MODELLING AND SIMULATION OF RESONANT TUNNELING DIODE

*Thesis submitted in partial fulfilment of the requirement
for the award of the degree of Master of Engineering in
Electronics and Telecommunication Engineering*

Of

JADAVPUR UNIVERSITY
2016

By

BANASREE DAS
(University Registration No.: 128919 of 2014-15**)**
(Examination Roll No.: M4ETC1605**)**

Under the supervision of

Prof. Chayanika Bose

**DEPARTMENT OF ELECTRONICS AND TELECOMMUNICATION
ENGINEERING
JADAVPUR UNIVERSITY, KOLKATA-700032
WEST BENGAL, INDIA**

FACULTY OF ENGINEERING & TECHNOLOGY
JADAVPUR UNIVERSITY

CERTIFICATE

This is to certify that the dissertation entitled **"Modelling and Simulation of Resonant Tunneling Diode"** has been carried out by **BANASREE DAS** (**University Registration No.:** 128919 of 2014-15) under my guidance and supervision and be accepted in partial fulfilment of the requirement for the degree of Master of Engineering in Electronics and Telecommunication Engineering. The research results presented in the thesis have not been included in any other paper submitted for the award of any degree to any other University or Institute.

Prof. Chayanika Bose
Project Supervisor
Department of Electronics and
Telecommunication Engineering
Jadavpur University
Kolkata- 700032

Prof. P. Venkateswaran
Head of the Department
Department of Electronics and
Telecommunication Engineering
Jadavpur University
Kolkata- 700032

----- ----------------------------------
Prof. Sivaji Bandyopadhyay
Dean
Faculty Council of Engineering and
Technology
Jadavpur University
Kolkata- 700032

FACULTY OF ENGINEERING & TECHNOLOGY

JADAVPUR UNIVERSITY

CERTIFICATE OF APPROVAL*

The forgoing thesis is hereby approved as a credible study of an engineering subject and presented in a manner satisfactory to warrant acceptance as pre-requisite to the degree for which it has been submitted. It is understood by this approval that the undersigned do not necessarily endorse or approve any statement made, opinion expressed or conclusion drawn there in but approve the thesis only for which it is submitted.

Committee on final examination for the evaluation of the Thesis.

....
External Examiner   **Project Supervisor**
                                                                               (Prof. Chayanika Bose)

*Only in case the thesis is approved

FACULTY OF ENGINEERING & TECHNOLOGY

JADAVPUR UNIVERSITY

DECLARATION OF ORIGINALITY AND COMPLIANCE OF ACADEMIC THESIS

It is hereby declared that the thesis titled **"Modelling and Simulation of Resonant Tunneling Diode"** contains original research work by the undersigned candidate, as a part of his degree of **Master of Electronics and Telecommunication Engineering**.

All information have been obtained and presented in accordance with academic rules and ethical conduct.

It is also asserted that, as required by these rules and conduct, the undersigned has fully cited and referenced all materials and results that are not original to this work.

Name: BANASREE DAS
Examination Roll No: M4ETC1605
Thesis Title: Modelling and Simulation of Resonant Tunneling Diode

_____
Signature of the Candidate with Date

Dedicated to

My Family members,

Especially to my beloved husband for his unconditional love, constant support and encouragement and

To the memory of my mother, who is no more to see today

ACKNOWLEDGEMENTS

BANASREE DAS

Department of Electronics and Telecommunication Engineering

Jadavpur University, Kolkata-700032

ABSTRACT

A simple model of resonant electronic transport through a GaAs-AlGaAs based double-barrier structure is developed. For each region of the system, analytical solutions to Schrödinger's equation are obtained, and the model is simulated in SILVACO-ATLAS software. The current-voltage characteristic of this Resonant Tunneling Diode (RTD) is considered as the reference one. Other models with various structural parameters like, well width, barrier width and barrier height are studied, and the corresponding I-V characteristics are compared with that of the previous one. This gives some insight about how each of the above parameters influences the device performance, mainly determined in terms of the peak-to-valley current ratio (PVCR). Two spacer layers are also included in the ideal model to get the more realistic behaviour of the device.

In order to improve the performance of RTD, In-based alloys viz. InGaAs-InAlAs and InGaAs-AlAs are used for simulation of RTDs, which exhibit much higher PVCRs, the latter performing better. However, in spite of the highest PVCR, the peak current appears at some higher voltage in the case of InGaAs-AlAs RTD. To eliminate the problem, a layer of InAs is introduced within the well layer of InGaAs, resulting in an InGaAs-AlAs-InAs RTD structure. The current-voltage characteristic of the RTD shows the similar qualitative features as reported in literature.

Table of Contents

Abbreviations

MBE: Molecular Beam Epitaxy.

MOCVD: Metal-Organic Chemical Vapour Deposition.

RTD: Resonant Tunneling Diodes.

NDR: Negative Differential Resistance.

PVCR: Peak to Valley Current Ratio.

HEMT: Single Material Gate

MODFET: Modulation Doped Field-Effect Transistors

HBT: Hetero-Junction Bipolar Transistors.

Xps: X-Ray Core Level Photoemission Spectroscopy.

QW: Quantum Well.

QWW: Quantum Well Wire.

QD: Quantum Dot.

QM: Quantum mechanical.

DBRTD: Double Barrier Resonant Tunneling Diode.

RITD: Resonant Intraband Tunneling Diode.

RTBT: Resonant-Tunneling Bipolar Transistor.

TCAD: Technology Computer-Aided-Design.

List of Figures

LIST OF TABLES

CHAPTER: 1

INTRODUCTION TO RESONANT TUNNELING DEVICES

Contents

CHAPTER: 1

INTRODUCTION TO RESONANT TUNNELING DEVICES

1.1. Beyond Si CMOS

Silicon based CMOS has been the dominant technology of the semiconductor industry for the last 50 years. The chip density and operating speed of Si based ICs have shown a regular trend of growth while the operating voltage has steadily decreased over the past decades. This has been achieved through continuous scaling of transistor dimensions. However as dimensions approach close to the wavelength of an electron, quantum effects such as tunneling, interference, quantization that arise due to wave nature of electron start playing an important role in determining device performance.

Novel devices with a different operational paradigm over conventional Field effect based devices can be built by utilizing these quantum mechanical effects. With the help of high mobility III-V compound semiconductors and advances in hetero epitaxial growth techniques such as Molecular Beam Epitaxy (MBE) and Metal-Organic Chemical Vapour Deposition (MOCVD), it has become possible to realize devices with very fast switching speeds and that are also capable of operating at low voltages, two very critical requirements for future digital logic technologies. Resonant Tunneling Diodes (RTD) hold a lot of promise in this regard. The negative differential resistance (NDR) characteristics exhibited by RTDs due to the resonant tunneling phenomenon have resulted in their usage in some niche applications. Since 1974, when the first GaAs-AlGaAs based RTD was demonstrated by Chang, Esaki and Tsu, [1] RTDs have been explored as alternatives to transistors for high frequency applications [2] such as microwave circuits and even logic circuits [3].

1.2. Motivation for studying Resonant Tunneling Devices

Among solid-state electronics the most promising devices are comprised of nanostructure to yield ultra small, ultrafast and power-efficient devices. The underlying physical phenomena to control the charge transport through such nano scale structures are quantum confinement. The fastest ever device is based on resonant tunneling and possesses current voltage characteristics with several negative-differential resistance (NDR) regions. Exploitation of such characteristics in memory cell or a logic family in nano-scale circuits is a widely accepted approach, especially to improve the computational functionality of basic circuit components.

From the technological point of view, resonant tunneling devices are presently the most mature type of quantum-effect device. Their interfacing with conventional transistors has reached an advanced level, and even in silicon, room temperature operations of NDR-devices are achievable. Besides the high-speed operation in the GHz regime, the combination of the NDR with electronic amplification is attractive to reduce circuit complexity i.e, the number of devices employed and the associated wiring. This has motivated the development of different three terminal devices. Significant examples are resonant hot electron transistors, gated resonant tunneling diodes and two dimensional electron gas tunneling field effect transistors.

Despite the advantages of high speed and low voltage operation offered by RTDs, there are some drawbacks too due to which RTDs have not become widespread. These are

1. RTDs are 2 terminal devices and cannot offer input to output isolation. They can therefore, only augment transistors but cannot replace them.

2. The load driving capabilities of RTDs are poor and hence overall throughput is affected. To increase the drive capabilities of RTDs, the peak current and the Peak to Valley Current Ratio (PVCR) need to be improved.

3. The most critical shortcoming is that RTDs with excellent PVRs can be grown using GaAs/AlGaAs, InGaAs/InAlAs and other III-V compound semiconductors, all of which are incompatible with the mainstream Si technology and are expensive to manufacture. Si/SiGe RTDs, those are compatible with Si

technology, have been demonstrated but they tend to have low PVCRs due to the short barrier height of SiGe.

So far, RTDs have been commonly used alongside III-V based HEMTs [4]. But as advances in fabrication techniques such as MBE continue, in the near future, we may have a viable and inexpensive way of manufacturing RTDs and integrating them with Si based circuits as well as III-V based HEMTs.

The various circuit design are accomplished in the area of binary and multiple-valued logic using resonant tunneling diodes (RTD's) in conjunction with high-performance III–V devices such as hetero-junction bipolar transistors (HBT's) and modulation doped field-effect transistors (MODFET's). New bistable logic families using RTD and HBT, RTD and MODFET are described that provide a single-gate, self-latching MAJORITY function in addition to basic NAND, NOR, and inverter gates. This forms the basis for design of high-speed nanopipelined 32- and 64-bit adders using only a single 4-bit adder block [3].

The immediate goal then is to understand and develop simulation models that can capture the underlying Physics of operation of RTDs accurately. Beginning with simple approximations, the models are then refined to account for effects happening in realistic devices such as scattering, thereby giving us a better understanding and a deeper insight into RTDs.

1.3. Project Problem Statement

In this thesis, novel features offered by Resonanant Tunneling diode are reviewed by simulating RTD in different conditions. The total work is divided into two parts: 1st part is totally based on a GaAs/AlGaAs RTD, which is the most common and popular type of RTD and will be used as the reference one. The effects of variations of different parameters on RTD's characteristics are mainly focused in this part. The 2nd part deals with the special structure of RTDs. The InGaAs/InAlAs, In GaAs/AlAs, InGaAs/AlAs/InAs based structures are studied in this chapter, and their performances are compared with respect to that of the standard GaAs/AlGaAs RTD investigated in part 1.

1.4. Thesis Outline

Following the introduction, the rest of the dissertation is organized as follows:

❖ **Chapter 2: Physical Background and History of Resonant Tunneling Diode.**

This chapter introduces the concept of Basic hetero structure, different types of hetero structure, and different types of quantum structures. The basic physics behind the square quantum well is first discussed, and then basics of tunneling for both single and double rectangular barrier are discussed. On the basis of the physics of tunneling *Resonant Tunneling* is derived and different factors of resonant tunneling is discussed. Finally the history behind the invention of RTD and its gradually evaluation are discussed.

❖ **Chapter 3: Software Used for Simulation of RTD.**

This chapter presents novel features offered by SILVACO TCAD-ATLAS software. This software is used as simulation tool to simulate the thesis work. Some common example is discussed in this chapter.

❖ **Chapter 4: Modelling and Simulation of Symmetric RTD.**

A physics based 2-D model of RTD is simulated by SILVACO software. At the beginning the basic requirements and details of its physical parameters used for simulation of GaAs-Al_xGa_{1-x}As based symmetric RTD are derived. Next different symmetric structures are simulated and their results are discussed.

❖ **Chapter 5: Modelling and Simulation of Asymmetric RTD.**

The current-voltage characteristics of a standard RTD may vary due to variation of its different parameters such as well widths, barrier widths, barrier height. The effects on characteristics curve due to these effects are observed and discussed in this chapter.

❖ **Chapter 6: Modelling and Simulation of Special Structure of RTD.**

This chapter demonstrates the development of RTD using different Material composition especially *Indium* based compound material. Different developments in RTD structure using *Indium* based compound material and their influence in current-voltage characteristics are derived here.

❖ **Chapter 7: Conclusions and future scope.**

In this final chapter overall conclusions are drawn, and depending on these conclusions what are the possible work left on RTD till date are discussed.

CHAPTER: 2

PHYSICAL BACKGROUND & HISTORY OF RESONANT TUNNELING DIODE

Contents

CHAPTER: 2

PHYSICAL BACKGROUND & HISTORY OF RESONANT TUNNELING DIODE

The seed of quantum well devices was planted when Esaki and Tsu [5] suggested in 1969 that a heterostructure consisting of alternating ultrathin layers of two semiconductors with different band gaps should exhibit some novel useful properties. The band-edge potential varies from layer to layer as a result of the difference in the band gaps and a periodically varying potential is produced in the structure with a period equal to the sum of the widths of two consecutive layers. For layer thicknesses of the order of ten 10 nm, the wavelength as well as the mean free path of the electrons extends over several layers and the periodic potential transforms the energy bands of the host lattice into mini bands. Phenomena like bloch oscillation and low-field negative differential resistance may be produced by the electrons in such mini bands. Attempts to fabricate the proposed structure and to demonstrate the predicted phenomena were only partially successful. Interest was, however, generated in fabricating heterostructures with transition regions extending over a few atomic layers. Structures were initially grown by using the technique of molecular beam epitaxy (MBE) but soon several other techniques were developed and realization of heterostructures may now be grown of any composition with crystalline perfection at the interfaces become feasible. Such structures form the basis of quantum well devices.

The nanostructure and resonant tunneling phenomena originate from the concept of heterostructures. So, the basics of heterostructures are presented first, followed by the concepts of nanostructure or resonant tunneling devices.

2.1. Theory of Heterostructures

Composite semiconductor structures consisting of two or more layers of different materials, one grown on another, are commonly referred as heterostructures. The structures were

mostly grown by the techniques of liquid phase epitaxy or chemical vapour deposition techniques [37]. Now a day, the fabrication of heterostructures by epitaxial growth is the cleanest and most reproducible method available. The properties of such structures are of critical importance for many heterostructure devices including Resonant Tunneling Diodes, Resonant Tunneling Transistors.

2.1.1 Formation of Heterostructure

In principle it must be possible to join the two materials perfectly in an ideal heterostructure.

i. This requires first that they have the same crystal structure (or at least symmetry), and this is satisfied for the common III-V compounds.

ii. A second requirement, if there is to be a minimum strain in the final structure, is that the two lattice constants must be nearly identical. The lattice constant of an alloy is usually given by linear interpolation between its constituents. This is known as **Vegard's law** and predicts, for example, that the lattice constant of $Al_xGa_{1-x}As$ is given by $xa_{AlAs} + (1 - x) a_{GaAs}$, where 'a' is the lattice constant and 'x' is the compound composition factor.

Growing the heterostructures is a complicated process and the behaviour of electrons and holes in this structure is manipulated through **band engineering**. For example, let's Consider a heterojunction between two materials *A* and *B,* with E_g (A) < E_g (B) where E_g is the energy gap between conduction band edge E_c and valence band edge E_v. Therefore Conduction band offset is given by: $\Delta E_C \approx E_C^B - E_C^A$

This Conduction band offset can be measured using different rules. There are two Emperical Rules. These are *Electron Affinity Rule, Common Anion Rule*. There are some Theoretical Methods. These are: *Tersoff Method, Van De Walle -Martin Method*. By some experimental method also band offset can find. Some common experiments are: *Absorption Measurement, Photoluminescence Measurement, X-Ray Core Level Photoemission Spectroscopy (Xps).*

2.1.2 Classification of Heterostructure

Depending on the alignment of the bands of two semiconductors, the hetero structures are divided into three types. Three possible alignments of the conduction band, valence band and forbidden gap in different heterostructures are shown in figure 2.1
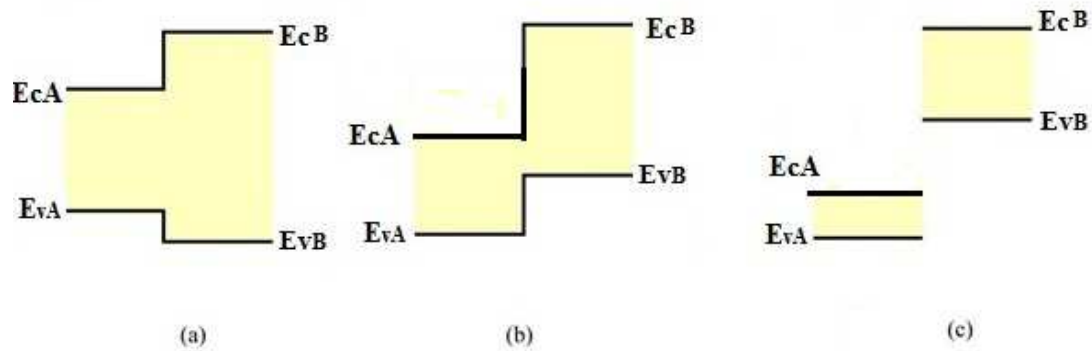
Figure 2.1 Various band alignment (a) Straddle or 'Type 1' alignment (b) Staggered or 'Type 2' alignment (c) Broken Gap or 'Type 3' alignment.

- ❖ *Straddle or 'Type 1' alignment:* In this type of alignment, the narrower band gap is enclosed within the wider band gap, as shown in Figure2.1 (a). Both electrons and holes are confined in the lower-band-gap material in these heterostructres. The common example of *type I* or *straddling* alignment is heterostructure formed by GaAs and AlGaAs composition.

- ❖ *Staggered or 'Type 2' alignment:* In this type of alignment the band offset for conduction band and valence band occurs in same direction, as shown in Figure2.1 (b). This happens due to the bands favour electrons in one material but holes in other material. Heterostructure of InP and $In_{0.52}Al_{0.48}As$ is an example of *type II* or *staggered* alignment.

- ❖ *Broken-gap or 'Type 3' alignment:* This is that where the two band gaps do not overlap at all, giving *type III or broken-gap alignment*. Heterostructure formed by InAs-GaSb combination is an example of this type.

Quantum well devices have been realized mostly by using the Type I heterostructures, either lattice matched or strained- layer systems. GaAs/$Ga_xA1_{-x}As$, $Ga_{0.47}In_{0.53}As/InP$,

Ga$_{0.47}$In$_{0.53}$As/Al$_{0.48}$In$_{0.52}$As and InP/GaxIn$_{1-y}$As$_{1-y}$Py are commonly used as lattice- matched systems while Al$_x$Ga$_{1-x}$As/Ga$_x$In$_{1-x}$As, Ga$_x$In$_{1-x}$As/ Al$_y$In$_{1-y}$As, Ga$_{0.47}$In$_{0.53}$AS/AlAs, Ga$_x$In$_{1-x}$As/InP and a few other combinations are used as strained layer systems.

2.2. Quantum Structure

As already mentioned the basic concept of **Quantum Structure** is established on the growth of Heterostructure. The formation of a structure by using different band gap materials together opens new era in devices physics. Keeping the widths of materials limited to few nanometres, the Quantum effects can be exhibited within the materials. Restricting the dimension of the materials at different directions, different quantum structure like Quantum well or 2D, Quantum wire or 1D or Quantum dot or 0D can be produced. The electrons become confined within the structure along the restricted dimension and behave more like free electron along other directions. This means that electronic wave functions become discrete in direction(s). This amazing nature of electron helps to reveal new device with advantageous features. The different quantum structures are discussed here.

❖ **Quantum Well:** Whenever a layer of small band gap material is sandwiched between large band gap materials, the structure results a type 1 heterostructure. If the thickness of small band gap material is kept comparable with electronic wavelength, then the conduction band gap discontinuity results in a well in the small band gap material and barrier in large band gap material. This structure is called *Quantum Well (QW) or 2-D electron gas system*. The wells are forms in both conduction band and valence band; the valence band well depth is of smaller than that of the conduction band well. The component of momentum and thereby, the carrier energy in the direction perpendicular to the interfaces are quantized.

❖ **Quantum Well Wire or 1-D electron gas System:** If the structure discussed above is made more complex such that electrons can move freely only in one dimension, then it is denoted as *Quantum Well Wire (QWW) or 1-D electron gas system*. It should be mentioned that the application of quantum wires to photonic devices requires good estimated values of the energy levels, so that the required dimensions of the well may be worked out with suitable design formula.

❖ **Quantum Dot or 0-D electron gas System:** If the carrier movement along all 3-diamentions are restricted, then it gives *Quantum Dot (QD) or 0-D electron gas system*. Here carriers occupy completely discrete energy levels, and thus such structure forms artificial atoms. Quantum effects one most pronounced in Quantum Dot.

⊕ *2.3. Quantum Well*

The phenomenon of *Resonant Tunneling* relies on the quantization of carrier energy in Quantum Well. However, the mathematical expression for quantized energy is available for an infinite QW and not valid for a real QW, which has barrier of height far from infinite. Therefore determination of such quantized energy levels in a QW is of uttermost importance, and is presented here.
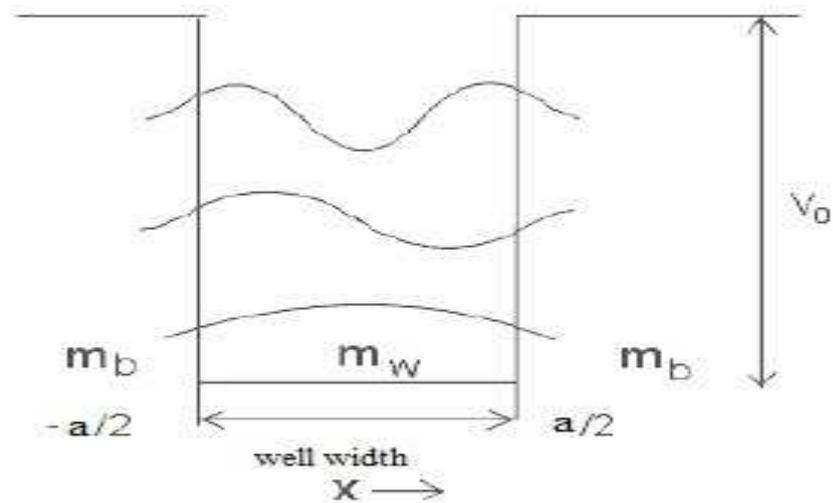
Figure 2.2 Rectangular Quantum Well with Vo Potential Barrier

The simplest Quantum well is a rectangular well which is characterized by a zero potential inside the well. The origin is chosen in the middle of such a well of width **'*a*'** and potential outside the well **'V_0'**

The Schrödinger equation for motion inside the well i.e., for - $a/2 < z < a/2$, is identical to that for free space, equation (2.1), because there is no potential energy.

$$-\frac{\hbar^2}{2m}\frac{d^2\psi}{dz^2} = E\psi(z) \dotfill 2.1$$

The solutions can be written as
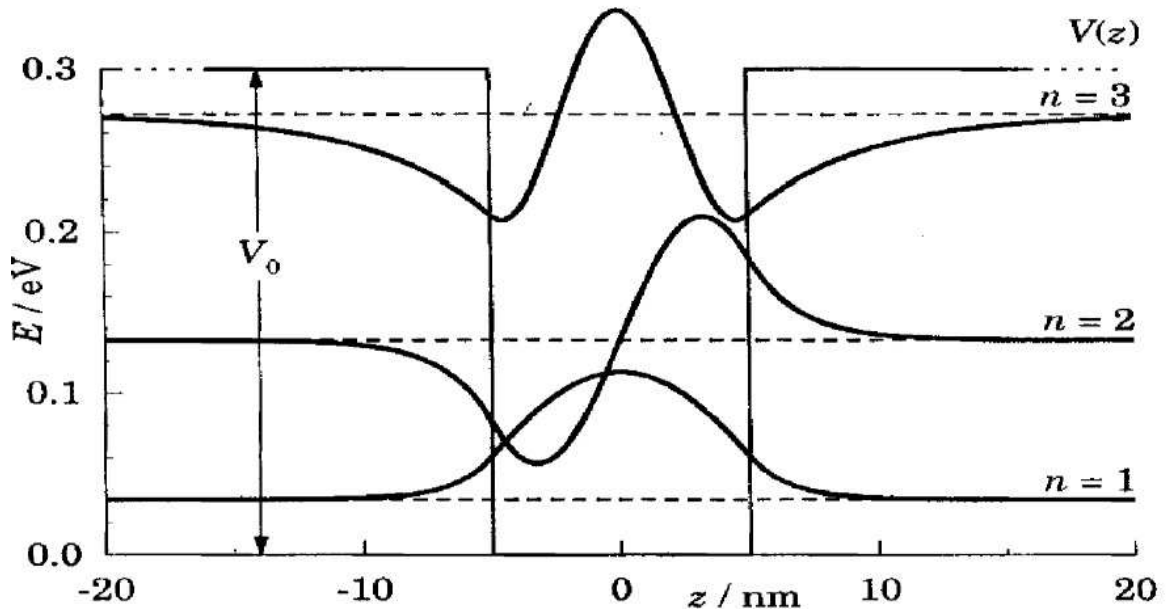
Figure 2.3 Finite Square Quantum Well showing three Bound States with barrier height 0.3eV and well width of 10nm [6]

$$\psi_w(z) = C\binom{\cos}{\sin}kz \dotfill 2.2$$

with $E = \hbar^2 k^2 / 2m$. Outside the well, $\psi(z)$ satisfies

$$-\frac{\hbar^2}{2m}\frac{d^2}{dz^2}\psi_B(z) + V_0\psi_B(z) = E\;\psi_B(z) \dotfill 2.3$$

with $E < V_0$. The solutions are $D = \exp(\pm\kappa z)$ \dotfill 2.4

with $\dfrac{\hbar^2\kappa^2}{2m} = V_0 - E = B$ \dotfill 2.5

where B is called **binding energy**. B is given as $B = \dfrac{ma^2 V_0^2}{2\hbar^2}$

Applying the boundary conditions at the interfaces (at $z = a/2$ and $z = -a/2$), continuity of ψ(z) requires

$$\psi\left(\frac{a}{2}\right) = C\begin{Bmatrix}\cos\\\sin\end{Bmatrix}\left(\frac{ka}{2}\right) = D\exp\left(-\frac{1}{2}\kappa a\right) \text{...} 2.6$$

Similarly matching the derivatives gives

$$\frac{d\Psi}{dz}_{z=a/2} = Ck\begin{Bmatrix}-sin\\cos\end{Bmatrix}\left(\frac{ka}{2}\right) = -D\kappa\, exp\left(\pm\frac{1}{2}\kappa a\right) \text{..} 2.7$$

By solving the equations 2.6 and 2.7 the values of 'k' and 'κ' will be derived in terms of energy 'E'. In case of heterostructure, the wave numbers inside and outsides are given by

$$k = \frac{\sqrt{2m_0 m_w(E - E_c^W)}}{\hbar} \qquad\qquad \kappa = \frac{\sqrt{2m_0 m_B(E_C^B - E)}}{\hbar} \text{..............................} 2.8$$

Where, m_w is the effective mass and E_c^W is the bottom of the conduction band of the well, and m_B and E_c^B are the effective mass of the barrier material and bottom of the conduction band of barrier respectively.

The depth of the well is given by $V_0 = E_c^B - E_c^W = \Delta E_c$

Simplifying the unchanged matching condition for ψ (a/2) gives

$$\begin{pmatrix}\tan\\-\cot\end{pmatrix}\left(\frac{ka}{2}\right) = \left(\frac{m_w \kappa}{m_B k}\right) = \sqrt{\frac{m_w}{m_B}\left(\frac{2m_0 m_w V_0}{\hbar^2 k^2} - 1\right)} \text{..} 2.9$$

Defining $\theta = ka/2$,

$$\theta^2 = \frac{m_0 m_w V_0 a^2}{2\hbar^2} \text{...} 2.10$$

which depends only on the mass inside the well. The matching condition then becomes

$$\begin{pmatrix}\tan\\-\cot\end{pmatrix}\theta = \sqrt{\frac{m_w}{m_B}\left(\frac{\theta_0^2}{\theta^2} - 1\right)} \text{...} 2.11$$

All the physical inputs the mass of the particle, the depth and width of the well has been absorbed into the dimensionless parameter θ_0^2. This parameter determine the allowed values of θ. The above transcendental equation (Eq. 2.11) is solved numerically in their dimensionless form.

Both sides of equation 2.11 are plotted against θ and solutions to equation 2.10 will occur when the lines of (tanθ) and(- cotθ) intersect the curve for the right hand side of equation 2.10. A typical example of this solution is shown in figure 2.4 for electrons in a well in GaAs. This has m = $m_0 m_e$, with m_e = 0.067, V_0= 0.3 eV, and a = 10 nm, which gives θ_0^2 = 13.2.

The difference in the energy between the two regions which forms the well is given by,

$$\Delta E_C + \frac{\hbar^2 k^2}{2m_0}(\frac{1}{m_0} - \frac{1}{m_w}) \quad \text{..} \quad 2.12$$

The energy is therefore given by $\varepsilon = \frac{\hbar^2}{2m_0 m_w} \frac{4}{a^2} \theta^2$ 2.13
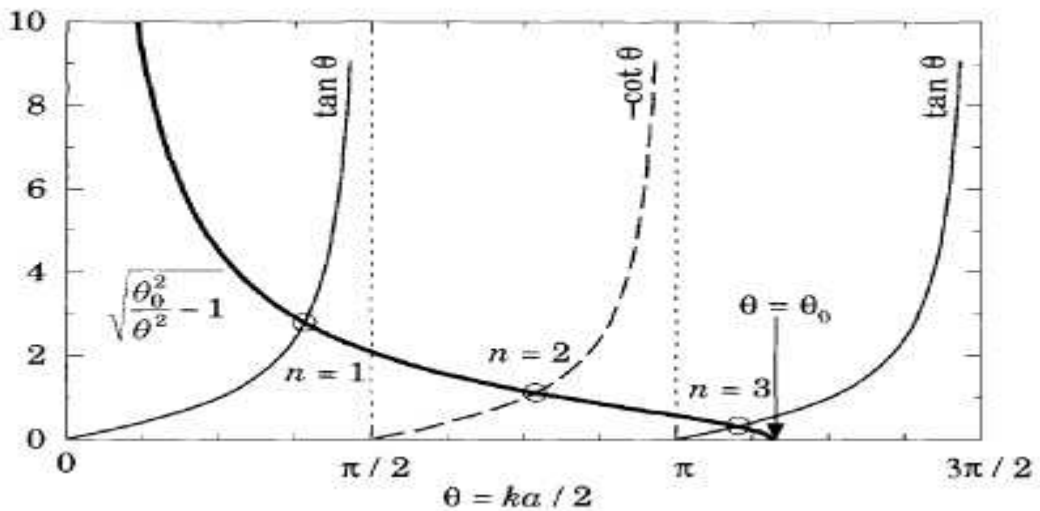
Figure 2.4 Graphical solution of equation 2.10 for a square well of GaAs with depth Vo = 0.3 eV and width *a* = 10 nm, The figure indicates three bound states [6].

2.4. Fundamentals of Tunneling

Tunneling is a Quantum mechanical (QM) phenomenon wherein a particle can penetrate a potential barrier higher than its kinetic energy. Classically, if a particle is incident on a potential barrier it is transmitted only when it has energy higher than the barrier height. However, quantum mechanically, if the barrier is thin enough and has a finite height, the electron wave can penetrate through the barrier and emerge on the other side. This is a result

of the wave nature of particles analogous to the evanescent waves observed in electromagnetic radiation. The tunneling phenomenon can be observed in semiconductor devices, where the potential barrier is created either by a difference in band alignment of semiconductors with different band gaps or by abrupt doping variations as in a p-n junction structure. The tunneling semiconductor devices are broadly classified into *intraband* and *interband* tunneling devices. *Intraband* tunneling involves tunneling within the same electronic band i.e. from conduction to conduction band or valence to valence band. These are unipolar and involve only one type of carrier i.e. either electrons or holes. The tunneling through RTD is an example of *Intraband tunneling*. In the case of *interband* tunneling, carriers tunnel from the conduction to the valence band or vice versa, and hence, tunnelling is bipolar in nature. The tunneling phenomenon in a tunnel diode is an example of this type of tunneling.

As the present thesis is focussed on the study of RTD, features of only intraband tunneling will be discussed in next sections.

The tunneling through a rectangular barrier is illustrated in Figure 2.5. Classically the electron would be reflected if $E < V_0$ but due to tunneling there is a probability that the electron penetrates the barrier. On the other hand, classically, if the electron has an energy $E > V_0$ it is certain to be transmitted through the barrier, but in quantum mechanics there is a probability of reflection even when the energy exceeds the barrier height.

Tunneling through a potential barrier is characterized by a transmission coefficient T so that $0 \leq T \leq 1$. The transmitted wave function Ψ_T is thus given by $T\Psi_I$ where Ψ_I is the wave function of the incident particle. In a single barrier structure like the one described here, the transmission coefficient is a monotonically increasing function of E when $E < V_0$ ($T (E_1) > T (E_2) \forall E_1 > E_2 | V_0 > E_1$).
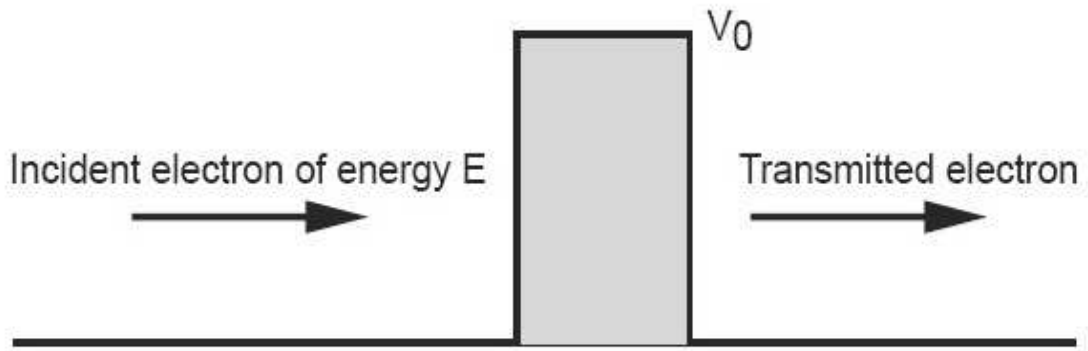
Figure 2.5 The basics of tunneling. An electron of energy E is incident on a potential barrier of height V0. Classically the electron is reflected when E < V0, but quantum mechanically there is a certain probability that the electron is transmitted through the barrier.

A double barrier structure like the one shown in Figure 2.6 gives rise to QM phenomena called resonant tunneling. In a quantum well in between the barriers the individual transmission coefficients of the left and right barriers, T_L and T_R respectively, are both much smaller than unity. This means that the energy levels in the well will be quantized. Strictly speaking this is not entirely true because T_R and T_L are in fact, of course, not equal to zero. This means that the energy levels are not clearly defined; there is some broadening of the levels. When an electron with an energy which is not coincident with one of the quasi-quantized levels in the well is incident on the barrier/well complex the global transmission coefficient T_G is much smaller than unity. The electron can be transmitted with a transmission coefficient on the order of unity only if the electron energy coincides with one of the energy levels in the well. This phenomenon is therefore called resonance tunneling and such structure is utilized in resonant tunneling diodes.
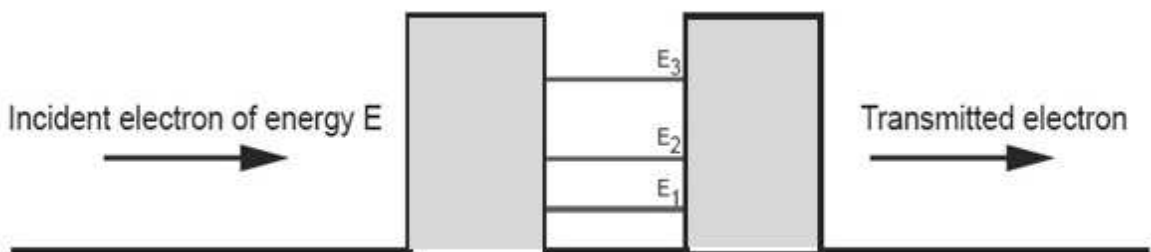
Figure 2.6 Tunneling through a double barrier. If T << 1 for both barriers the region between the two barriers will act as a quantum well with quantized energy levels. This gives rise to resonant tunneling

2.4.1 Single Rectangular Barrier

The simplest barrier to analyze is a rectangular potential $E_{pot}(x)$, with barrier height E_0, larger than the electron total energy E as illustrated in Fig. 2.7. The potential exists in the finite interval $0 < x < a$, and is zero outside. In the region external to the potential i.e. $x < 0$ and $x > a$, the electron is free. For practical tunneling devices implemented using semiconductor heterostructures, the effective mass of electrons may not be equal in the regions inside and outside the barrier. This is taken into consideration by assuming an electron effective mass of m_1 outside the barrier and m_2 inside the barrier.

To calculate the tunneling probability, the wave function Ψ is determined using the general time-independent Schrödinger equation:
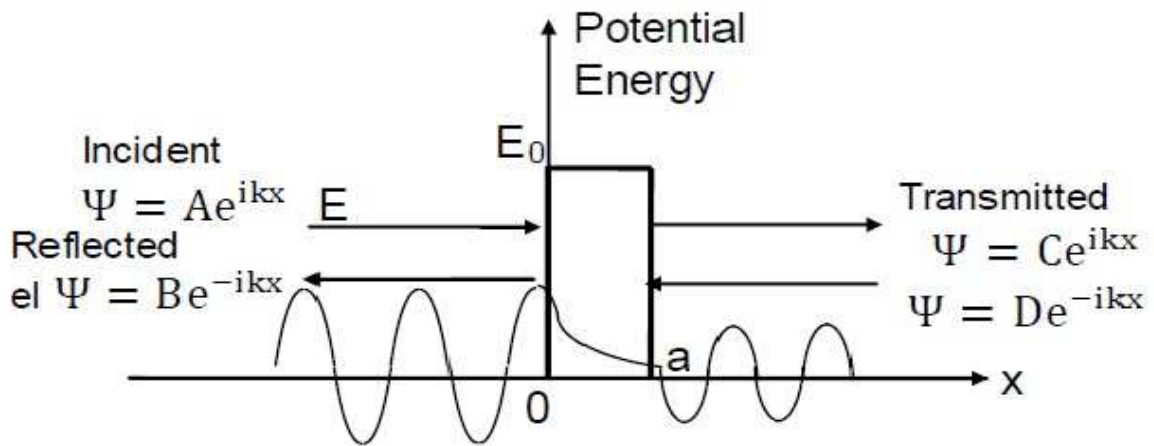
Figure 2.7 Rectangular tunneling barrier showing incident, reflected and transmitted wave functions

$$(-\frac{\hbar^2}{2m}\nabla^2 + E_{pot}(r))\psi = E\psi \quad\text{.. 2.14}$$

Here positional vector 'r' represents the three dimensional position. Reducing to a one-dimensional problem,

$$\frac{\hbar^2}{2m}\frac{d^2\psi}{dx^2} + (E - E_{pot}(x))\psi = 0 \quad\text{.. 2.15}$$

$$\frac{\partial^2\psi}{\partial x^2} + k^2\psi = 0 \text{ where, } k = \frac{\sqrt{2m_1(E - E_{pot}(x))}}{\hbar} \quad\text{... 2.16}$$

In the region outside the barrier i.e. for $x < 0$ and $x > a$, $E_{pot} = 0$ and k reduces $\frac{\sqrt{2m_1 E}}{\hbar}$

The general solution of the Schrödinger's equation is given by:

$$\psi(x) = \begin{cases} Ae^{ikx} + Be^{-ikx}, & x < 0 \\ Ce^{ikx} + De^{-ikx}, & x > a \end{cases}$$ 2.17

where, A, B, C, D are constants.

Inside the barrier, $\dfrac{\sqrt{2m_2(E-E_0)}}{\hbar}$. Since E < E₀, k is imaginary. The Schrödinger's equation is now written as

$$\frac{d^2\psi}{dx^2} + \kappa^2\psi = 0 \text{ where } \kappa = \frac{\sqrt{2m_2(E_0-E)}}{\hbar}$$ 2.18

and the general solution is given by $\psi(x) = Fe^{\kappa x} + Ge^{-\kappa x}$, where F and G are constants.

Now, $\psi(x)$ and $1/\mathrm{m}\left(\dfrac{d\psi(x)}{dx}\right)$ should be continuous at $x = 0$ and $x = a$. At $x = 0$,

$$(A+B) = (F+G)$$ 2.19

and $\dfrac{ik}{m_1}(A-B) = \dfrac{k}{m_2}(F-G)$ 2.20

$$\left[\frac{A}{B}\right] = \begin{bmatrix} \dfrac{ik + \dfrac{m_1}{m_2}\kappa}{2ik} & \dfrac{ik - \dfrac{m_1}{m_2}\kappa}{2ik} \\ \dfrac{ik - \dfrac{m_1}{m_2}\kappa}{2ik} & \dfrac{ik + \dfrac{m_1}{m_2}\kappa}{2ik} \end{bmatrix}\left[\frac{F}{G}\right]$$ 2.21

While at $x = a$,

$$Ce^{ika} + De^{-ika} = Fe^{\kappa a} + Ge^{-\kappa a}$$ 2.22

$$ikCe^{ika} - ikDe^{-ika} = \frac{m_1}{m_2}\kappa(Fe^{\kappa a} + Ge^{-\kappa a})$$ 2.23

$$\begin{bmatrix} F \\ G \end{bmatrix} = \begin{bmatrix} \left(\dfrac{ik + \dfrac{m_1}{m_2}\kappa}{2\dfrac{m_1}{m_2}\kappa}\right)e^{(ik-\kappa)a} & -\left(\dfrac{ik - \dfrac{m_1}{m_2}\kappa}{2\dfrac{m_1}{m_2}\kappa}\right)e^{-(ik+\kappa)a} \\[4mm] -\left(\dfrac{ik - \dfrac{m_1}{m_2}\kappa}{2\dfrac{m_1}{m_2}\kappa}\right)e^{-(ik+\kappa)a} & \left(\dfrac{ik + \dfrac{m_1}{m_2}\kappa}{2\dfrac{m_1}{m_2}\kappa}\right)e^{(ik-\kappa)a} \end{bmatrix}\begin{bmatrix} C \\ D \end{bmatrix} \dots\dots\dots\dots\dots 2.24$$

Combining equations (2.21) and (2.24)

$$\begin{bmatrix} A \\ B \end{bmatrix} = \begin{bmatrix} \dfrac{ik + \dfrac{m_1}{m_2}\kappa}{2ik} & \dfrac{ik - \dfrac{m_1}{m_2}\kappa}{2ik} \\[4mm] \dfrac{ik - \dfrac{m_1}{m_2}\kappa}{2ik} & \dfrac{ik + \dfrac{m_1}{m_2}\kappa}{2ik} \end{bmatrix}\begin{bmatrix} \left(\dfrac{ik + \dfrac{m_1}{m_2}\kappa}{2\dfrac{m_1}{m_2}\kappa}\right)e^{(ik-\kappa)a} & -\left(\dfrac{ik - \dfrac{m_1}{m_2}\kappa}{2\dfrac{m_1}{m_2}\kappa}\right)e^{-(ik+\kappa)a} \\[4mm] -\left(\dfrac{ik - \dfrac{m_1}{m_2}\kappa}{2\dfrac{m_1}{m_2}\kappa}\right)e^{-(ik+\kappa)a} & \left(\dfrac{ik + \dfrac{m_1}{m_2}\kappa}{2\dfrac{m_1}{m_2}\kappa}\right)e^{(ik-\kappa)a} \end{bmatrix}\begin{bmatrix} C \\ D \end{bmatrix} =$$

$$\begin{bmatrix} M_{L11} & M_{L12} \\ M_{L21} & M_{L22} \end{bmatrix}\begin{bmatrix} M_{R11} & M_{R12} \\ M_{R21} & M_{R22} \end{bmatrix}\begin{bmatrix} C \\ D \end{bmatrix} =$$

$$\begin{bmatrix} M_{L11}M_{R11} + M_{L12}M_{R21} & M_{L11}M_{R12} + M_{L12}M_{R22} \\ M_{L21}M_{R11} + M_{L22}M_{R21} & M_{L21}M_{R12} + M_{L22}M_{R22} \end{bmatrix}\begin{bmatrix} C \\ D \end{bmatrix} = \begin{bmatrix} M_{11} & M_{12} \\ M_{21} & M_{22} \end{bmatrix}\begin{bmatrix} C \\ D \end{bmatrix} \dots\dots\dots\dots 2.25$$

where, $M_{11} = M_{22}^{*}$ and $M_{12} = M_{21}^{*}$

Assuming incidence only at the left side of the barrier, $D = 0$

$$A = (M_{L11}M_{R11} + M_{L12}M_{R21})C \dots\dots\dots\dots\dots\dots\dots\dots\dots\dots\dots\dots\dots\dots\dots\dots\dots 2.26$$

$$B = (M_{L21}M_{R11} + M_{L22}M_{R21})C \dots\dots\dots\dots\dots\dots\dots\dots\dots\dots\dots\dots\dots\dots\dots\dots\dots 2.27$$

$$\frac{B}{A} = \frac{M_{L21}M_{R11} + M_{L22}M_{R21}}{M_{L11}M_{R11} + M_{L12}M_{R21}} = \frac{-i\dfrac{\left(k^2 + \left(\dfrac{m_1}{m_2}\right)^2 \kappa^2\right)}{2\left(\dfrac{m_1}{m_2}\right)k\kappa}\sinh(\kappa a)}{\cosh\cosh(\kappa a) - i\dfrac{\left(k^2 - \left(\dfrac{m_1}{m_2}\right)^2 \kappa^2\right)}{2\left(\dfrac{m_1}{m_2}\right)k\kappa}\sinh(\kappa a)} \quad\text{.................. 2.28}$$

$$\frac{C}{A} = \frac{1}{M_{11}} = \frac{1}{\left(M_{L11}M_{R11} + M_{L12}M_{R21}\right)} = \frac{e^{-ika}}{\cosh(\kappa a) - \dfrac{i\left(k^2 - \left(\dfrac{m_1}{m_2}\right)^2 \kappa^2\right)}{2\left(\dfrac{m_1}{m_2}\right)k\kappa}\sinh(\kappa a)} \quad\text{................. 2.29}$$

and the reflection (R) and transmission (T) coefficients are given by:

$$R = \frac{|B|^2}{|A|^2} = \frac{\dfrac{\left(k^2 + \left(\dfrac{m_1}{m_2}\right)^2 \kappa^2\right)^2}{4k^2\kappa^2}\sinh^2(\kappa a)}{\cosh^2(\kappa a) + \dfrac{\left(k^2 - \left(\dfrac{m_1}{m_2}\right)^2 \kappa^2\right)^2}{4k^2\left(\dfrac{m_1}{m_2}\right)^2 \kappa^2}\sinh^2(\kappa a)} = \left[1 + \frac{4\left(\dfrac{m_1}{m_2}\right)^2 k^2\kappa^2}{\left(k^2 + \left(\dfrac{m_1}{m_2}\right)^2 \kappa^2\right)^2\sinh^2(\kappa a)}\right]^{-1}$$

For $m_1 = m_2$ this reduces to: $R = \left[1 + \dfrac{4E(E_0 - E)}{E_0^{\,2}\sinh^2(\kappa a)}\right]^{-1}$ 2.30

$$T = \frac{|C|^2}{|A|^2} = \frac{1}{|M_{11}|^2} = \frac{1}{\cosh^2(\kappa a) + \dfrac{\left(k^2 - \left(\dfrac{m_1}{m_2}\right)^2 \kappa^2\right)^2}{4k^2\left(\dfrac{m_1}{m_2}\right)^2 \kappa^2}\sinh^2(\kappa a)} = \left[1 + \frac{\left(k^2 - \left(\dfrac{m_1}{m_2}\right)^2 \kappa^2\right)^2\sinh^2(\kappa a)}{4k^2\left(\dfrac{m_1}{m_2}\right)^2 \kappa^2}\right]^{-1}$$

For $m_1 = m_2$ this reduces to: $T = \left[1 + \dfrac{E_0^{\ 2} \sinh^2(\kappa a)}{4E(E_0 - E)} \right]^{-1}$ 2.31

(a)

(b)
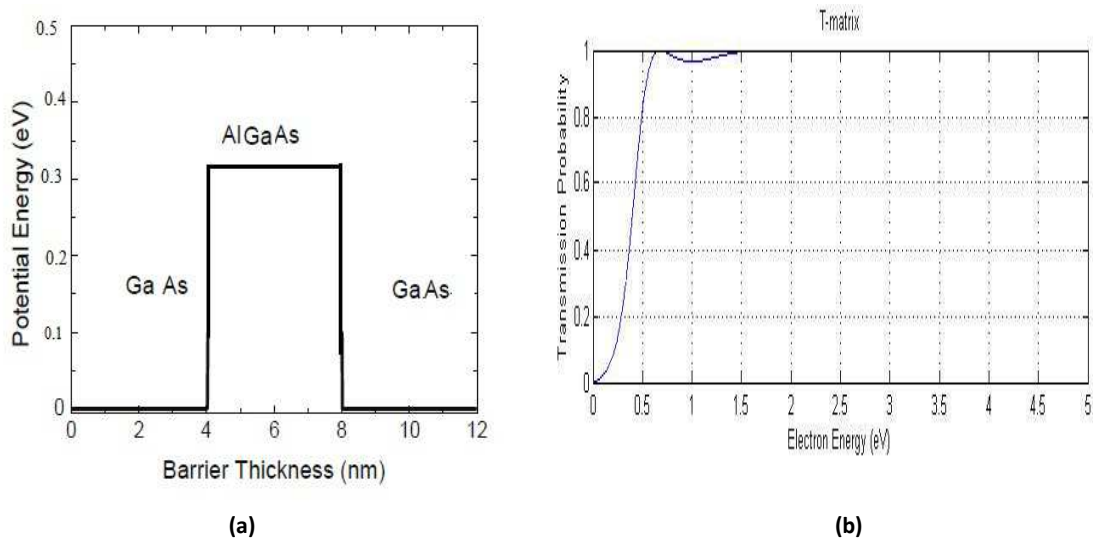
Figure 2.8 Transmission Coefficient for a GaAs/AlGaAs barrier with barrier width 4 nm and barrier height of 0.33eV.

Figure 2.8 shows the transmission coefficient; **T** for a single potential barrier formed using an GaAs/AlGaAs heterostructure where the electron effective mass used for GaAs is $0.067m_0$ and for AlGaAs is $0.087m_0$. In contradiction to classical prediction, for $E \geq E_0$ the transmission coefficient is not always '1' but is oscillatory and equal to one only for "**κa=nπ**" i.e. when the thickness of the barrier is a half-integral or integral number of the de-Broglie wavelength in the barrier region. This is due to destructive interference between waves caused by reflections at $x = 0$ and $x = a$. As $E \gg E_0$, 'T' asymptotically tends to unity.

A more complex but practical situation appears is when the momentum on the two sides of the barrier is not constant. If the wave vector on the left and right side of the barrier are **k** and **k'** respectively, then the transmission coefficient is given by [7]:

$$T = \frac{k'}{k} \frac{1}{|M_{11}|^2} = \frac{4kk' / (k + k')^2}{1 + \dfrac{(k^2 + \kappa^2)(k'^2 + \kappa^2)}{\kappa^2(k^2 + k'^2)} \sinh^2(\kappa\alpha)}$$ 2.32

2.4.2 Double Rectangular Barrier - Resonant Tunneling
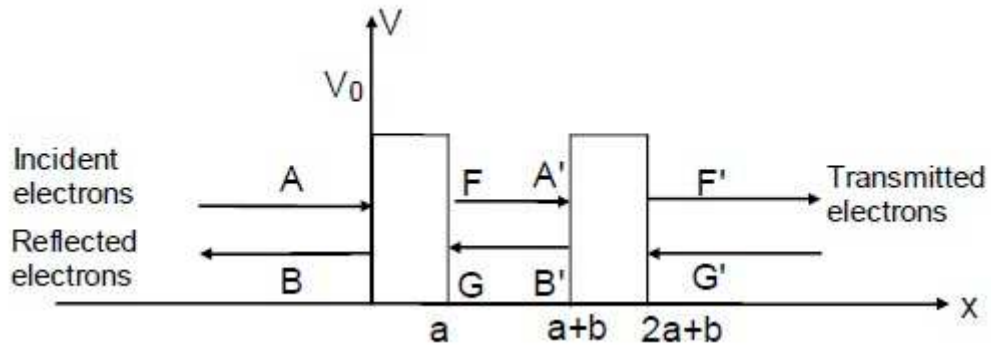
Figure 2.9 Double barrier structure showing amplitudes of forward and backward wave functions in each region

In a quantum well of width 'b' existing between two barriers (Fig. 2.9), discrete energy levels are formed due to quantum confinement. When the incident wave energy coincides with the energy level in the well, resonant tunneling occurs, and the transmission through the barriers equals unity. The wave amplitude F transmitted through the left barrier can be related to the wave incident on the right barrier A' by the relation:

$A' = Fe^{ikb}$. Similarly $B' = Ge^{-ikb}$

Thus, $\begin{bmatrix} F \\ G \end{bmatrix} = \begin{pmatrix} e^{-ikb} & 0 \\ 0 & e^{ikb} \end{pmatrix} \begin{bmatrix} A' \\ B' \end{bmatrix}$ describes the matrix for the well region. $\mathbf{M_L}$ and $\mathbf{M_R}$ are matrices representing the two barrier regions and are identical to that obtained in Eq. (2.25). The composite transmission matrix can now be written as:

$$\begin{bmatrix} A \\ B \end{bmatrix} = [M_L] \begin{bmatrix} e^{-ikb} & 0 \\ 0 & e^{ikb} \end{bmatrix} [M_R] \begin{bmatrix} F' \\ G' \end{bmatrix} = \begin{bmatrix} M_{T11} & M_{T12} \\ M_{T21} & M_{T22} \end{bmatrix} \begin{bmatrix} F' \\ G' \end{bmatrix}$$

.... 2.33

where $M_{T11} = M_{L11}M_{R11}e^{ikb} + M_{L12}M_{R21}e^{-ikb}$

For barrier's with equal width and height, the wave vector in the regions left and right of the structure is the same as the wave vector in the quantum well. Further the wave vectors in the barriers are also the same. Hence, $M_{L11} = M_{R11} = M_{11}$ and $M_{L12} = M_{R21}^* = M_{21}$.

$$M_{T11} = |M_{11}|^2 e^{-i\theta} e^{ikb} + |M_{21}|^2 e^{-ikb}$$

where from Eq. 2.29 $\theta = \tan^{-1}\left[\left(\dfrac{k^2\kappa^2}{2k\kappa}\right)\tanh(\kappa a)\right]$

Hence, $|M_{T11}|^2 = 1 + 4|M_{11}|^2 |M_{21}|^2 \cos^2(kb+\theta)$ 2.34

From Eq. (2.32), transmission probability

$$T = \frac{1}{|M_{T11}|^2} \sim \frac{1}{4|M_{11}|^2 |M_{21}|^2 \cos^2(kb+\theta)} = \frac{T_{\sin gle-barrier}}{4|M_{21}|^2 \cos^2(kb+\theta)}$$ 2.35

(a)

(b)
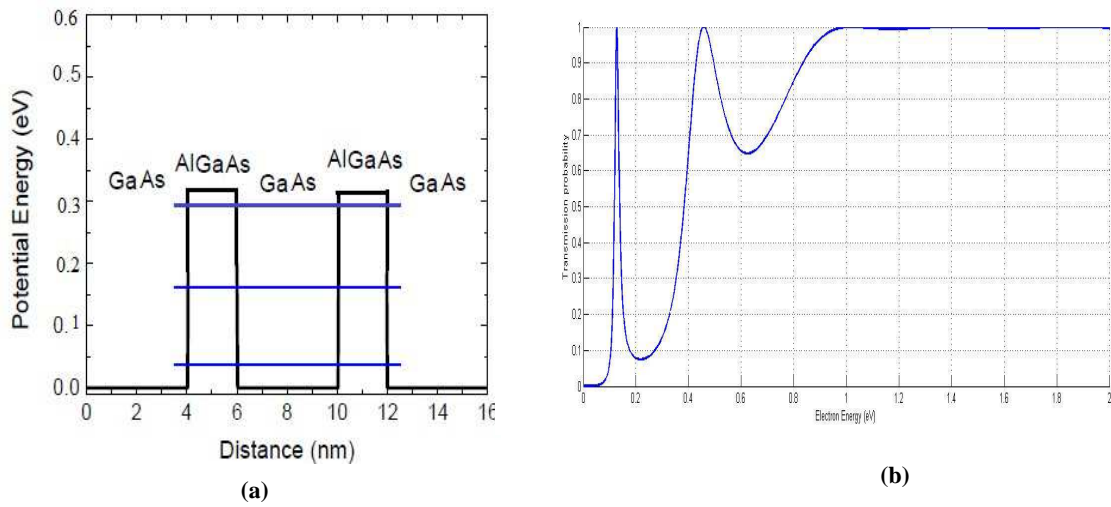
Figure 2.10Transmission probability for a GaAs/AlGaAs double barrier, separated by a quantum well. Showing resonance energy levels. In contrast to the single barrier case, the transmission probability shows a sharp resonance peak below the barrier height with unity transmission probability.

Thus, off resonance, the transmission probability for a double barrier structure is lower than that of a single barrier. However, at resonance, $\cos^2(kb+\theta) = 0$ and the transmission probability is unity. Thus, the condition for resonance is

$(kb+\theta) = (2n+1)(\pi/2)$ 2.36

In practical tunneling devices, application of voltage bias results in reduction of device symmetry and hence reduced transmission probability.

Figure 2.10 shows the transmission probability for a double barrier structure formed using an GaAs/AlGaAs heterostructure with barrier width of 2 nm, separated by a quantum well of 4 nm width and barrier height is 0.33 eV, showing the unity transmission probability. From Fig. 2.10 (b) it is apparent that the transmission probability exhibits a sharp resonance at the resonant energy level. This is often approximated by a Lorentzian shape. Thus, the transmission probability as a function of energy is given by [7]:

$$T(E) = \left[1 + \frac{E - E_{res}}{\frac{1}{2}\Gamma} \right]^{-1} \qquad \text{.. 2.37}$$

where, E_{res} is the resonance energy level and Γ is the full-width at half-maximum.

2.5. Resonant Tunnel Diode

A resonant tunnel diode (RTD) consists of an undoped quantum well between two undoped barrier layers formed by the conduction or valence band edge discontinuity between the two materials. The double barrier is sandwiched between heavily doped emitter and collector regions serving as contacts. Figure 2.11(a) shows the zero bias conduction band diagrams. The emitter and collector are 3D systems with electron density of states which are continuously distributed in energy while the 2D well consists of quantized energy states. As an appropiate bias is applied to the device, the electron energy in the emitter is raised with respect to the well and the collector. The applied bias is primarily dropped across the undoped double-barrier structure. When the electron energy in the emitter coincides with the quasi-bound state energy in the well ($E_F = E_n$), resonant tunneling starts through the double-barrier, resulting in a tunneling current [Fig. 2.11(b)]. Tunneling occurs for $E_C < En < E_{FL}$.
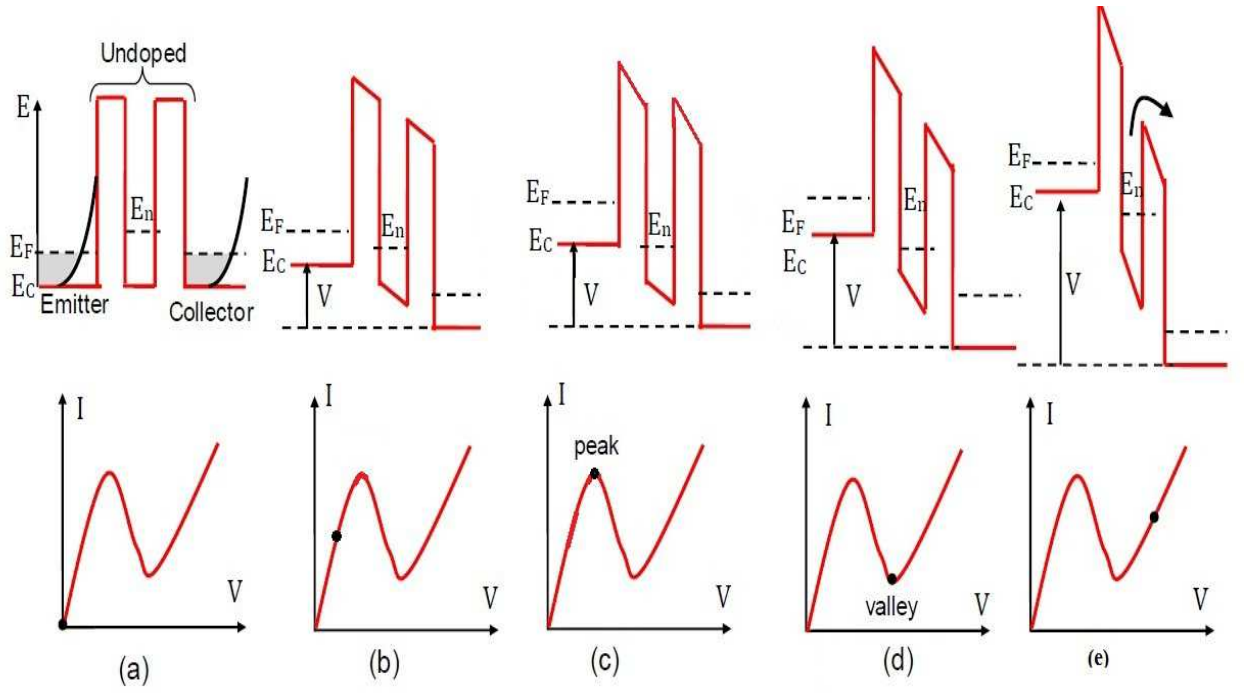
Figure 2.11 Band diagram and current voltage-characteristics of a RTD

In the above process energy and lateral momentum of electron are conserved. The electron energy in the emitter is given by: $E = E_C + \dfrac{\hbar^2 k_\perp^2}{2m^*} + \dfrac{\hbar^2 k_\parallel^2}{2m^*}$ where, $\perp$ and $\parallel$ denote perpendicular to and parallel to the direction of tunneling respectively and m^* is the electron effective mass. A parabolic, isotropic, conduction band minima is chosen. Energy of electrons in the quasi-bound state of size quantization no.'n' is denoted by:

$E = E_n + \dfrac{\hbar^2 k_\perp^2}{2m^*}$. Hence, from conservation of energy and lateral momentum

$k_\perp, E_C + \dfrac{\hbar^2 k_\parallel^2}{2m^*} = E_n$ is the condition for tunneling. This is known as *coherent tunneling* since the particle maintains phase coherence across the tunneling structure. Maximum tunneling occurs when E_{CL} aligns with E_n [Fig. 2.11(c)].

As the applied bias is increased further and the conduction band on the left side, E_{CL} crosses E_n, tunneling current stops to flow and a negative differential resistance (NDR) region appears. Ideally, the current should fall to zero. However a valley current is observed as a result of off-peak transmission due to phonon and impurity scattering, tunneling via impurity states in the potential barrier, interface roughness scattering. Scattering also results in broadened transmission resonance. Further increase in bias results in thermionic emission

of carriers over the tunneling barrier and an increase in current. The PVCR is most important figure of merit for tunneling devices. A high peak current is desirable for achieving high speed operation, while the valley current contributes to power dissipation and should be as low as possible. Hence, a high PVCR is a critical design goal for tunnel diodes.
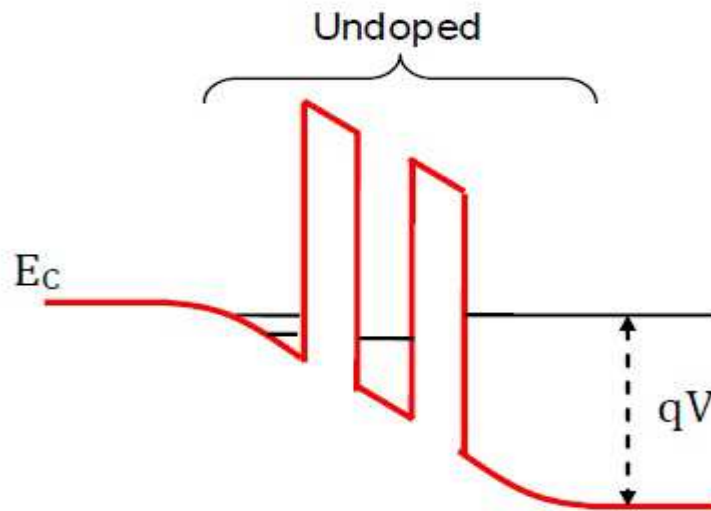
Figure 2.12 Use of undoped spacer regions adjacent to the tunneling barrier structure resulting in 2D-2D tunneling instead of 3D-2D, improving PVCR

PVCR can be further improved by adding an undoped spacer region on the emitter side. The applied bias now falls across this undoped region in addition to the double barrier structure forming a triangular quantum well as shown in Fig. 2.12. Tunneling now occurs between 2D-to-2D instead of 3D-2D states resulting in sharper resonance and larger PVCR. Introduction of spacer layers also increases the depletion width, reducing the capacitance which is beneficial for high frequency applications.

2.5.1 Coherent Tunneling Current

Current density is given by the total particle flux, $J=qnv$, where, 'q' is the electron charge, 'n' is the carrier density and 'v' is the velocity of carriers. For tunneling through a barrier, the number of carrier is proportional to the tunneling probability and the number of

available electrons which depends on the density of k-states and their Fermi occupation probability $f(E)$. Hence,

$$J = 2q \int_0^\infty \frac{d^3k}{(2\pi)^3} v_\parallel T(E_\parallel) f(E)$$

where, the factor '2' is due to spin degeneracy, $(2\pi)^3$ is the normalized volume occupied by a k-state, $T(E_\parallel)$ is the tunneling probability, $f(E)$ is the Fermi-Dirac distribution function, $v_{//}$ is the electron velocity in the tunneling direction. Now the net tunneling current is the difference between current flow from left of the barrier to right and from the right of the barrier to left.

$$J = \frac{2q}{(2\pi)^3} \int_0^\infty v_\parallel T_{L \to R}(E_\parallel) f_L d^3k - \frac{2q}{(2\pi)^3} \int_0^\infty v_\parallel T_{R \to L}(E_\parallel) f_R d^3k \dots\dots\dots\dots\dots\dots\dots\dots 2.36$$

From time reversal symmetry, $T_{L\to R} = T_{R\to L} = T$

Hence, $J = \frac{2q}{(2\pi)^3} \int_0^\infty v_\parallel T(E_\parallel)(f_L - f_R) d^3k$

$$J = \frac{2q}{(2\pi)^3} \int_0^\infty d^2k_\perp \int_0^\infty v_\parallel T(E_\parallel)(f_L - f_R) dk_\parallel \dots\dots\dots\dots\dots\dots\dots\dots\dots\dots\dots\dots 2.37$$

Velocity $v_\parallel = \frac{1}{\hbar}\frac{dE_\parallel}{dk_\parallel}$, substituting, $J = \frac{2q}{\hbar(2\pi)^3} \int_0^\infty d^2k_\perp \int_0^\infty T(E_\parallel)(f_L - f_R) dE_\parallel$

Number of k-states at energy E in the two-dimensional space transverse to the tunneling direction is given by $2\pi k dk_\perp$.

$$J = \frac{2q}{\hbar(2\pi)^3} \int_0^\infty 2\pi k dk_\perp \int_0^\infty T(E_\parallel)(f_L - f_R) dE_\parallel$$

Using $E_\perp = \frac{\hbar^2 k_\perp^2}{2m^*}$, or $k_\perp dk_\perp = \frac{m^*}{\hbar^2} dE_\perp$ where, m^* is the effective mass in the well. Hence,

$$J = \frac{qm^*}{2\pi^2\hbar^3} \int_0^\infty dE_\perp \int_0^\infty (f_L - f_R) T(E_\parallel) dE_\parallel$$

$$J = \frac{qm^*}{2\pi^2\hbar^3} \int_0^\infty \left(\frac{1}{1+\exp(E-E_{FL})/k_BT} - \frac{1}{1+\exp(E-E_{FR})/k_BT} \right) dE_\perp \int_0^\infty T(E_\parallel)dE_\parallel \dots\dots\dots 2.38$$

The total energy E can be split into the longitudinal and transverse components. Hence,

$$J = \frac{qm^*k_BT}{2\pi^2\hbar^3} \int_0^\infty \ln\left(\frac{1+\exp((E-E_{FL\parallel})/k_BT)}{1+\exp((E-E_{FR\parallel})/k_BT)} \right) T(E_\parallel)dE_\parallel \dots\dots\dots\dots\dots\dots\dots\dots 2.39$$

which is the same as the expression derived by Esaki and Tsu [8] and is the general expression for tunneling current.

2.5.2 Tunneling Current for a Resonant Tunnel Diode

Some simplifications can be made for a resonant tunnel diode. The contribution from the right can be ignored for a large bias, and the Fermi function can be approximated as a step function. Hence,

$$J = \frac{qm^*}{2\pi^2\hbar^3} \int_0^\infty \left(E_{FL} - E_\parallel \right) T(E_\parallel)dE_\parallel$$

From the Eq. 2.37 the Lorentzian approximation for the tunneling probability is substituted in the above equation to get

$$J = \frac{qm^*}{2\pi^2\hbar^3} \int_0^\infty \left(E_{FL} - E_\parallel \right) \left[1 + \frac{E_\parallel - E_n}{\frac{1}{2}\Gamma} \right]^{-1} dE_\parallel \dots\dots\dots\dots\dots\dots\dots\dots 2.40$$

where, $E_n = E_{n0} - (qV/2)$ and gives the location of the resonance peak with applied bias.

2.5.3 Valley current

The actual I-V characteristics of Double Barrier Resonant Tunneling Diode (DBRTD) at room temperatures do not show zero current beyond the peak current. This discrepancy from the I-V shown in Fig.2.13 is attributed to the valley current flow off-resonance. At finite temperature major contributors to valley current are -

1. Thermionic emission over the barriers

2. Tunneling through higher order subbands at finite temperatures

3. Inelastic scattering processes that provide alternative tunneling channels
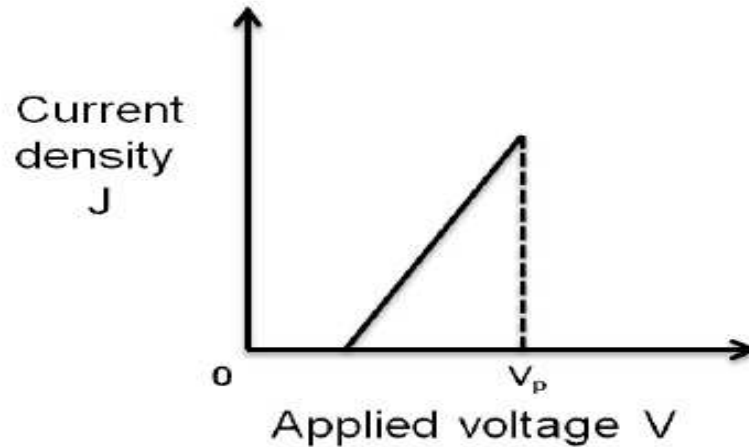
Figure 2.13 Expected I-V characteristics at 0K

The valley current can be suppressed mainly by lowering the operating temperature of the device. But a low temperature of operation makes the device cumbersome and reduces its usefulness. Apart from lowering the operating temperature, using the right combination of material systems and dimensions for the well and barrier layers, some fraction of the valley current can be minimized. These alternate approaches are discussed in next subsection.

2.5.4 Minimizing thermionic emission current

It can be minimized by using tall barriers, such as by using *AlAs* instead of *AlGaAs*. However, increasing the barrier heights will result in sharp resonances with a reduced transmission probability at off-resonance and scattering can then broaden the transmission causing a drop in the current. The barriers will then have to be made thin in order to improve the current density.

2.5.5 Minimizing current due to higher resonances

The component of current due to tunneling through higher order resonance levels can be reduced by shifting these resonances upward in energy and away from the first

resonance. This can be done by using a low effective mass material for the well or by using narrow wells as evident from the following expressions of subband energy and inter subband separation in an infinite QW.

$$E_n = \frac{n^2 \pi^2 \hbar^2}{2m^* a^2}$$ 2.41

$$E_{n+1} - E_n = \frac{\hbar^2 \pi^2}{2m^* a^2}(2n+1)$$ 2.42

where 'm^*' is the effective mass of electrons in well material, 'a' is the well width and 'n' is the size quantization no. and characterizing the subband and n= 1,2,3...........

However, for finite QW, the qualitative features remain same as those in an infinite QW.

2.5.6 Effect of scattering

The various scattering mechanisms that can contribute to valley current are optical and acoustic phonon scattering, inter-valley scattering, scattering due to impurity atoms, interface roughness and alloy disorder in the case of $Al_xGa_{1-x}As$ barriers. Polar optical phonon scattering is the dominant phonon scattering mechanism in polar semiconductors such as GaAs. When the resonance level E_0 drops below the emitter conduction band edge, tunneling can still occur if the electron loses energy corresponding to the difference $E_C - E_0$ by emitting a phonon.

In the presence of phase-breaking scattering, resonant tunneling can be described as two continuous tunneling processes - tunneling from emitter into the quantum well followed by tunneling from the well to the collector. Between these two processes, electrons suffer phase-breaking scattering in the quantum well and are relaxed into local quasi-equilibrium states [9]. This is the sequential tunneling model and is an alternative to the global coherent tunneling model when scattering is present [10], [11], [12].

Due to the open nature of the system, the resonances in the well exhibit an intrinsic broadening Γ. The transmission probability for energies close to resonances can be approximated using the following Lorentzian form

$$T(E_z) = \frac{\Gamma^2}{(E_z - E_0)^2 + \Gamma^2} \quad \text{..} \quad 2.43$$

The dwell time (t_d) of the electrons in the quantized states is related to the intrinsic broadening as

$$t_d = \hbar / \Gamma \text{..} \quad 2.44$$

The effect of scattering is to broaden the resonance levels in the well further and thus the transmission.

$$T(E_z) = \frac{\Gamma}{\Gamma_{tot}} \frac{\Gamma_{tot}^2}{(E_z - E_0)^2 + \Gamma_{tot}^2} \quad \text{..} \quad 2.45$$

where $\Gamma_{tot} = \Gamma + \Gamma$s, is the sum of broadenings due to intrinsic and extrinsic scattering. As in Eq.(2.43) a phase coherence breaking time t_s corresponding to Γ_s can be defined as

$$t_s = \hbar / \Gamma_s \text{...} \quad 2.46$$

The ratio Γ_s / Γ acts as boundary between global coherent tunneling and sequential tunneling. When $\Gamma_s / \Gamma > 1$, the transmission peak decreases and becomes broader. If steps are not taken to enhance the peak current through the DBRTD, then scattering can degrade the PVCR, by increasing the valley current.

Two important measures to be taken to minimize phase-breaking scattering are

    i.   The usage of high quality interfaces to minimize roughness and alloy disorder scattering, and

    ii.   Undoped layers for barriers and well to minimize impurity scattering.

However to enhance the current density peak, heavily doped contacts are regularly used. This introduces unwanted diffusion of impurities into the barrier and well layers and hence impurity as well as electron-electron scattering is always present in RTDs that are operated at nominal temperatures. An interesting technique to minimize valley current is then through using *Resonant Intraband Tunneling Diode* (RITD)s [13] .

2.6. History of Resonant Tunneling Devices

The first interest of quantum well devices was grown when Esaki and Tsu [14] suggested in 1969 that a heterostructure consisting of alternating ultrathin layers of two semiconductors with different band gaps should exhibit some novel useful properties. The band-edge potential varies from layer to layer as a result of the difference in the band gaps and a periodically varying potential is produced in the structure with a period equal to the sum of the widths of two consecutive layers.

In their pioneer work on tunnelling through superlattice in 1973[8], they computed the transport properties of a finite superlattice from the tunneling point of view. The computed 1-*V* characteristic describes the experimental cases of a limited number of spatial periods or a relatively short electron mean free path. For layer thicknesses of the order of electronic wave length, the wavelength as well as the mean free path of the electrons extends over several layers and the periodic potential transforms the energy bands of the host lattice into mini-bands. Phenomena like Bloch oscillation and low-field negative differential resistance may be produced by the electrons in such mini-bands.

In 1974 Esaki, Chang and Tsu observed the resonant tunnelling in semiconductor double barrier [1].In their work resonant tunneling of electrons has been observed in double-barrier structures having a thin GaAs sandwiched between two GaAlAs barriers. The resonance manifests itself as peaks or humps in the tunneling current at voltages near the quasi-stationary states of the potential well. The structures have been fabricated by molecular beam epitaxy which produces extremely smooth films and interfaces.

Attempts to fabricate the proposed structure and to demonstrate the predicted Phenomena were only partially successful. Interest was renewed in these devices with the advancement in epitaxial growth techniques, like MBE, and the work of Sollner et al. in1983-84 [15]. In their work resonant tunneling through a single quantum well of GaAs had been observed. The current singularity and negative resistance region are dramatically improved over previous results, and detecting and mixing had been carried out at frequencies as high as 2.5 THz. Resonant tunnelling features were visible in the conductance-voltage curve at room temperature and become quite pronounced in the *J-V* curves at low temperature. The high-frequency results proved that the charge transport is faster than about 10 - 13s. As a result it is now possible to construct practical nonlinear devices using quantum wells at millimetre and sub-millimetre wavelengths.

Resonant tunnel diodes (RTDs) are most commonly implemented using the III-V material system due to the large selection of binary, tertiary, and ternary compounds which can be combined to form a variety of heterostructures with varying conduction band offsets. Early RTDs were developed in the AlGaAs/GaAs material system [1], [16]. [17]. High peak current densities (Jp) were obtained with the use of AlGaAs as barrier, however the PVCR was reduced due to thermionic emission over the barrier and thermal-assisted tunneling through higher subbands. Use of AlAs as barrier could reduce this but also deteriorated the peak current. High PVCRs of 3.9 were obtained using undoped spacer regions [17]. A switch to InGaAs/InAlAs material system significantly improved [18--20]. Only GaInAs replaces GaAs and AlInAs replaces GaAlAs. The peak current density is reported to be 5.5×10^4 A/cm^2 and the PVCR ratio is 21.6 at 77 K and 6 at 300 K. Even a PVCR ratio of 14 has been reported [21-22] at 300 K by using the GaInAs/AlAs system.

PVCRs and Jp with improved barrier height and increased subband separation [23], [24]. Use of In0.53Ga0.47As/AlAs system led to PVCRs of 24 and Jp of 15 kA/cm^2 [25]. Inata *et al* obtained dramatically improved characteristics, with peak-to-valley current ratios as high as 14 at 300 K [26]. Reducing the barrier thickness from 2.4 nm to 1 nm resulted in the Jp boosted to 450 kA/cm^2[27]. Based upon the results of these experiments, it was determined that a 1 monolayer increase in AlAs barrier width, InGaAs quantum-well width, or InAs subwell width results in a peak current reduction of 56%±7%, 19%±2%, and 18%±3%, respectively. Further, a 1% decrease Inindium mole fraction of the InGaAs quantum well has been found to increase the peak current by l0%±1%. Sensitivity parameters have been tabulated for both the peak current and the peak voltage of the RTD. Through the use of these parameters, the maximum allowed fluctuation in the RTDs structural parameters has been estimated for a given tolerance in the RTDs electrical characteristics. Further, these data can also be used to evaluate the feasibility of in situ epitaxial growth control of resonant tunneling devices [28]. Addition of strained InAs, sandwiched between In0.53Ga0.74As in the quantum well, greatly increased the PVCR to as high as 50 with Jp of 5.8 kA/cm2 [29]. Higher current densities were obtained for the InAs/AlSb system, which also benefitted from the lower contact resistance of InAs, with Jp of 490 kA/cm2 and PVCR of 2.2 [30].

Si-based RTDs did not meet with a lot of success due to the lack of lattice-matched heterostructure materials. The Si/SiGe system, with strained SiGe grown on Si substrates, allowed formation of heterostructures but were limited due to the very small conduction

band offset. Almost all the bandgap difference is accommodated in the valence band resulting in a hole RTD. RTDs grown using both molecular beam epitaxy and chemical vapor deposition exhibited negative differential characteristics only when cooled down to 77K and no room temperature results were obtained [31], [32], [33]. Conduction band offset of ~ 150 meV can be obtained by growing a strained Si/relaxed Si1-xGex structure on a relaxed Si1-yGey substrate [34]. Room temperature PVCRs up to 1.2 were obtained [35], [36].

In 1984, Capasso and Kiehl proposed the concept of a resonant-tunneling bipolar transistor (RTBT) [37]. Independently, Riccb and Solomon [38] discussed a similar device. Resonant Tunneling transistors allow the implementation of a large class of circuits (e.g., analog-to-digital converters, parity checkers, frequency multipliers, etc.) with greatly reduced complexity (i.e., less transistor per function compared to a circuit using conventional transistors). The inherent functionality of these and other quantum electron devices has led a group at Texas Instruments to project an intriguing scenario for the future of electronics.

Depending on the basic inventions on RTD and RTBT, a lot of experiments were carried on for different aspects. Experiments followed by either RTD or RTBT were carried on simultaneously.

Combinations of different resonant tunneling devices with other semiconductor devices create a new emerging field of nanotechnology. RTD-FET based digital circuits, RTD incorporated with HBT are common field of application of such combine devices

CHAPTER: 3

SOFTWARE USED FOR SIMULATION OF RTD

Contents

CHAPTER: 3

SOFTWARE USED FOR SIMULATION OF RTD

In this chapter a brief over view of the software used for simulation of the RTD structure is presented. This structure is implemented and simulated using SILVACO-TCAD software. Among many sub parts of the mentioned software, "ATLAS" is used to obtain the result of simulation in this thesis work.

3.1. SILVACO TCAD-ATLAS: An Introduction

TCAD-ATLAS Device simulates the electrical behaviour of a single semiconductor device using numerical integration and associated device physics either in isolation or several devices combined in a circuit. Terminal currents, voltages, surface potential, electric field and charges are computed based on a set of physical device equations that describes the carrier distribution and conduction mechanisms. A real semiconductor device, such as a transistor, is represented in the simulator as a "virtual" device whose physical properties are discretized onto a non- uniform "grid" (or "mesh") of nodes.

Therefore, a virtual device is an approximation of a real device. Continuous properties such as doping profiles are represented on a sparse mesh and, therefore, are only defined at a finite number of discrete points in space. The doping at any point between nodes (or any physical quantity calculated by TCAD-ATLAS Device) can be obtained by interpolation. Each virtual device structure is described in the Synopsys TCAD tool suite by a STR file containing the following information:

- The "mesh" (or geometry) of the device contains a description of the various regions, that is, boundaries, material types, and the locations of any electrical contacts. It also contains the locations of all the discrete nodes and their connectivity.
- The data fields contain the properties of the device, such as the doping profiles, in the form of data associated with the discrete nodes. By default, a device simulated in 2D is assumed to have a "thickness" in the third dimension of 1 μm.

3.2. Silvaco CAD Environment:

Silvaco TCAD software is divided in many sub software. Among them some important parts are ATLAS, Deckbuild, Tonyplot, Tonyplot3D, DEVEDIT and ATHENA.

ATLAS is a physically-based device simulator. It provides general capabilities for two (2D) and three-dimensional (3D) simulation of semiconductor devices. It specifies the device simulation problems by defining: the physical structure to be simulated, the physical models to be used, and the bias conditions for which electrical characteristics are to be simulated. ATLAS can be used in conjunction with the V.W.F. (Virtual Wafer Framework) Interactive Tools. These include Deckbuild, Tonyplot, DEVEDIT (Device Edit), MaskViews, and Optimizer. Deckbuild provides an interactive run time environment. Tonyplot supplies scientific visualization capabilities. DEVEDIT is an interactive tool for structure and mesh specification. MaskView is an IC Layout Editor. The Optimizer supports black box optimization across multiple simulators. ATLAS is often used in conjunction with the Athena process simulator which predicts the physical structures that result from processing steps. The resulting physical structures are used as input by ATLAS, which then predicts the electrical characteristics associated with specified bias conditions. The combination of ATHENA and ATLAS makes it possible to determine the impact of process parameters on device characteristics. The electrical characteristics predicted by ATLAS can be used as input by the UTMOST device characterization and SPICE modelling software. Compact models based on simulated device characteristics can then be supplied to circuit designers for groundwork circuit design. Combining ATHENA, ATLAS, UTMOST, and SmartSpice makes it possible to predict the impact of process parameters on circuit characteristics. ATLAS can be used as one of the simulators within the V.W.F. Automation tools. V.W.F. makes it convenient to perform highly automated simulation-based experimentation. It therefore links simulation very closely to technology development, resulting in significantly increased benefits from simulation use.

3.2.1 Tool Flow:

Figure 3.1 shows the types of information that flow in and out of ATLAS. Most ATLAS simulations use two input files. The first input file is a text file that contains commands for ATLAS to execute. The second input file is a structure file that defines the structure that will be simulated.

ATLAS produces three types of output files. The first type of output file is the run-time output, which gives us the progress and the error and warning messages as the simulation proceeds. The second type of output file is the log file, which stores all terminal voltages and currents from the device analysis. The third type of output file is the solution file, which stores 2D and 3D data relating to the values of solution variables within the device at a given bias point. These log and structure files can be viewed by TonyPlot and TonyPlot3d and from there the data can be extracted for further calculations.
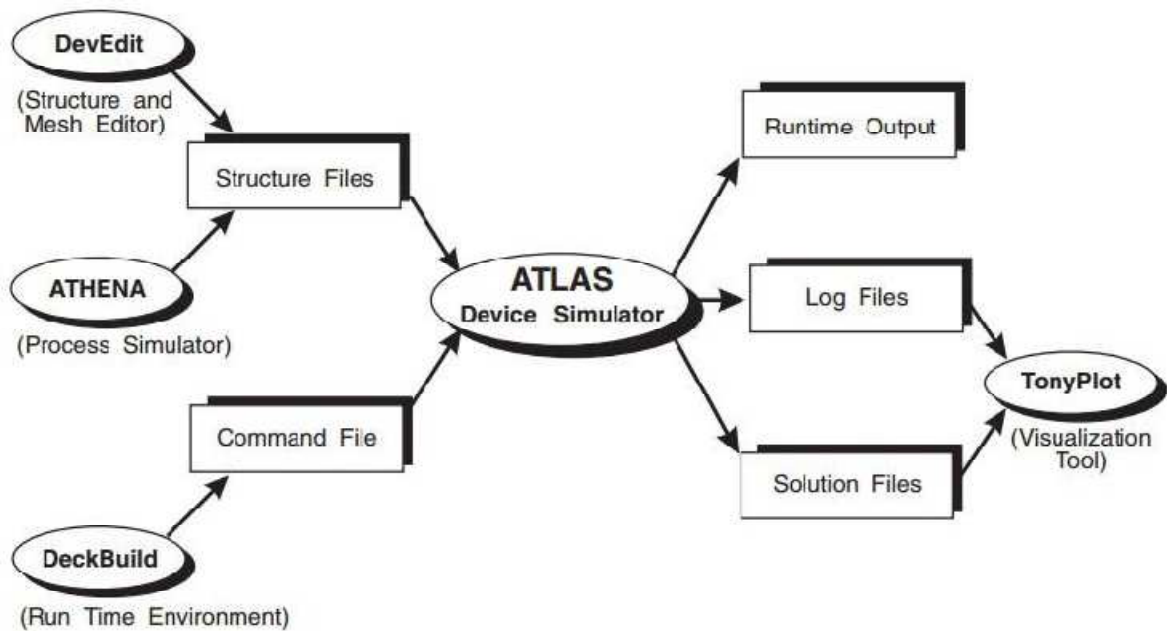
Figure 3.1Typical tool flow with device simulation using Silvaco TCAD Device.

3.3. ATLAS

As discussed in the aforesaid section, ATLAS of the Silvaco EDA Tools software is the part which simulates the device with device physics. For simulating the device, direct command input to the ATLAS can be given or DECKBUILD can be used to get a GUI based interpreter. Now, for any volume or region based structure, there should be some minimal structural unit or part and adding up these minimal units, the MESH forms. There are simple commands to create two dimensional, rectangular three dimensional and cylindrical three dimensional mesh structures with a parameter of the minimal unit as desired. Then the mesh is divided in some regions with which region contain what material like silicon, silicon oxide, gate material etc. Contacts and doping profiles are defined in the desired mesh regions. The construction of the desired MOSFET is now complete and we have to simulate

the device. First, the simulation environment should be defined. That is what device physics should be used (as suitable for the device to be analyzed) and what calculation/solving methods (NEWTON, GUMMEL etc. solving methods) to be used with what precision are stated. Then the required calculated parameters (like electric field, potential, mobility, current by carriers, drift and diffusion currents etc.) are mentioned as required in current analysis. After declaring the simulation environment, simulation output storage LOG and STRUCTURE files are given followed by the electrical inputs with initial values. Then the simulation occurs and stores the results in the files specified. These files are then viewed by various softwares including TONYPLOT. We can further extract other parameter from the files/data.

3.4. Typical flow of SILVACO TCAD Device Simulator

The command used to simulate the device is presented. Each statement section is explained individually.

3.4.1 Mesh information part:

```
go atlas

mesh three.d cylindrical

r.mesh location=0.0 spacing=0.001
r.mesh location=0.005 spacing=0.001
r.mesh location=0.008 spacing=0.001
r.mesh location=0.011 spacing=0.001
r.mesh location=0.014 spacing=0.001
r.mesh location=0.015 spacing=0.001

a.mesh location=0 spacing=60
a.mesh location=360 spacing=60

z.mesh location=-0.050 spacing=0.001
z.mesh location=-0.048 spacing=0.001
z.mesh location=-0.030 spacing=0.001
z.mesh location=-0.015 spacing=0.001
```

```
z.mesh location=0.015 spacing=0.001
z.mesh location=0.030 spacing=0.001
z.mesh location=0.048 spacing=0.001
z.mesh location=0.050 spacing=0.001


region num=1 material=silicon z.min=-0.030 z.max=0.030 r.min=0.000
r.max=0.010
region num=2 material=hfo2 r.min=0.010 r.max=0.014 z.min=-0.030
z.max=0.030
region num=3 material=si3n4 r.min=0.010 r.max=0.015 z.min=-0.050
z.max=-0.030
region num=4 material=si3n r.min=0.010 r.max=0.015 z.min=0.030
z.max=0.050


electrode name=gate z.min=-0.030 z.max=-0.010 r.min=0.014
r.max=0.015
electrode name=gate1 z.min=-0.010 z.max=0.010 r.min=0.014
r.max=0.015
electrode name=gate2 z.min=0.010 z.max=0.030 r.min=0.014
r.max=0.015
electrode name=source z.min=-0.050 z.max=-0.030 r.min=0.000
r.max=0.010
electrode name=drain z.min=0.030 z.max=0.050 r.min=0.000
r.max=0.010


doping uniform region=1 conc=1e16 p.type

#contact name=gate wsi2
#contact name=gate1 chromium common=gate
#contact name=gate2 ti common=gate1
#contact name=source sb
#contact name=drain sb


save outf=tmgsbsd.str
tonyplot3d tmgsbsd.str


quit
```

3.4.2 Simulation Part:

```
go atlas


mesh inf=tsrgsbsd.str


contact name=gate workfunction=4.8
contact name=gate1 workfunction=4.6 common=gate
contact name=gate2 workfunction=4.4 common=gate1
contact name=source workfunction=4.68
contact name=drain workfunction=4.68


models cvt srh auger


solve init
solve vgate=0.01
solve vgate=0.02
solve vgate=0.05
solve vgate=0.1
solve vgate=0.2
solve vdrain=0.01
solve vdrain=0.02
solve vdrain=0.05
solve vdrain=0.1
solve vdrain=0.2


save outf=tmsrgsbsd1.str
tonyplot tmsrgsbsd1.str


quit
```

3.4.3 File Section:

Each ATLAS run inside DECKBUILD should start with the line:

go atlas

A single input file may contain several ATLAS runs each separated with a go atlas line. Input files within DECKBUILD may also contain runs from other programs such as ATHENA or DEVEDIT along with the ATLAS runs.

This essential input file (default extension .tdr) defines the mesh and various regions of the device structure, including contacts.

In our program output file (default extension .str) is saved as "`tmgsbsd.str`".

Dimensionality of the problem from this file. It also contains the doping profiles data for the device structure.

"`doping uniform region=1 conc=1e16 p.type`".

3.4.4 Electrode Section:

The Electrode section defines all the electrodes to be used in the Silvaco TCAD-ALTAS Device simulation, with their respective boundary conditions and initial biases. Any contacts that are not defined as electrodes are ignored by Silvaco TCAD-ALTAS Device.

"`electrode name=gate`", "`electrode name=gate1`", "`electrode name=gate2`", "`electrode name=source`", "`electrode name=drain`".

Each electrode is specified by a case-sensitive name that must match exactly an existing contact name in the structure file. Only those contacts that are named in the Electrode section are included in the simulation.

"`solve vgate=0.01`"

This defines a applied gate voltage boundary condition with an initial value.

"`solve vgate=0.2`"

This defines a applied gate voltage boundary condition with an final value. One or more boundary conditions must be defined for each electrode, and any value given to a boundary condition applies in the initial solution. In this example, the simulation commences with a bias on the drain.

`solve vdrain=0.01`

```
solve vdrain=0.02
solve vdrain=0.05
solve vdrain=0.1
solve vdrain=0.2
```

where initial value is defined by "`solve vdrain=0.01`" and final value is defined by "`solve vdrain=0.2`".

The metals work function used as three different gate region are defined as

```
contact name=gate workfunction=4.8
contact name=gate1 workfunction=4.6 common=gate
contact name=gate2 workfunction=4.4 common=gate1
contact name=source workfunction=4.68
contact name=drain workfunction=4.68
```

3.4.5 Physics Section:

The Physics section allows a selection of the physical models to be applied in the device simulation. In this example, it is sufficient to include basic mobility models and a definition of the band gap (and, therefore, the intrinsic carrier concentration). Potentially important effects, such as impact ionization (avalanche breakdown at the drain), are ignored at this stage.

"`models cvt srh auger`".

Mobility models including doping dependence and different types of recombination processes are specified for this simulation.

3.4.6 Plot Section:

In our program finally plot section is defined as "tonyplot tmsrgsbsd.str".
The Plot section specifies all of the solution variables that are saved in the output plot files (.str). Only data that Silvaco TCAD-ATLAS Device is able to compute, based on the selected physics models, is saved to a plot file.
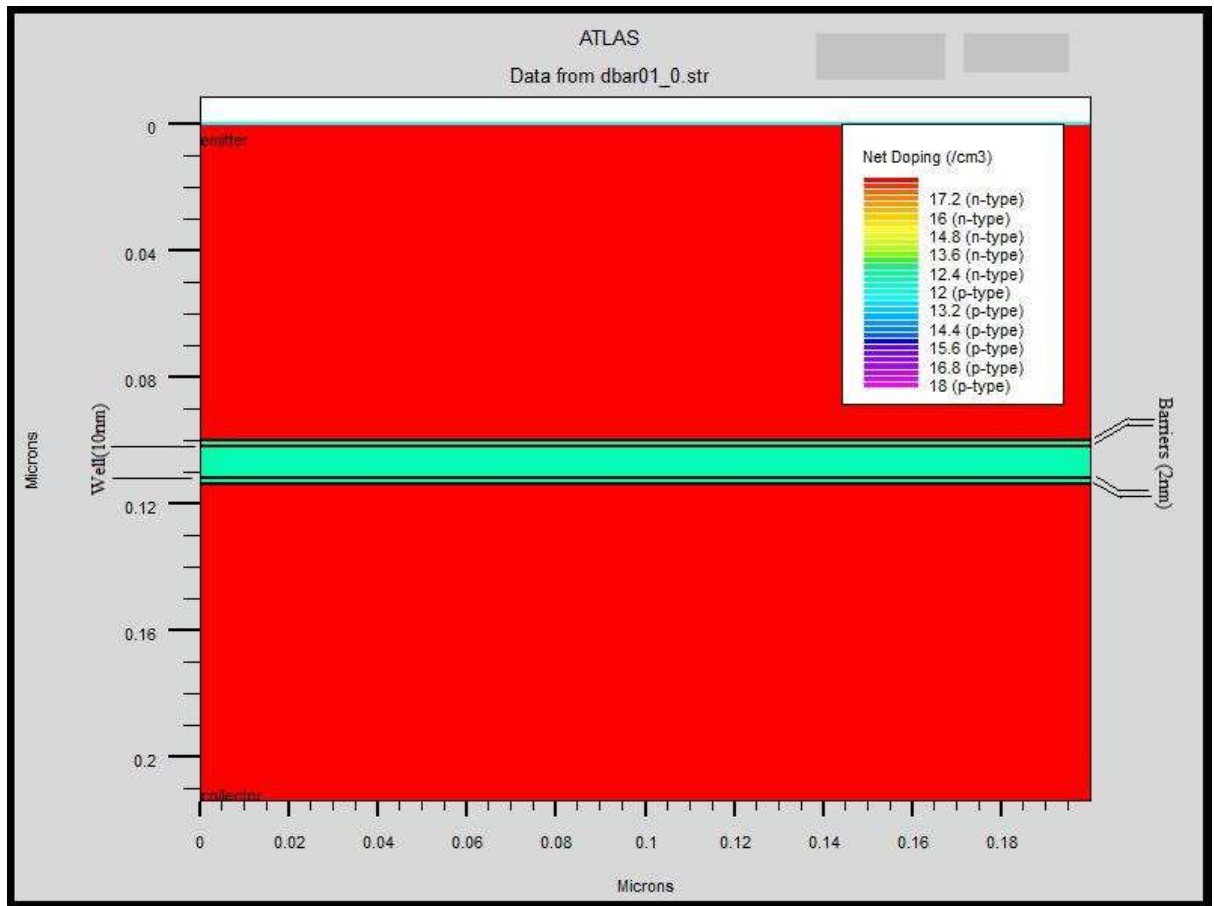
Figure 3.2 The simulated 2D structure in Silvaco TCAD-ATLAS

The program of the proposed structure is given in appendix - A.

CHAPTER: 4

MODELLING & SIMULATION OF RTD: SYMMETRIC STRUCTURE

Contents

CHAPTER: 4

MODELLING & SIMULATION OF RTD: SYMMETRIC STRUCTURE

The present chapter deals with the modelling and simulation of RTD of symmetric structure using SILVACO software are discussed. The device parameter calculations and simulation results are presented in different sections.

First part of this chapter includes modelling and simulation of a symmetric DBRT and its resulting I-V curve. The rest of the chapter presents simulation of basic structure with some deviation from the standard one and their influences on I-V characteristics of the performance.

4.1. Choice of Material for Resonant Tunneling Diode

The 1st structure of RTD demonstrated by Esaki and Tsu was on GaAs-AlGaAs based system. Since then GaAS-AlGaAs material system is used as popular material system.

The material chosen is an *n-type* GaAs as a host semiconductor on which potential barriers with the height of a fraction of 0.3eV were formed by introducing epitaxial layers of $Al_{0.3}Ga_{0.7}As$. Because of the similar properties of the chemical bond of Ga and Al, together with their almost equal ion size, the introduction of *'Al'* makes the least disturbance to the continuity and thus the quality of the epitaxial films.

Experiments were done on the proposed heterostructures in 1974 with gallium arsenide (GaAs) and aluminum gallium arsenide ($Al_xGa_{1-x}As$), the mismatch in the lattice constant of GaAs and AlAs being negligible; it is easy to grow layers of GaAs and mixed compounds of GaAs and AlAs on each other with crystalline perfection. Experiments were done with structures consisting of GaAs layers sandwiched between $Al_xGa_{1-x}As$ layers, which form potential-barriers as the band gap of $Al_xGa_{1-x}As$ is larger than that of GaAs [39]. The

component of the electron wave vector is quantized in such structures in the direction of potential variation [25].

For the above mentioned advantages, the GaAs-AlGaAs system is mainly selected for standard structure of simulation.

4.2. Mathematical Calculation Required for Simulation

4.2.1 Calculation of basic device parameters:

A. *Device Materials:*

For the standard RTD structure, studied is a GaAs/AlGaAs based heterostructures where both barrier and well materials are kept undoped. The following parameters are used to study the normal behaviour of the structure.

- The well material: GaAs, with Eg^{Γ} =1.424eV at 300K
- The barrier material: The two barrier regions are formed with alloy of GaAs and AlAs (Eg^{Γ} = 3.018 eV). The material is undoped $Al_xGa_{1-x}As$ with x= **'0.3'**.
- Emitter and collector region: These regions formed by heavily doped n-type GaAs material with doping concentration (1×10^{18}) /cm^3

B. *Barrier Height Calculation:*

According to **Anderson's rule** the vacuum levels of the two materials of a heterojunction should be lined up, as in Figure 4.1. This shows immediately that $\Delta E_C \approx E_C^B$ - $E_C^A = \chi A$ - χB where 'χ' denotes the electron affinity of the materials.

For example, GaAs has χ = 4.07 eV and $Al_{0.3}Ga_{0.7}As$ has χ = 3.74 eV, predicting ΔEc = 0.33eV. The band gap changes by ΔEg = 0.3eV, so ΔE v = 0.04eV. The fraction of the band gap that has gone into the conduction band $Q = \Delta E_C / \Delta E_g$ = 0.85 according to this model [26].
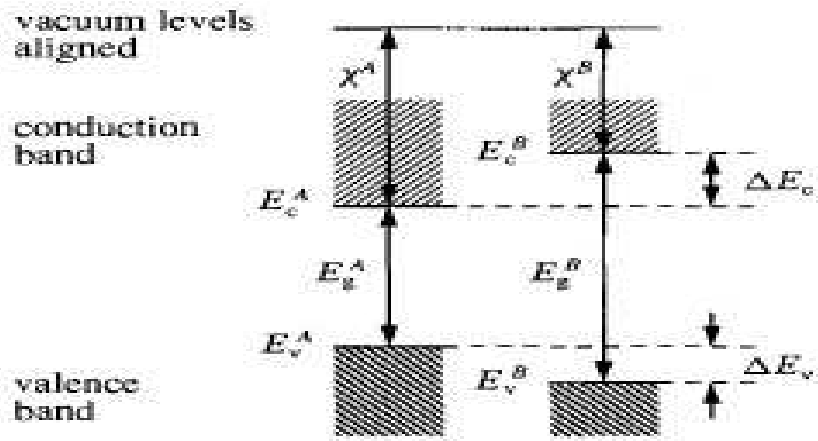
Figure 4.1 Anderson's rule for the alignment of the bands at a heterojunction between materials *A* and *B*, based on aligning the vacuum levels [6]

The barrier height depends on the value of alloy composition *'x'* in $Al_xGa_{1-x}As$ as well as the value of the 'Q' $(=\Delta E_c/\Delta E_g)$. Various calculated parameters are given bellow:

E_g ($Al_{0.3}$ $Ga_{0.7}$ As) = {(0.7x1.424) + (0.3x3.018)}

$\qquad$ = 1.9022eV

E_g ($Al_{0.3}$ $Ga_{0.7}$ As) - E_g (GaAs) = ΔEg = (1.9022-1.424) = 0.478eV

The Q is set to 0.65 for this thesis work the most accepted value for the heterostructure, ΔEc = (0.65 x 0.478) eV = 0.31083eV.

Therefore, Barrier height is taken as **'0.3eV'** in the RTD structure considered here.

C. *Lattice Constant Calculation:*

Lattice constant matching is very important factor to maintain crystalline perfection in the resultant heterostructure. The detail calculation of lattice constant for the materials used in this thesis i.e GaAs and $Al_{0.3}Ga_{0.7}As$ is given bellow:

- Lattice constant of (GaAs) = 5.6533 Å
- Lattice constant of (AlAs) = 5.6611 Å
- Lattice constant of $Al_{0.3}Ga_{0.7}As$ = (0.3 x 5.6611) + (0.7 x 5.6533)

$\qquad$ = 5.65564 Å

Therefore mismatch in lattice constant of the barrier material $Al_{0.3}Ga_{0.7}As$ and host material GaAs = (5.65564 – 5.6533) Å = 0.00234 Å = **0.041%** only.

This enables epitaxial growth of $Al_{0.3}Ga_{0.7}As$ and GaAs layers, one alone other without any restriction, and thus makes practical realization of such RTD structure feasible.

Estimation of all the above parameters enables us to simulate the standard RTD presented in the next section.

4.3. RTD: Conventional Structure

Considering the conventional structure as reference, variation of characteristics for other structures is studied. The details for simulation of this conventional structure are given in the following subsections.

4.3.1. Device Specification of Conventional RTD Structure:

The device considered for theoretical calculation, consist of only basic structure that means only two barriers in between those a well. However for Silvaco simulation the total structure consists of one emitter region, one collector and the main structure (well, sandwiched between two barriers). However the specifications are all same for common structure in both cases. The followings describe the device structure:

- Well width: 10nm (100Å)
- Barrier Width: 2nm (20Å)
- Emitter Width:100nm (1000Å)
- Collector Width: 100nm (1000Å)
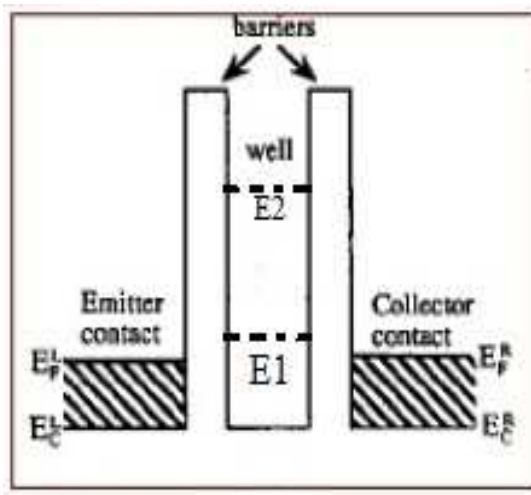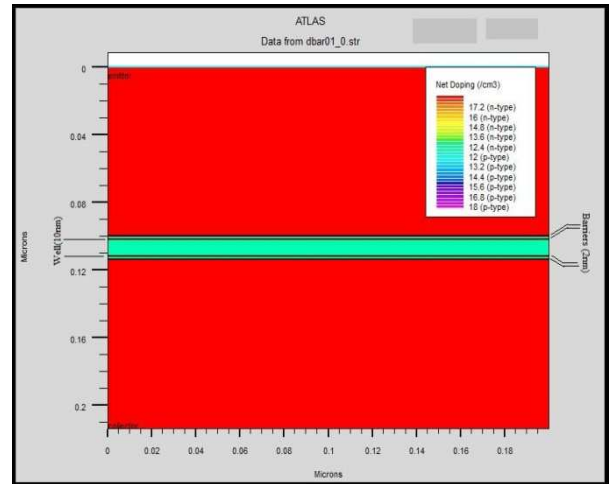
Figure 4.2 (a) Basic Structure of Double barrier Resonant Tunnel Diode, (b) Complete Structure in SILVACO Simulation

4.3.2 Calculation of bound Energy states of the well:

As discussed in Chapter 2, the bound states of a well depend upon the well width, effective mass of the well material and barrier height. So, it is necessary to determine the bound states in the quantum well sandwiched between two barriers well before analysing the characteristics of an RTD.

In section 2.3, the details for calculation of bound states of electron in a finite QW were derived. Using MATLAB simulation, the transcendental equation of that section was solved and it is shown in Figure 4.3, and the bound states for structure used in the thesis were obtained as follows.

Here a GaAs well and Al_xGa_{1-x} As barrier structure which has $m = m_0 m_e$, where $m_e = 0.067$, with depth $V_0 = 0.3$ eV and width $a = 10$ nm. The bound states of the well are calculated as:

1st bound state of energy E_1:0.0316 eV

2nd bound state of energy E_2:0.1266 eV, and

3rd bound state of energy E_3: 0.26 eV

From the above calculated value of bound states, it is clear that only three bound states can be supported in structure considered here. From the values of energy states, it is found that the differences of the energy levels are not even. The upper bound states are at larger value than lower one. The last one is comparable with barrier height. So, it has less effect in I-V characteristics.
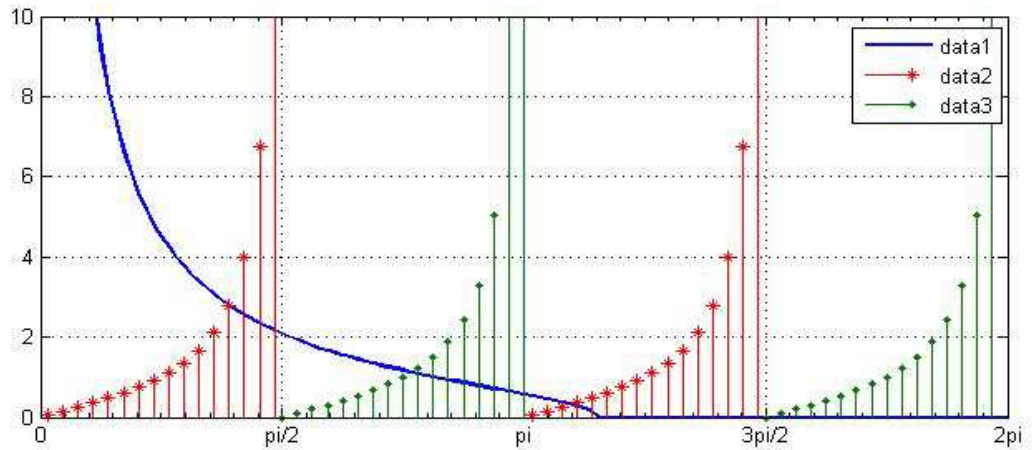
Figure 4.3 Graphical solutions in MATLAB to find bound states of a finite QW

4.3.3 Current Density as a function of Applied Voltage:

(a)   (b)
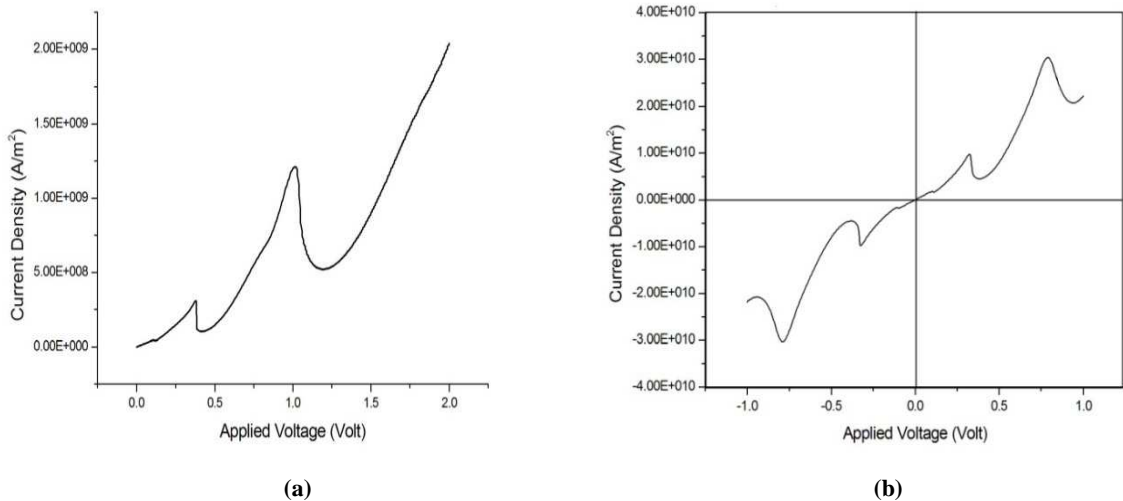
Figure 4.4 Plot of Current Density as a Function of Applied Voltage. (a) Application of forward bias only, (b) Application of both positive and negative bias, this indicates the symmetry in nature.

As discussed in Chapter 2, the Current density Vs applied voltage curve shows peak currents followed by valley currents indicating multiple NDR regions in RTD characteristic graph. Two distinct NDR regions are shown in figure 4.4. This is because of the main two bound states in the well are distinguished and higher states are very close to or above barrier height. From the calculation of bound states within the well, it found that there are three bound states, but the 3rd one is comparable with barrier height. So, the NDR due to that bound state is not so prominent in the graph. The energy bound states are shown in figure 4.5. From Figure 4.4.(b), it is clear that I-V characteristics is symmetric on both positive and negative biases. This is because of symmetric structure of the device.
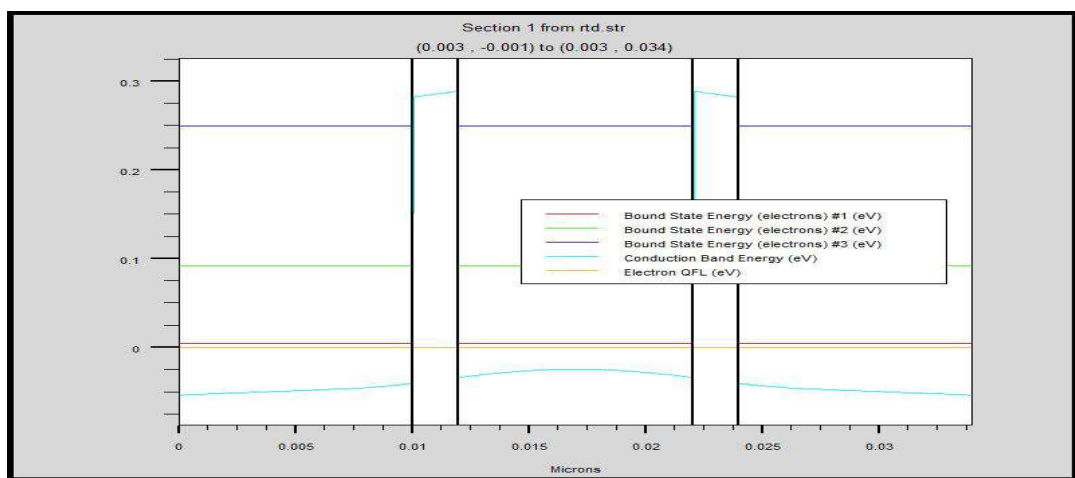
Figure 4.5 Electron bound states of well of standard RTD structure

Table 4.1 Comparison of calculated and simulated data of Bound Energy levels of Well of standard RTD

Energy bound states	Theoretical Value (eV)	From simulated Structure (eV)
E_1	0.0316	0.058
E_2	0.1266	0.1455
E_3	0.26	0.3037

4.3.4 Analysis of the Simulated Result

The following table shows the different data from simulated result.

Table 4.2 Simulated Data for Symmetrical 2nm-10nm-2nm RTD at 300K

Characteristics	*Peak*		*Valley*		*PVCR*
	J_p (A/m^2)	V_p (V)	J_v (A/m^2)	V_v (V)	
1st NDR	9.73 x 10^9	0.325	4.51 x 10^9	0.385	2.17
2nd NDR	3.04 x 10^{10}	0.79	2.08 x 10^{10}	0.995	1.46

Discussion: Bias has three main effects on the electronic structure:

    i.   it changes Fermi levels,

    ii.   sifts the energy of the resonant state,

    iii.   alters the profiles and transmission properties of the barriers.

The appropriate bias V pulls down the resonant state by about V/2, if the structure is symmetric. So $E_{pk}(V) \approx E_{pk}(0)-(1/2)eV$. Hence, resonance is pulled through the range of applied field.

Table 4.3 Theoretical and simulated voltage differences

Energy Level Differences (eV)		Theoretical Voltage Differences (V)		Practical Voltage Differences (V)	
$E_2 – E_1$	0.095	$\{(2x\ (E_2 – E_1))\ /q\}$	0.19	$V_2 – V_1$	0.465
$E_3 – E_2$	0.1334	$\{(2x\ (E_3 – E_2))\ /q\}$	0.1334	$V_3 – V_2$	0.71

On the other hand current depends on the applied bias through the factor of $(E_{FL}-E_{FR}) \approx$ $[E_{FL}-E_{pk}(0) + (1/2)\ eV]$. From the table 4.2, it is found that only two NDRs are supported by the structure. The peak currents appear at 0.325V and 0.79V respectively and a weak peak occurs at 1.5V (Approx). This clearly shows that the differences of the voltages at which peaks occur are not same as said in sub-section 4.3.2 that resonance energy differences are also not same. The total theoretical and simulated values are tabulated in table 4.3. Theoretically, the 1st peak of the RTD should appear at $\{$**(2 x 0.057) /q} V= 0.114V** and 2nd peak at $\{$**(2 x 0.2279)/q} V = 0.4558 V**. But from the data it is clear that practically peak voltages are larger than theoretical values. It is due to the drops across the undoped barriers as well as emitter and collector regions.

4.4. Resonant Tunneling Diode: Well Width Variation

Whenever well width of a RTD is varied, it plays very significant role on the I-V characteristics. Variation of widths varies the position of the bound states. The energy associated with the states of a quantum well as discussed in section 4.3.2, depends on the well thickness. From Eq. 2.41, it is found that energy states associated with well are inversely proportional with well width. So, as the well width decreases quantized energy states occur at higher levels.

For this simulation keeping the other parameters of the device fixed, only the well width is varied. Five different well widths, viz. 2nm, 4nm, 6nm, 8nm and 10nm are considered for simulation.

4.4.1. Current Density Vs Applied Voltage Characteristics for different well width:

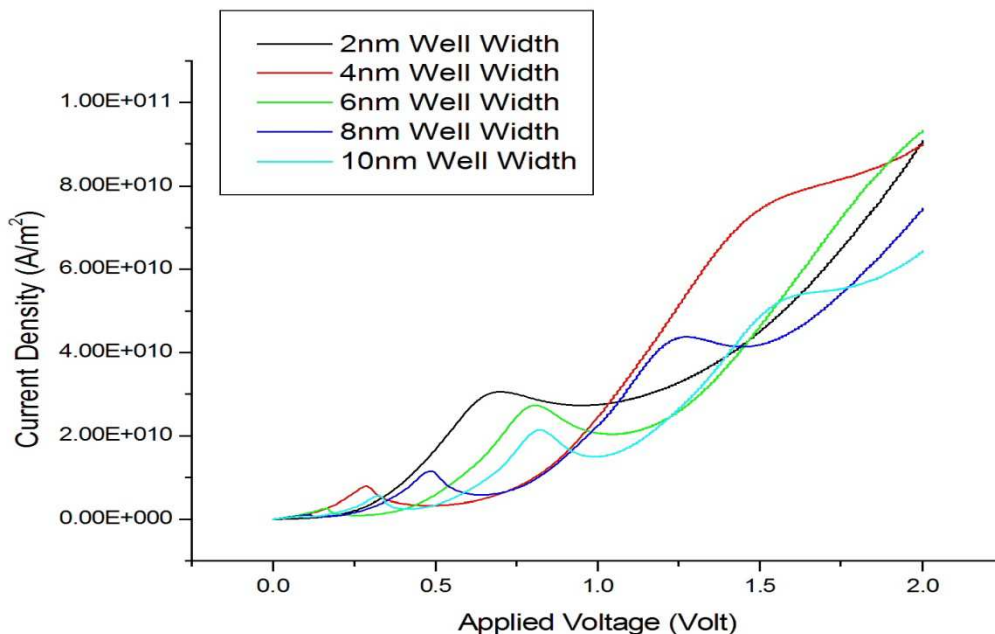Different current –voltage characteristics are of different well widths are shown in figure 4.6.

Figure 4.6 I-V Characteristics of RTD with varying well width

4.4.2. Analysis of the Simulated Result:

The following table indicates the different data from simulated result.

Table 4.4 Simulated result of RTD of different well widths

Well width (nm)	1st NDR					2nd NDR				
	1st Peak		1st Valley		PVCR	2nd Peak		2nd Valley		PVCR
	J_p (A/m²)	V_p (V)	J_v (A/m²)	V_v (V)		J_p (A/m²)	V_v (V)	J_p (A/m²)	V_v (V)	
2	3.065×10^{10}	0.7	2.728×10^{10}	0.95	1.123					
4	7.87×10^{9}	0.285	3.318×10^{9}	0.48	2.372					
6	2.688×10^{9}	0.165	9.77×10^{8}	0.26	2.75	2.725×10^{10}	0.81	2.035×10^{10}	1.04	1.338
8	1.14×10^{9}	0.11	6.41×10^{8}	0.145	1.778	1.149×10^{10}	0.485	5.78×10^{9}	0.64	1.987
10	6.83×10^{8}	0.085	5.66×10^{8}	0.1	1.2	5.61×10^{9}	0.325	2.496×10^{9}	0.415	2.247

Discussion: From the simulated data and figure 4.6, it is found that for 2nm and 4nm well widths only one peak appear at higher voltage. As discussed above that narrow well means the energy bound states occurs at higher energy values, so peak current density also occurs at higher voltages as more voltage required to align the Fermi-level with resonant states. The tunneling through higher order sub band levels of well, which is mainly responsible for valley current, can be reduced at narrow well as the energy sub band separations are higher. Hence increase in PVCR. As the inter subband separation are increased; only single subband becomes bound in the well. So, only one peak appears.

From the table 4.4, it is found that as the well width increases peak current and its' occurring voltage decreases as well as after a limit PVCR decreases.

On the other hand, when the energy Eigen value, E_n, is comparable in magnitude to the barrier potential V_0 [= $(E_{CB} - E_{CW})$]. It is then found that E_n's have lower values than those given by the infinite-barrier-potential model. The lowering depends on the magnitude of barrier height 'V_0' and well width 'a' [39].

From the table 4.4, it is also clear that for narrower well widths, subband separation are so large that higher states are comparable with barrier height and as a result, higher peaks are absent.

4.5. Resonant Tunneling Diode: Barrier Width Variation

In the standard case of RTD, 2 nm barrier widths are considered. Here in this section, influence of variation in barrier thickness on the device characteristics will be studied. In this section two types of structure are used to review the result. These are:

A. 3nm-10nm-3nm RTD

B. 4nm-10nm-4nm RTD

A. Device performance of 3nm-10nm-3nm RTD:

4.5.1. Structure of 3nm-10nm-3nm RTD:

The structure and energy bound states of present structure are shown in figure 4.7.

(a)   (b)

Figure 4.7 3nm-10nm-3nm RTD (a) Device structure and (b) bound energy states of electrons

4.5.2. Current Density as a function of Applied Voltage Characteristics:
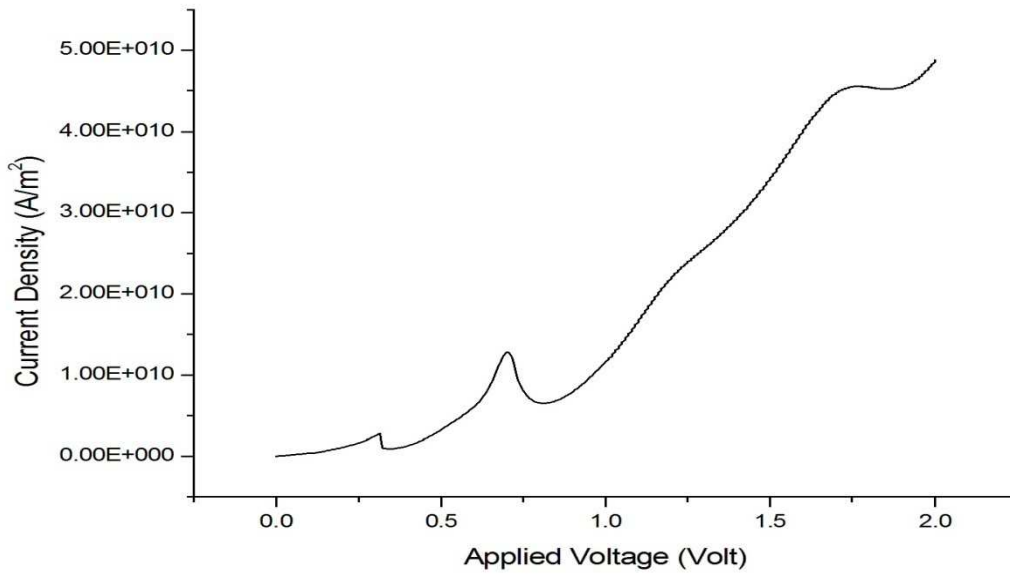
Figure 4.8 I-V Characteristics of 3nm-10nm-3nm RTD

4.5.3. Analysis of the Simulated Result:

The different data from simulated result are tabulated in the following table.

Table 4.5 Simulated result of 3nm-10nm-3nm RTD

Characteristics	*Peak*		*Valley*		*PVCR*
	J_p (A/m^2)	V_p (V)	J_v (A/m^2)	V_v (V)	
1st NDR	2.77 x 10^9	0.315	9.3 x 10^8	0.34	2.978
2nd NDR	1.28 x 10^{10}	0.705	6.49 x 10^9	0.815	1.97

Discussion: From the simulated data, it is pointed that the peaks occurred at lower voltages than normal structure. The 1st peak occurs at 0.315V whereas in standard case 1st peak occurs at 0.325V. However Peak current density is lower than standard case. This is due to decrease in the tunneling coefficient with barrier width, hence, results in decreasing current density.

B. Device performance of 4nm-10nm-4nm RTD:

4.5.4. Structure of 4nm-10nm-4nm RTD:

The software simulated structure and associated bound states are shown in figure 4.9.
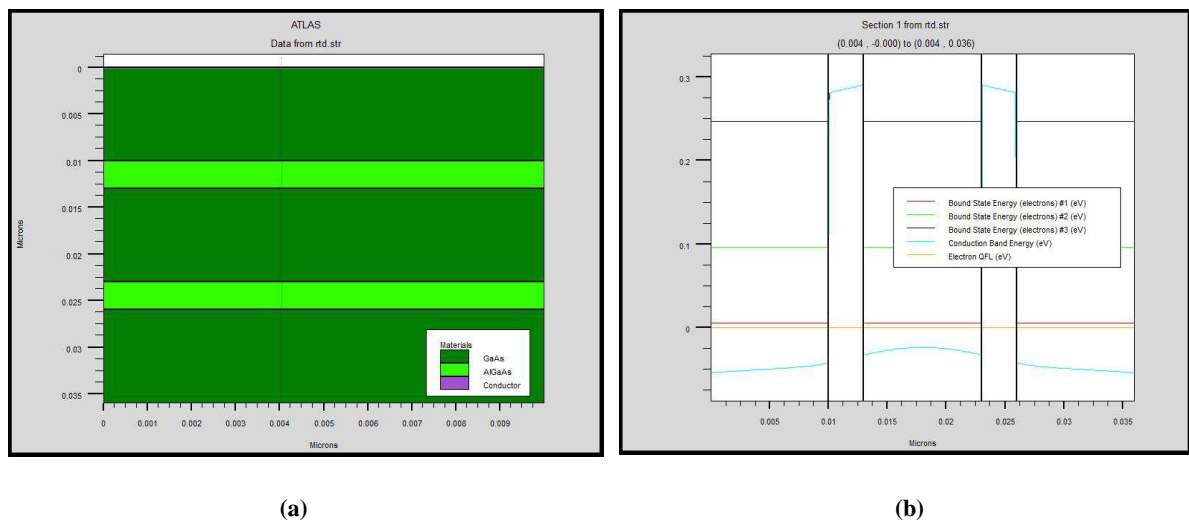

Figure 4.9 4nm-10nm-4nm RTD (a) Device structure and (b) bound energy states of electrons

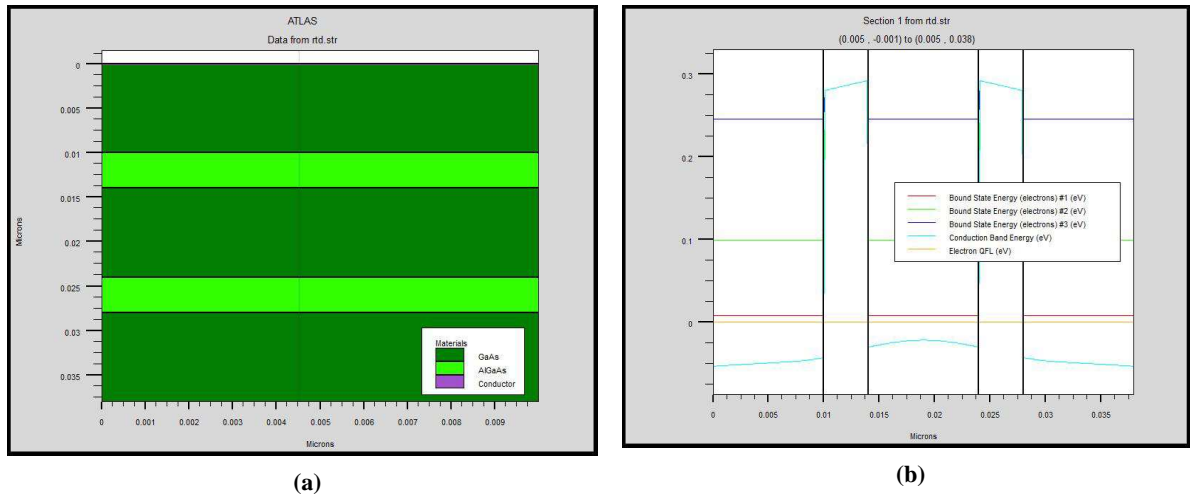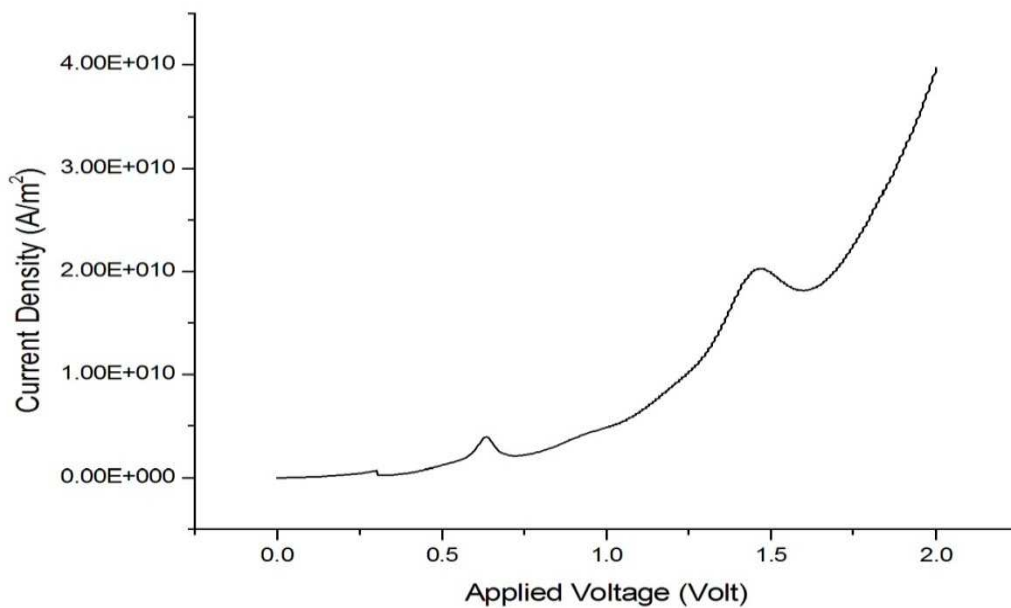### 4.5.5. Current Density as a function of Applied Voltage Characteristics:

Figure 4.10 I-V Characteristics of 4nm-10nm-4nm RTD

4.5.6. Analysis of the Simulated Result:

The following table shows the different data from simulated result.

Table 4.6 Simulated result of 4nm-10nm-4nm RTD

Characteristics	Peak		Valley		PVCR
	J_p (A/m^2)	V_p (V)	J_v (A/m^2)	V_v (V)	
1st NDR	6.79 x 10^8	0.3	2.36 x 10^8	0.325	2.8
2nd NDR	3.92 x 10^9	0.63	2.09 x 10^9	0.73	1.875

Discussion: In this case the peaks occur at lower voltages than previous case as the barrier width is thicker than previous one. The peak current density also decreases as discussed due to decrease in tunneling coefficient. In this case PVR also decrease than previous case. Hence it can be concluded that peak current density and PVR decreases with increase of barrier width, but peak occurs at lower voltage.

4.6. Resonant Tunneling Diode: Barrier Height Variation

The barrier height mainly depends on the composition factor *'x'* of the barrier material. In this case barrier material is *Al$_x$Ga$_{1-x}$As* which is combination of AlAs and GaAs. The details are described in section 4.2.1. In this case the value of *'x'* is set as **'0.38'**, thus barrier heights raise from **'0.3 eV'** to **'0.4 eV'.**

4.6.1. Structure of RTD with Higher Potential Barrier:

The structure and bound states are shown in figure 4.11.

(a)   **(b)**
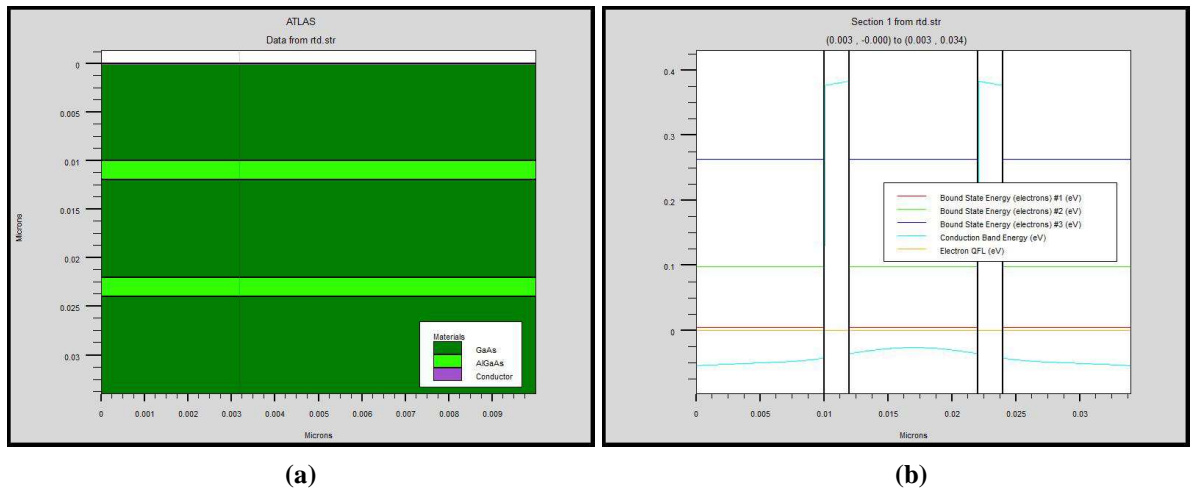
Figure 4.11 RTD with higher potential barrier (a) Device structure and (b) bound energy states of electrons

4.6.2. Current Density as a function of Applied Voltage Characteristics:

Figure 4.12 I-V Characteristics of RTD with Higher Potential Barrier

4.6.3. Analysis of the Simulated Result:

The following table shows the different data from simulated result.

Table 4.7 Simulated result of RTD with higher potential barrier

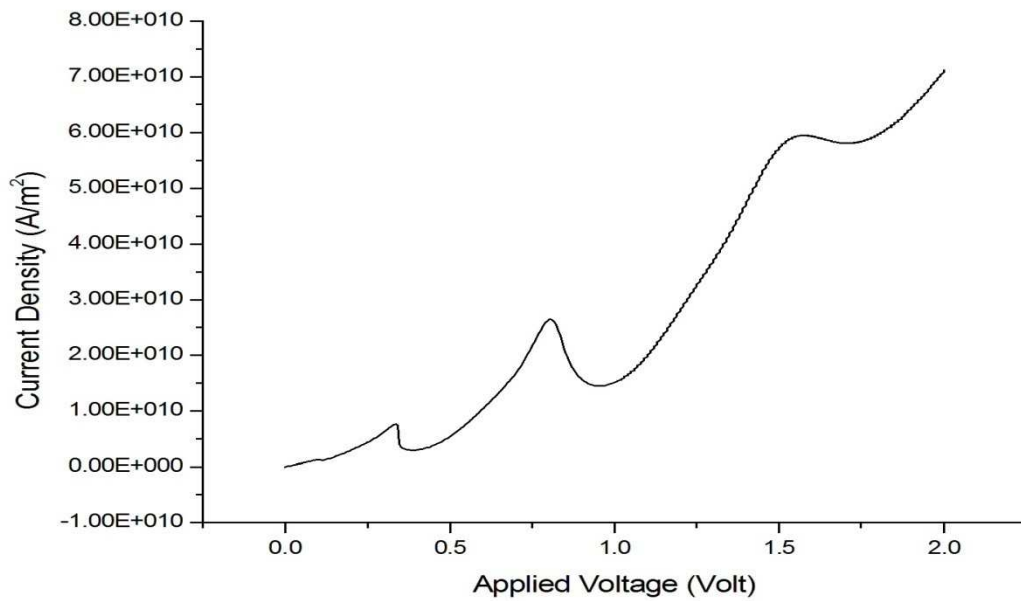| Characteristics	Peak		Valley		PVCR
	J_p (A/m^2)	V_p (V)	J_v (A/m^2)	V_v (V)	
1st NDR	6.79 x 10^8	0.3	2.36 x 10^8	0.325	2.8
2nd NDR	3.92 x 10^9	0.63	2.09 x 10^9	0.73	1.875
3rd NDR	5.955 x 10^{10}	1.58	5.814 x 10^{10}	1.71	1.0242

Discussion: This case the peaks occur at higher voltages than the standard case as the barrier heights are higher than standard structure. This makes the well deeper, as a result greater no. of bound states become confined in the well. From the table and graph, it is shown that there is extra 3rd peak. It indicates 3rd resonance level in the well. The inter subband separation also increases due to higher potential barrier. This results a lower valley current which increases PVCR. But peaks appear at higher voltages.

4.7. Resonant Tunneling Diode: With Spacer Layer

In real structure, a thin layers of undoped spacers ($\approx$15 Å same as electrode material [40]) adjacent to the barrier layers is used to ensure that dopants of the electrode do not diffuse to the barrier layers. This structure helps to improve PVCR of the device. In this section improvement in I-V characteristics using spacer with standard symmetric RTD structure, will be discussed.

4.7.1. Structure of RTD with spacer layer:

The structure and bound states of RTD with spacer layer are shown in figure 4.13.

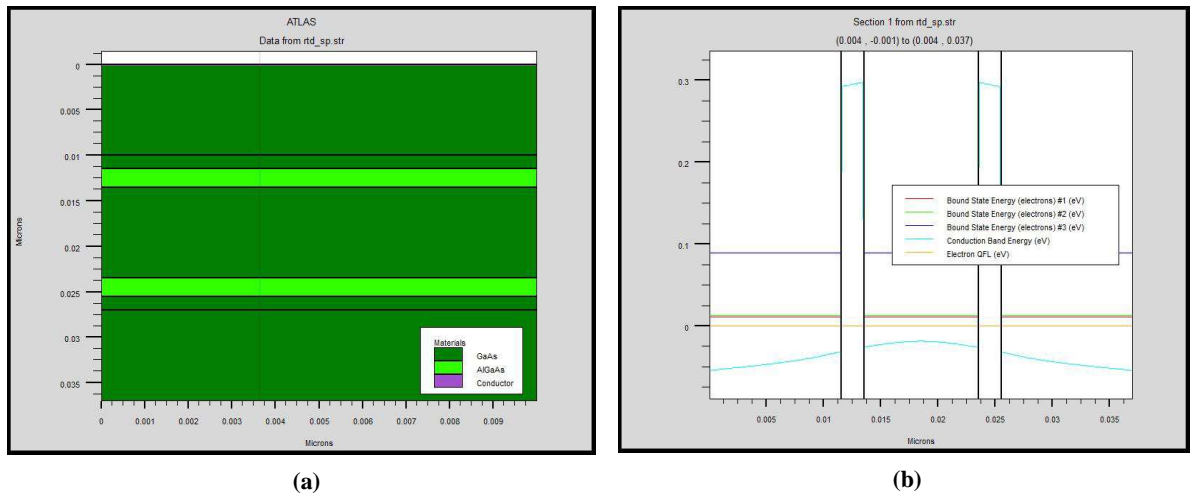(a)   (b)

Figure 4.13 RTD with spacer layer (a) Device structure and (b) bound energy states of electrons

4.7.2. Current Density as a function of Applied Voltage Characteristics:
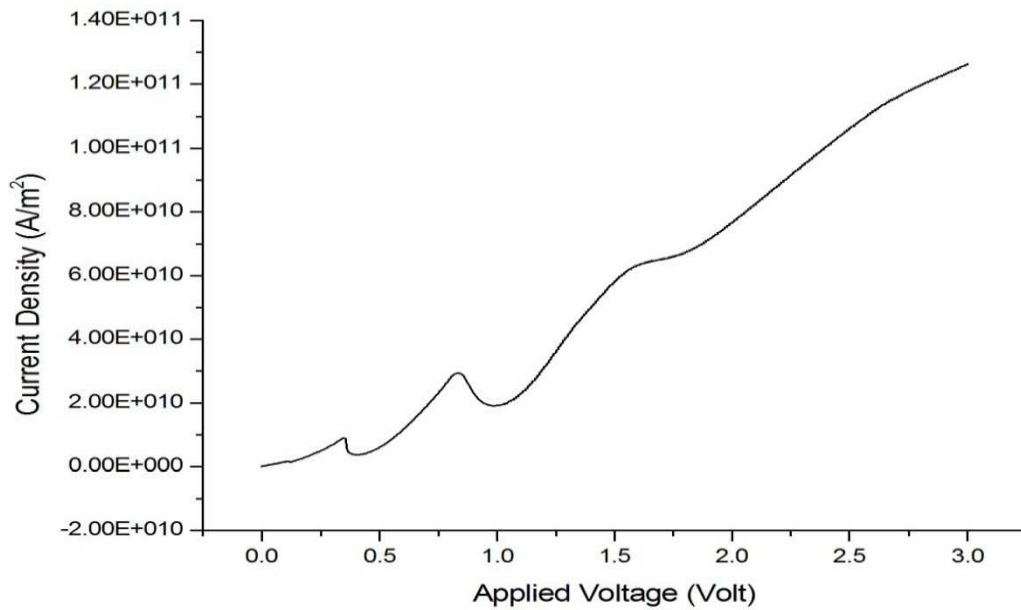

Figure 4.14 I-V Characteristics of RTD with spacer layer

4.7.3. Analysis of the Simulated Result:

The simulated results are given in the following table.

Table 4.8 Simulated result of RTD with spacer layer

Characteristics	Peak		Valley		PVCR
	J_p (A/m^2)	V_p (V)	J_v (A/m^2)	V_v (V)	
1st NDR	8.99 x 10^9	0.35	3.68 x 10^9	0.405	2.44
2nd NDR	2.945 x 10^{10}	0.835	1.909 x 10^{10}	0.99	1.5

Discussion: Using the spacer layer the PVCR is improved as unintentional doping from electrode region is reduced. The peak occurs at higher voltage as the structure now includes undoped spacer layers across which additional voltage drops will occurs.

4.8. Conclusion

From the graphs and simulated data obtained from simulation of RTD structure, the following conclusions may be drawn:

- Increase in the barrier width results in more voltage drops across the barrier layers. Therefore, peak current densities and NDR appear at higher voltages. But due to the asymmetric nature induced in the structure by the external field, the overall current density along with J_P also decrease here.

- In choice of well width, there is also a trade off between no. of NDR and value of PVCR in the resulting current-voltage characteristics. From simulation of various RTD structures, it may be concluded that a well widths comparable to double of the barrier widths is best suitable. When the well width *'a'* is increased, the resonant tunneling current is predicted to be reduced because of following reasons. The increase of *'a'* lowers first the resonance level E_{n1}, which leads to the increase of the effective barrier height $V_0' = V_0 - E_{n1}$ for electrons. This rise of V_0' causes the sharpening of the transmission coefficient around the resonance peak, or equivalently, the decrease of the peak width E_{n1}, which results in the decrease of the resonant tunneling current J_P. Also the valley current Jv depends on *'a'* as shown in table 4.4. This *'a'* dependence of J_v is similar to that of some tunneling-limited currents. Since J_v has appreciable temperature dependence, the excess current is

likely to be due to the tunneling currents of electrons thermally excited up to higher lying subbands. As clear from Fig. 4.6 that the first peak is nearly overshadowed by the tail current of the second peak, which supports this interpretation. Hence, we can conclude that the *PVCR* of DBRT with wide wells are severely lowered by the current due to tunneling through the higher lying level [41].

- The maximum available current density in the NDR region is directly related to the barrier thickness of the device. It is found experimentally that increasing the barrier width keeping well width fixed, results a peak current at lower voltage. But increasing barrier width means decrease of *tunneling probability*, hence total current will decrease [26]. High J_p and PVCR values have been achieved by using very thin barriers. The barrier thickness does not only limit J_p and PVCR, but also influence the quasibound lifetime of electrons in the quantum well (QW) and in turn, determine the speed of the RTD. It already verified that the reduction in barrier widths leads to the exponential increase in the resonant tunneling current J_p in AIAs/GaAs/ AlAs diodes [42].

- Higher barrier height implies deeper well, which supports a greater no. of energy bound state and thereby, results in greater no. of NDR regions. In a deeper well, inter-subband separation also increases. As a result, the valley current due to unintentional tunnelling thro' higher subbands gets suppressed, improving the PVCR. Again, the larger inter-subbsnd separation needs higher bias voltage to make E_{FL} aligned with E_n.

- Finally, introducing spacer layer decreases unintentional doping from heavily doped electrode region to undoped barrier region. This results a high PVCR than without spacer layer.

CHAPTER: 5

MODELLING & SIMULATION OF RTD: ASYMMETRIC STRUCTURE

Contents

CHAPTER: 5

MODELLING & SIMULATION OF RTD: ASYMMETRIC STRUCTURE

This Chapter deals with asymmetric structure of RTD. Different parameter variation and its influence in device characteristics are discussed in previous chapter. Here also the variation of parameter and its effects on device characteristics will be studied, but variation is asymmetric in nature. First RTD with asymmetric barrier width and then with asymmetric barrier height will be discussed in this chapter.

5.1. Resonant Tunneling Diode: Asymmetric Barrier Widths

Barriers have important role in RTD device performance. In previous chapter it is found that if the widths of the barrier be thinner, it results a good tunneling characteristics. From the Eq.2.31, if the width of the barrier increases, the transmission probability 'T' decreases. In this section the effects on device characteristics due to variation of widths in asymmetric way. The asymmetric barrier may be of two types.

(A) First barrier is thinner than second one, and

(B) Second barrier is thinner than first one.

A. Device Performance of RTD with First barrier thinner than second one:

5.1.1 Structure of RTD with Asymmetric barrier width:

Figure 5.1 shows the schematic structure of the above mentioned device and figure 5.2 shows the simulated structure and energy bound states of the same. This is asymmetric barrier RTD, 1st barrier width is taken as **2 nm** and 2nd one as **3 nm** and other parameters are same as standard one.
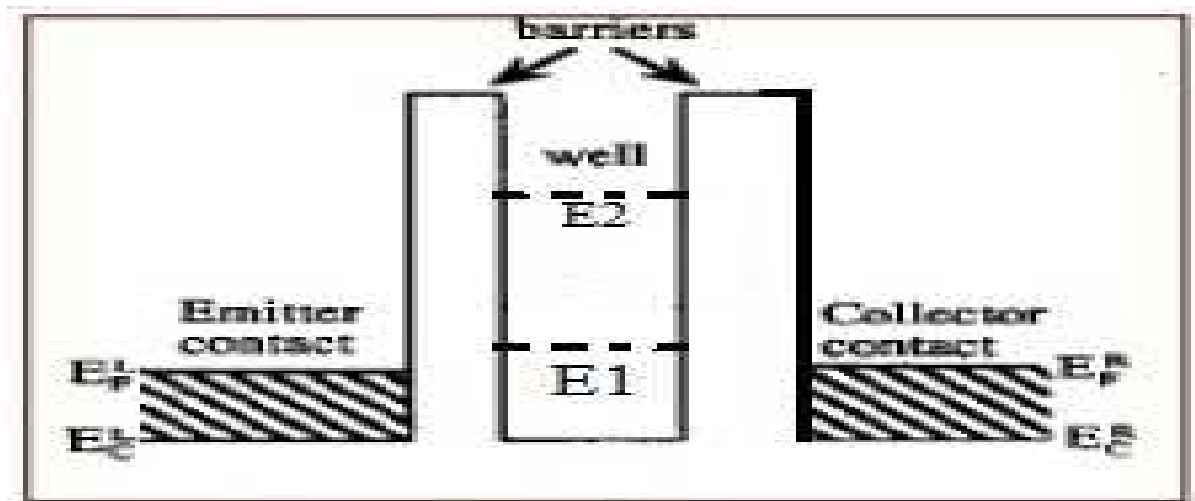
Figure 5.1 Schematic Device structure of RTD with Asymmetric barrier width
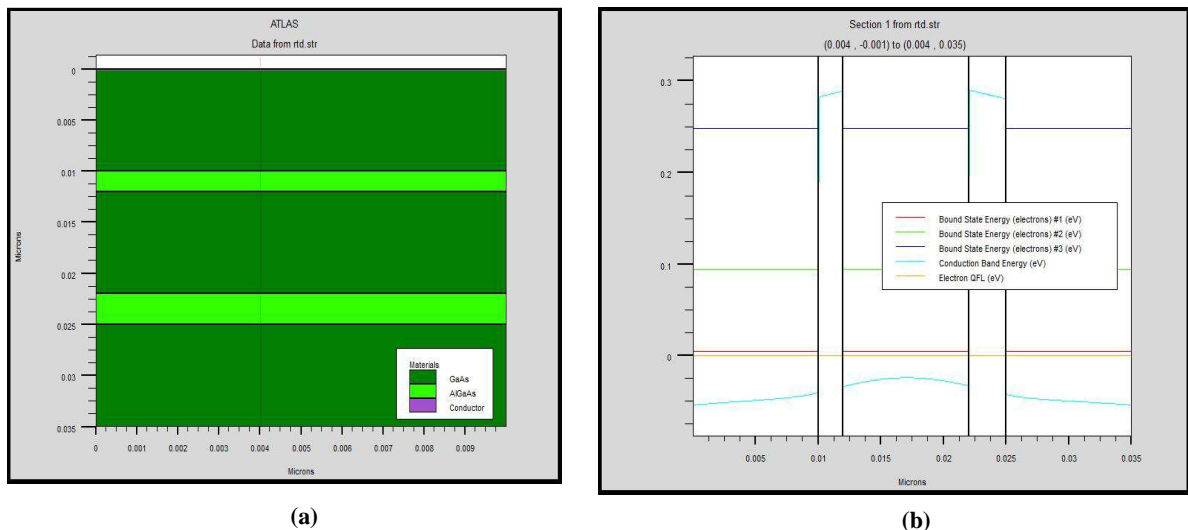
(a)

(b)

Figure 5.2 RTD with asymmetric Barrier widths (a) Simulated structure and (b) bound energy states of electrons

5.1.2 Current Density as a function of Applied Voltage Characteristics:

(a)

(b)
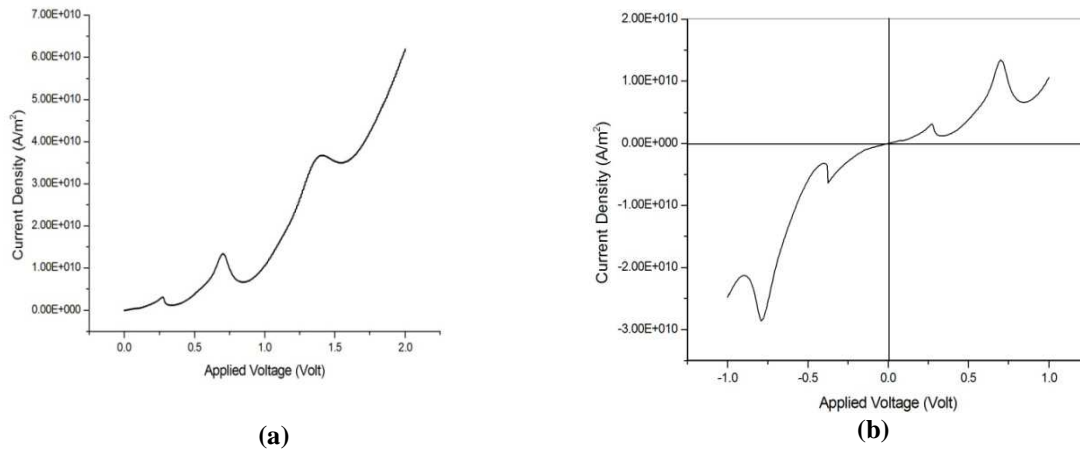
Figure 5.3 I-V Characteristics of RTD with 1st barrier thinner than 2nd one (a) Forward Bias (b) Both forward and reverse Bias

5.1.3 Analysis of the Simulated Result

The following table shows the different data from simulated result.

Table 5.1 Simulated result of RTD with 1st barrier thinner than 2nd one

Characteristics	Peak		Valley		PVCR
	J$_p$ (A/m^2)	V$_p$ (V)	J$_v$ (A/m^2)	V$_v$ (V)	
1st NDR	3.12 x 10^9	0.275	1.23 x 10^9	0.34	2.5
2nd NDR	1.34 x 10^{10}	0.75	6.65 x 10^9	0.845	2.015

Discussion: The simulated data shows 1st peak occurs at lower voltage than the standard operation of RTD as previously discussed. This is because that the total applied voltage drops across the total structure. When 1st barrier is thinner than 2nd one, then the voltage drops less at 1st barrier than 2nd one. Though the total current density is less than symmetric structure, but PVCR is improved than symmetric structure. This is due to less valley current than standard structure. So, keeping the 2nd barrier thinner the PVCR can be improved by making the valley current less. The asymmetric nature of the structure is also verified and it shown in figure 5.3(b). From this graph, it is clear that the I-V characteristics are not same under forward and reverse bias.

B. Device Performance of RTD with Second barrier thinner than first one:

5.1.4. Structure of RTD with Asymmetric barrier width:

In this section for asymmetric barrier RTD structure the 1st barrier width is taken as **3 nm** and 2nd barrier width as **2 nm.** Figure 5.4 shows the schematic diagram of of RTD with 1st barrier thicker than 2nd one and figure 5.5 shows the simulated structure and bound states of the device.

Figure 5.4 Schematic Device structure of RTD with Second barrier thinner than first one

| (a) | (b) |

Figure 5.5 RTD with Second barrier thinner than first one (a) Simulated structure and (b) bound energy states of electrons

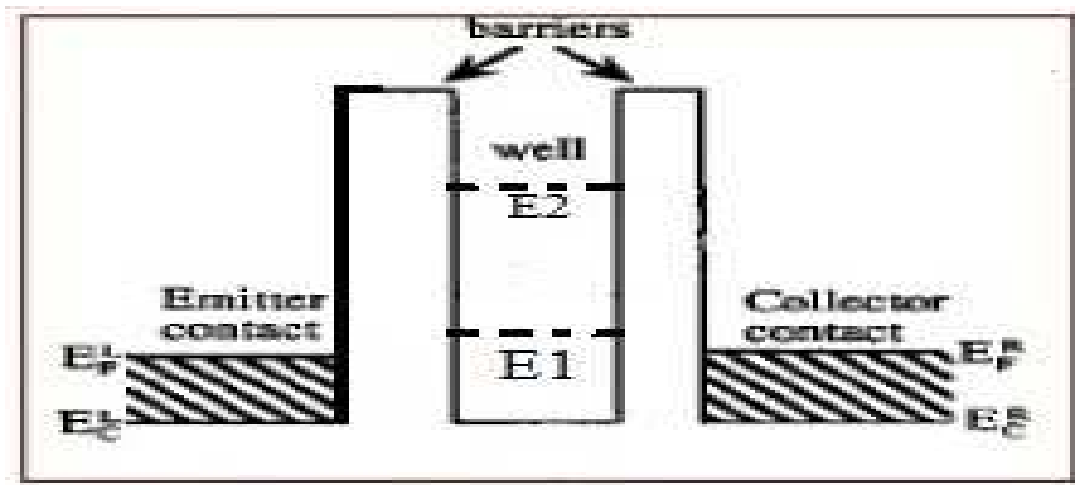## 5.1.5. Current Density as a function of Applied Voltage Characteristics:

Figure 5.6(a) shows the current-voltage characteristics of RTD in forward bias condition with 1st barrier thicker than 2nd one, and figure 5.6 (b) shows the characteristics under forward and reverse bias.

(a)   (b)
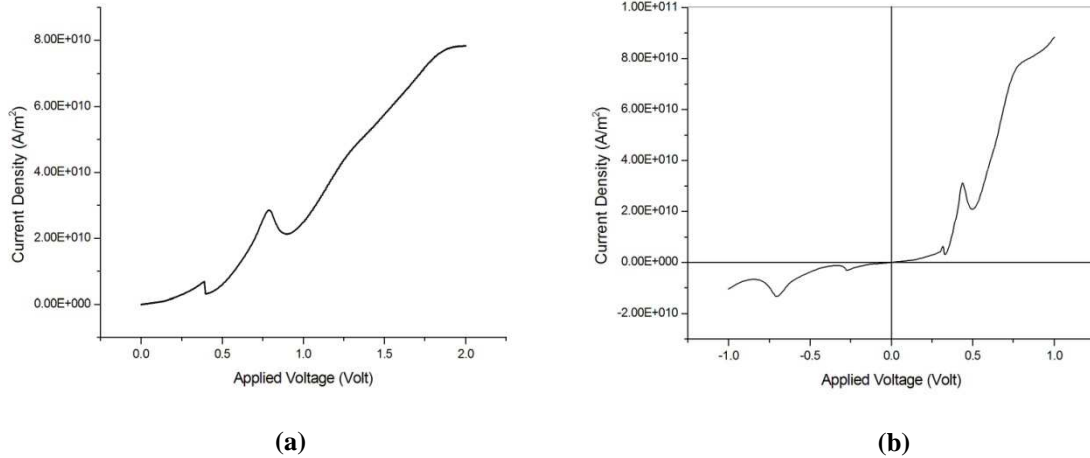
Figure 5.6 I-V Characteristics of RTD with 1st barrier thicker than 2nd one (a) Forward bias (b) Both Bias

5.1.6. Analysis of the Simulated Result:

The following table shows the different data from simulated result.

Table 5.2 Simulated result of RTD with 1st barrier thicker than 2nd one

Characteristics	*Peak*		*Valley*		*PVCR*
	J_p (A/m^2)	V_p (V)	J_v (A/m^2)	V_v (V)	
1st NDR	6.86×10^9	0.39	3.2×10^9	0.4	2.14
2nd NDR	2.85×10^{10}	0.79	2.13×10^{10}	0.9	1.9

Discussion: The simulated data show 1st peak occurs at higher voltage than the standard operation of RTD as discussed in 4.3. This is because that the total applied voltage drops across the total structure. When 1st barrier is wider than 2nd one, then the voltage drops more across the 1st barrier than 2nd one. The total current density and PVR is less than symmetric structure. This is because of presence of wider barrier. The 1st barrier is wider which is

mainly responsible for matching with resonance level. As the tunneling coefficient decreases with barrier width, current density in this case also decreases.

5.2. Resonant Tunneling Diode: Asymmetric Barrier Height

As mentioned in sub-section 4.6.1, to maintain the barrier height of **'0.4 eV'**, the composition factor *'x'* of the barrier material must be equal to **0.38**. In this section one of the barrier heights is kept **'0.3 eV'** i.e., same value considered for conventional structure and another one is kept **'0.4 eV'**. Here in this section the variations of RTD characteristics due to asymmetric barrier height will be studied.

This asymmetric structure is studied in two ways:

A. 1st barrier is smaller than 2nd one, and

B. 2nd barrier is smaller than 1st one.

A. Asymmetric RTD with 2nd barrier higher than 1st one:

5.2.1. Structure of Asymmetric barrier height RTD:

The barrier height is calculated in section 4.2.1 for standard case. Here the 1st barrier height is kept as same as standard structure, whereas 2nd barrier height is kept as **'0.4'eV**. For this *'x'* composition of $Al_xGa_{1-x}As$ is taken as **0.38.** The schematic structure is shown in figure 5.7 and simulated structure and bound states are shown in figure 5.8.
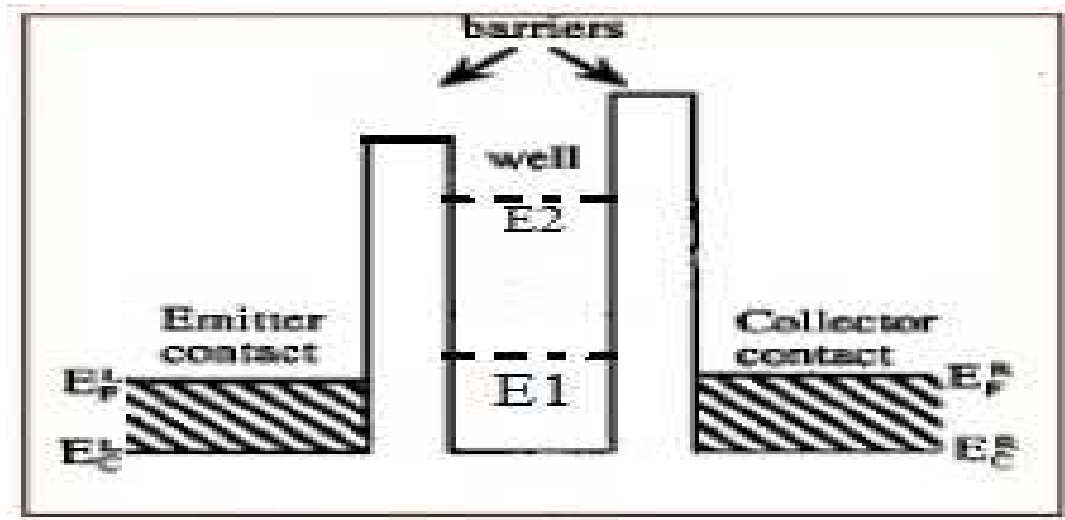
Figure 5.7 Schematic Device structure of RTD with Second barrier larger than first one
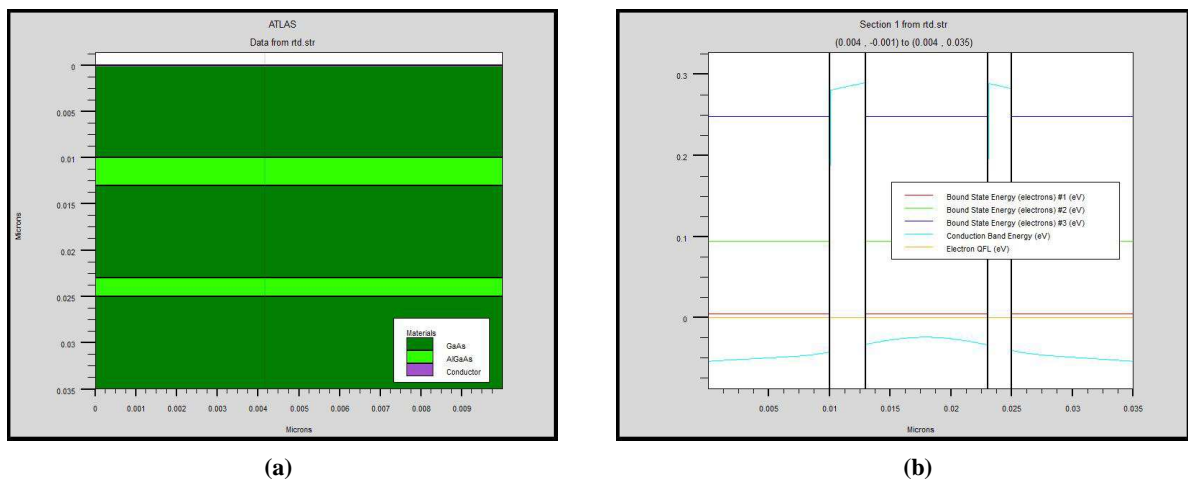

(a)	(b)
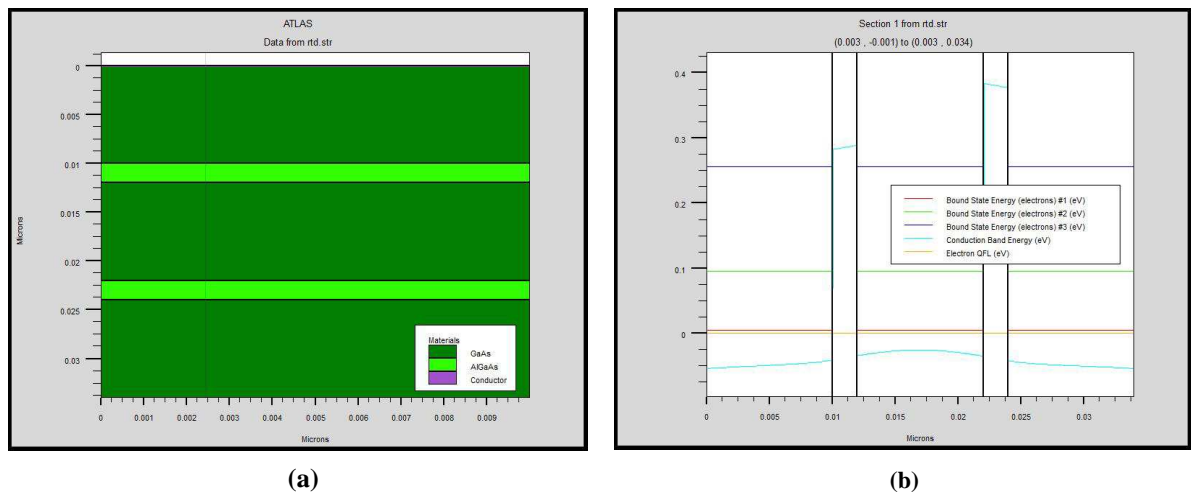
Figure 5.8 Asymmetric RTD with 2nd barrier higher than 1st one (a) Simulated structure and (b) bound energy states of electrons

5.2.2. Current Density as a function of Applied Voltage Characteristics:

I-V characteristics of the device under forward bias condition is shown in Figure 5.9(a), and both forward and reverse bias condition is shown in Figure 5.9(b).

(a)   (b)
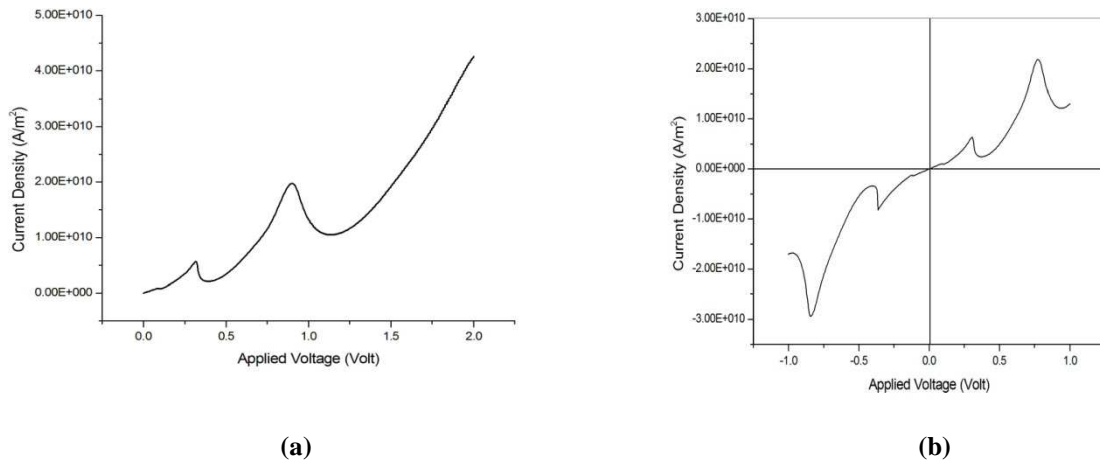
Figure 5.9 I-V Characteristics of Asymmetric RTD with 2ⁿᵈ barrier higher than 1ˢᵗ one (a) Forward Bias (b) Both Biases

5.2.3. Analysis of the Simulated Result:

The following table shows the different data from simulated result.

Table 5.3 Simulated result of Asymmetric RTD with 2ⁿᵈ barrier higher than 1ˢᵗ one

Characteristics	Peak		Valley		PVCR
	J_p (A/m²)	V_p (V)	J_v (A/m²)	V_v (V)	
1ˢᵗ NDR	6.36×10^9	0.305	2.46×10^9	0.37	2.585
2ⁿᵈ NDR	2.18×10^{10}	0.77	1.21×10^{10}	0.935	1.8

Discussion: Increasing barrier height makes resonance sharper i.e higher no of states become bound. But for discussed case, as the first barrier is same as standard structure the effect will be little. The 1ˢᵗ peak occurs at 0.305V and peak current density is 6.36×10^9 A/m². This is also smaller than symmetric structure. Though the current density is smaller than symmetric structure, PVCR is 2.585, higher than symmetric structure. The bias reduces the heights of barriers, the right hand one being most affected, as well as the energy of the resonance. So, Device under bias condition is no longer a symmetric structure. For this case with higher barrier at right hand side, keeps the device symmetric under bias condition. This also reduces valley current, hence increases PVCR.

B. RTD with 1st barrier higher than 2nd one:

5.2.4. Structure of Asymmetric barrier height RTD:

In this case 1st barrier height is kept as 0.4eV and 2nd one is 0.3eV. The schematic structure and bound states are shown in figure 5.10 and 5.11 respectively.

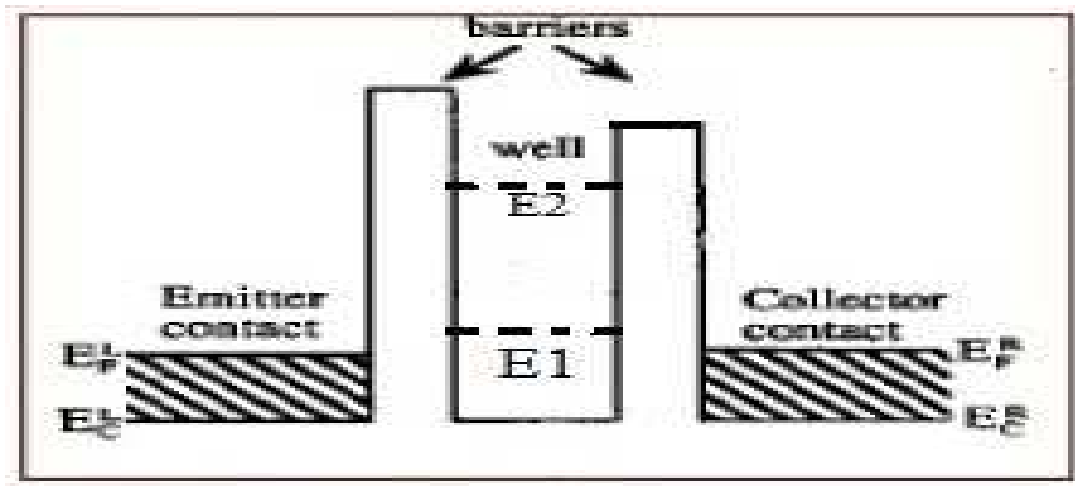

Figure 5.10 Schematic Device structure of RTD with 1st barrier higher than 2nd one
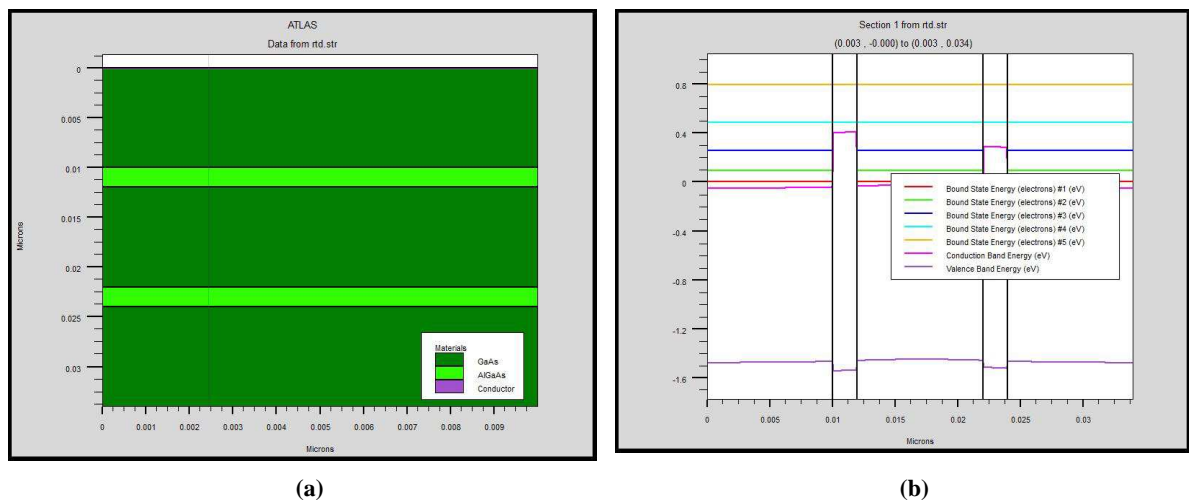
Figure 5.11 Asymmetric RTD with 1st barrier higher than 2nd one (a) Simulated structure and (b) bound energy states of electrons

5.2.5. Current Density as a function of Applied Voltage Characteristics:

The forward bias I-V characteristic of the device is shown in Figure 5.12(a) and both forward and reverse bias I-V characteristic is shown in Figure 5.12(b).

(a)   (b)
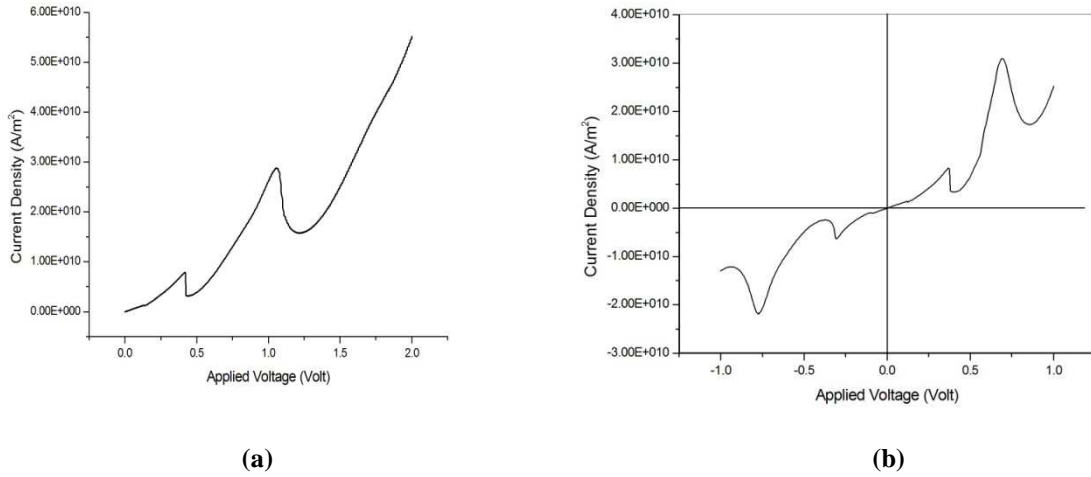
Figure 5.12 I-V Characteristics of Asymmetric RTD with 1st barrier higher than 2nd one (a) Forward Bias (b) Both Biases

5.2.6. Analysis of the Simulated Result:

The following table shows the different data from simulated result.

Table 5.4. Simulated result of Asymmetric RTD with 1st barrier higher than 2nd one

Characteristics	*Peak*		*Valley*		*PVCR*
	J_p (A/m^2)	V_p (V)	J_v (A/m^2)	V_v (V)	
1st NDR	8.3 x 10^9	0.37	3.37 x 10^9	0.4057	2.46
2nd NDR	2.94 x 10^{10}	0.85	1.68 x 10^{10}	0.97	1.78

Discussion: In this case 1st barrier is larger than the 2nd barrier height. The 1st peak occurs at 0.37V and peak current density is 8.3×10^9 A/m^2. This is also smaller than symmetric structure. Though the current density is smaller than symmetric structure, PVCR is 2.46, higher than symmetric structure. Here as the 1st barrier height is larger than 2nd one, the peak current occurs at higher voltage.

🞂 *5.3 Conclusion*

From the graphs and simulated data discussed in this chapter on simulation of asymmetric RTD structure, the following conclusions may be drawn:

- It is found that whenever the device structure is asymmetric (asymmetric in barrier widths or asymmetric in barrier height) the current is always less than the symmetric one. Though increase in barrier height means more confinement of energy states in the well. But as in this thesis work two barriers suffer changes in asymmetric way due to the bias applied to the RTD, and this causes reduction in current density. But changing barrier height means change in composition of 'x' in $Al_xGa_{1-x}As$. There is limitation to change the value of 'x'. As it is established that band gap remains direct up to x=0.45 [6].
- From the simulated result it was found that barrier width or barrier height larger in right side, results better PVCR. Bias reduces the heights of barriers, particularly of the right hand one, as well as the energy of the resonance. So, device under bias condition is no longer a symmetric structure. If they are to be reasonably symmetric, yielding higher peaks in T(E), when under bias, device should be designed with alternately thicker or higher right hand barrier at equilibrium.

CHAPTER: 6

MODELLING & SIMULATION OF SPECIAL STRUCTURE OF RTD

Contents

CHAPTER: 6

MODELLING & SIMULATION OF SPECIAL STRUCTURE OF RTD

In the previous chapter GaAs-AlGaAs based of RTD have been simulated and effects of variations in its parameters on their characteristics have been studied. In this chapter simulation of RTD using different material especially of lower effective mass, will be discussed and their characteristics will be compared with respect to those of GaAs based RTD.

In this chapter the following special structure are studied:

- InGaAs-InAlAs based RTD
- InGaAs-AlAs based RTD
- InGaAs-AlAs-InAs based RTD

6.1. Choice of Material for Resonant Tunneling Diode

In based material is mainly preferable due to low carrier effective mass in it compared to that in GaAs. $In_{0.53}Ga_{0.47}As$ and $In_{0.52}Al_{0.48}As$, which are matched to a substrate of InP.

A much wider range of materials opens up if the restriction of equal lattice constant is relaxed. For example, an attraction of $In_{0.53}Ga_{0.47}As$ — $In_{0.52}Al_{0.48}As$ for electronic systems is the large value of ΔEc and small m* for electrons in $In_{0.53}Ga_{0.47}As$. Raising the fraction of indium above **'0.53'** further improves the both properties, at the cost of introducing strain. Adjusting the fraction of indium also allows the band gap to be matched to the needs of optical fibres.

III/V heterostrucutures grown by sophisticated growth methods like metal-organic vapour phase epitaxy (MOVPE) or molecular beam epitaxy (MBE), far away from thermal

equilibrium, offer atomic control of layer thickness and composition. On atomic levels in order to take full advantage of all III/V-based band-gap engineering highly strained layers with abrupt interface are indispensable [30]. III/V growth is performed under excess group-V in order to maintain the stoichiometry at the growth front despite the higher group-V vapour pressure. Interfaces incorporating a group-V exchange (e.g. InGaAs to InP) intrinsically exhibit non-perfect abruptness. In addition, interface intermixing, compositions close or within the miscibility gap and segregation effects may damage the interface within a very few nanometer range [43].

6.2. InGaAs-InAlAs BasedResonant Tunneling Diode

As discussed in previous section that earlier works were focused on the GaAsl-$Al_xGa_{1-x}As$ heterostructures. More recently, improved peak-to-valley current ratios were obtained in the InGaAs-lnA1As material system, lattice matched to InP. In this section the I-V characteristics of RTD using *InGaAs-InAlAs* will be studied.

6.2.1. Structure of *InGaAs-InAlAs* based RTD:

The detail specifications of the structure used for this simulation are given below:

- Emitter width: 100nm
- Collector width: 200nm
- Barrier width: 50nm
- Well width: 40nm

Emitter and collector regions are formed by $In_{0.54}Ga_{0.46}As$ alloy with dopping concentration of (1.7×10^{17}) cm^{-3}. $In_{0.38}Al_{0.62}As$ is used as barrier material and $In_{0.59}Ga_{0.41}As$ is used as well material. Both the well and barriers are undoped. The SILVACO simulated structure and bound states are shown in figure 6.1.

(a)   (b)

Figure 6.1 *InGaAs-InAlAs* **based RTD (a) Device structure and (b) bound energy states of electrons**

6.2.2. Current Density as a function of Applied Voltage Characteristics:
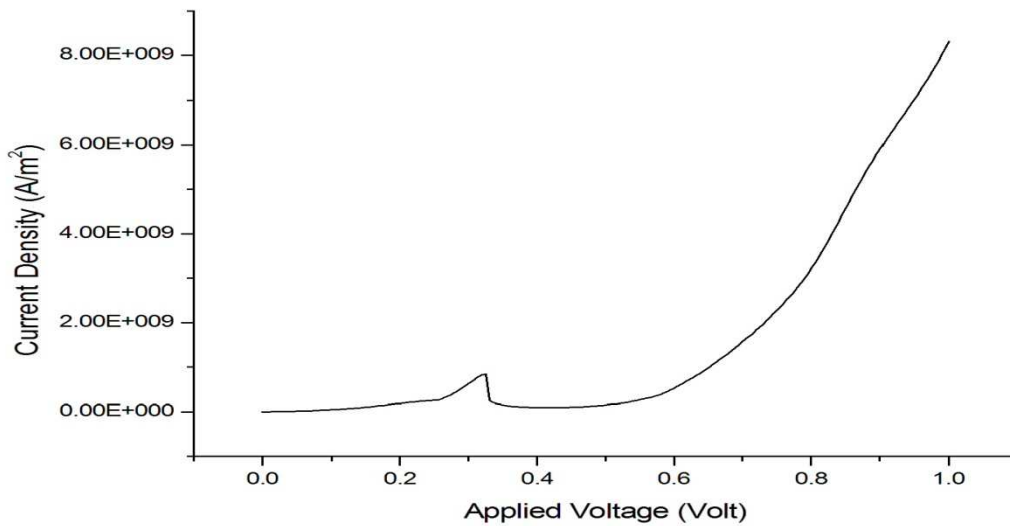
Figure 6.2 I-V Characteristics of *InGaAs-InAlAs* based RTD

6.2.3. Analysis of the Simulated Result:

The following table shows the different data from simulated result.

Table 6.1 Simulated result of *InGaAs-InAlAs* based RTD

Characteristics	Peak		Valley		PVCR
	J_p (A/m^2)	V_p (V)	J_v (A/m^2)	V_v (V)	
1st NDR	8.43 x 10^8	0.325	9.5 x 10^7	0.415	8.86

Discussion: From the expression of Transmission coefficient, it is found that effective mass of the material has great influence on Transmission coefficient. If material with lower effective mass is used, transmission coefficient and hence PVCR will improve,. From the above table, it is clear that the PVCR in case of $In_{0.53}Ga_{0.47}As$ — $In_{0.52}Al_{0.48}As$ RTD with respect to GaAs- $Al_{0.3}Ga_{0.7}As$ RTD discussed in chapter 4 is improved.

➕ *6.3. InGaAs-AlAs Based Resonant Tunneling Diode*

Though improved peak-to-valley current ratios were obtained in the InGaAs-lnAlAs material system, lattice matched to InP. By replacing the $In_{0.52}Al_{0.48}As$ barrier with a strained-layer AlAs barrier, the effects of characteristics will be discussed in this section.

6.3.1. Structure of *$In_{0.53}Ga_{0.47}As$-AlAs* base RTD:

For the simulation of this structure, as mentioned above AlAs is used for barrier material instead of $In_{0.52}Al_{0.48}As$ and $In_{0.53}Al_{0.47}As$ is used as well material. Both the emitter and well regions are undoped. The details about the structure dimensions are given below:

- Emitter width: 20 nm
- Collector width: 20nm
- Barrier width: 2nm
- Well width: 4nm

Both the emitter and collectors are n-type doped with dopping concentration of (2×10^{17}) cm^{-3}. The structure and bound states are shown in figure 6.3.
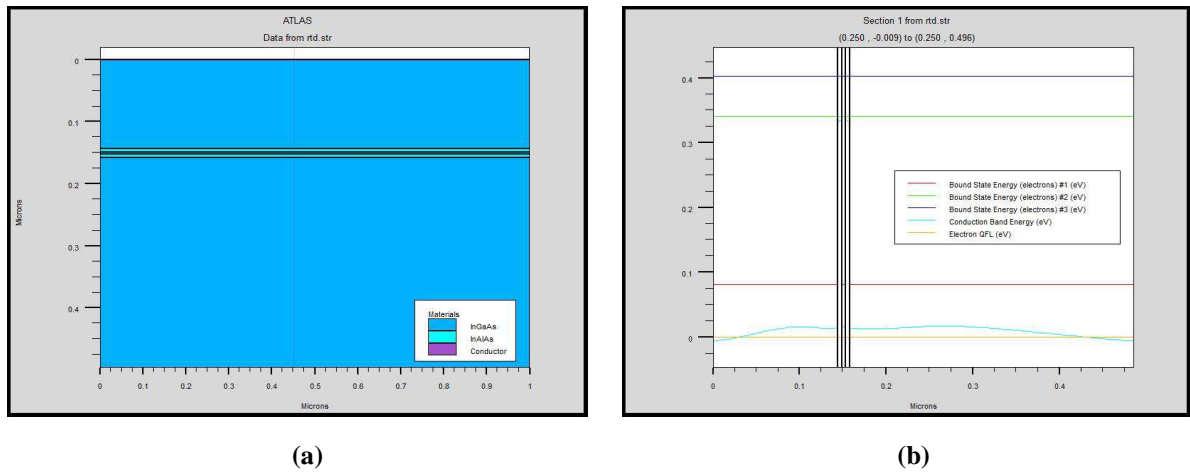
Figure 6.3 *InGaAs-AlAs* **based RTD (a) Device structure and (b) bound energy states of electrons**

## 6.3.2. Current Density as a function of Applied Voltage Characteristics:
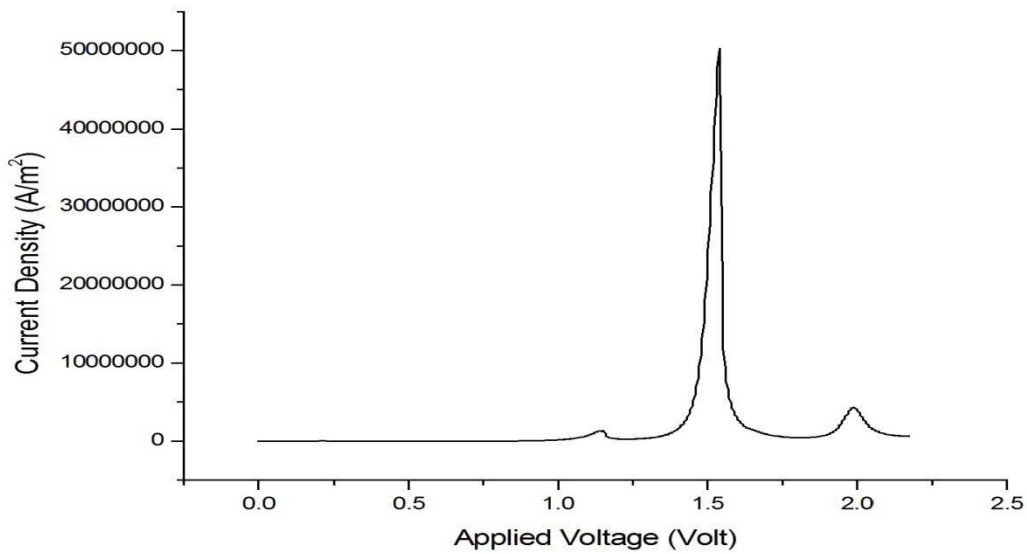
Figure 6.4 I-V Characteristics of *InGaAs-AlAs* based RTD

6.3.3. Analysis of the Simulated Result:

The following table shows the different data from simulated result.

Table 6.2 Simulated result of *InGaAs-AlAs* based RTD

Characteristics	Peak		Valley		PVCR
	J_p (A/m^2)	V_p (V)	J_v (A/m^2)	V_v (V)	
1st NDR	5x10^7	1.54	465745	1.81	107.922
2nd NDR	4178733	1.98	656011	2.17	6.37

Discussion: From the simulated result tabulated in Table 6.2, it is found that PVCR is improved using AlAs barrier instead of InAlAs. It is increases rapidly than previous one. But problem associated with it is that PVCR is found at higher voltage. The PVCR at lower voltage is possible using wider barrier widths.

6.4. InGaAs-AlAs-InAs Based Resonant Tunneling Diode

In the previous section, it was found that PVCR can be improved using AlAs barrier than InAlAs barrier material, but NDR appears at higher voltage. So, a very thin layer of InAs is introduced within the well region. In this section the characteristics of this RTD structure will be investigated.

6.4.1. Structure of *InGaAs-AlAs-InAs* base RTD:

The structure of this case is same as *InGaAs-AlAs* based RTD. The only modification is a extra thin layer of InAs within the InGaAs wel layer. The structure specifications are given bellow:

- Emitter width: 20nm
- Collector width: 20nm
- Barrier width: 2nm
- Total well width: 4nm

The details specification of the well in this case is as follows:

- Width of InAs layer: 0.8nm (8 Å)
- Width of each InGaAs layer: 1.6nm (16 Å)

In this case also well and barrier are undoped and emitter and collector are n-typed doped withdoping concentration of (2×10^{17}) cm^{-3}. The schematic structure of this device is shown in figure 6.5. and the simulated structure and bound states are shown in figure 6.6.
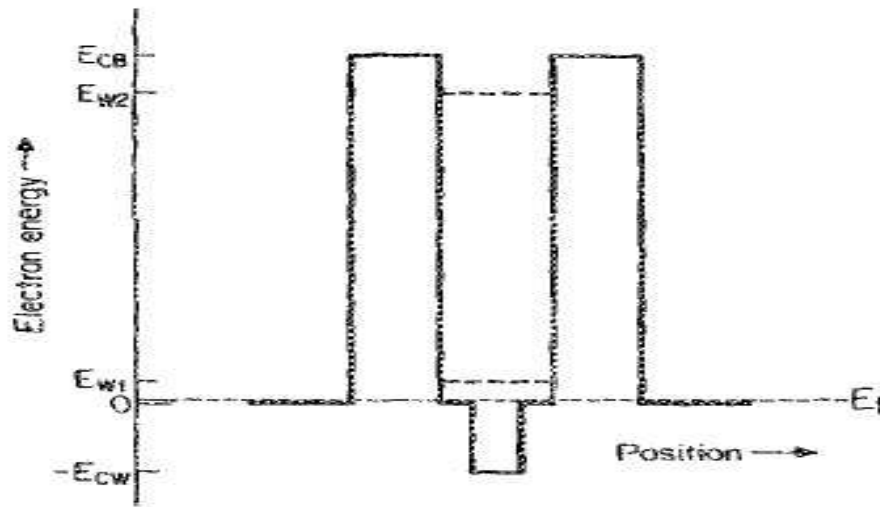
Figure 6.5 Schematic cross-sectional layer structure of the pseudomorphic InGaAs/ AIAs/ lnAs double-barrier resonant tunneling diode grown on InP substrate
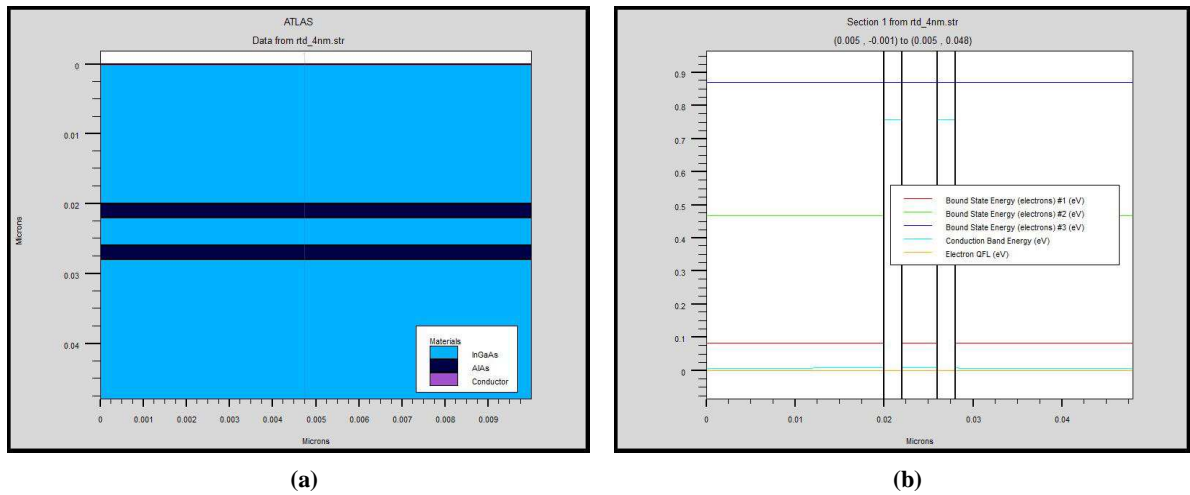

(a)

(b)
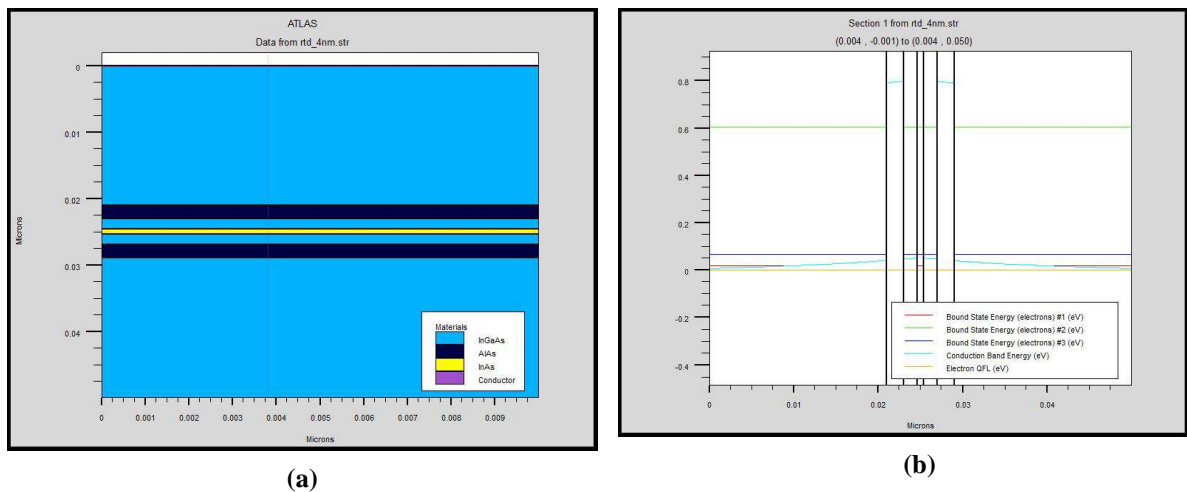
Figure 6.6 *InGaAs-AlAs-InAs* based RTD (a) Device structure and (b) bound energy states of electrons

## 6.4.2. Current Density as a function of Applied Voltage Characteristics:
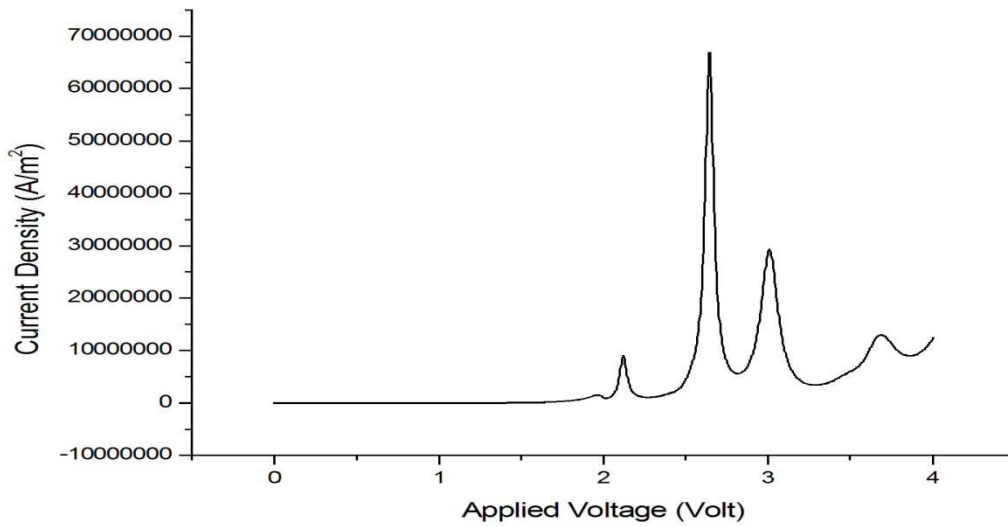
Figure 6.7 Current-Voltage Characteristics of *InGaAs-AlAs-InAs* based RTD
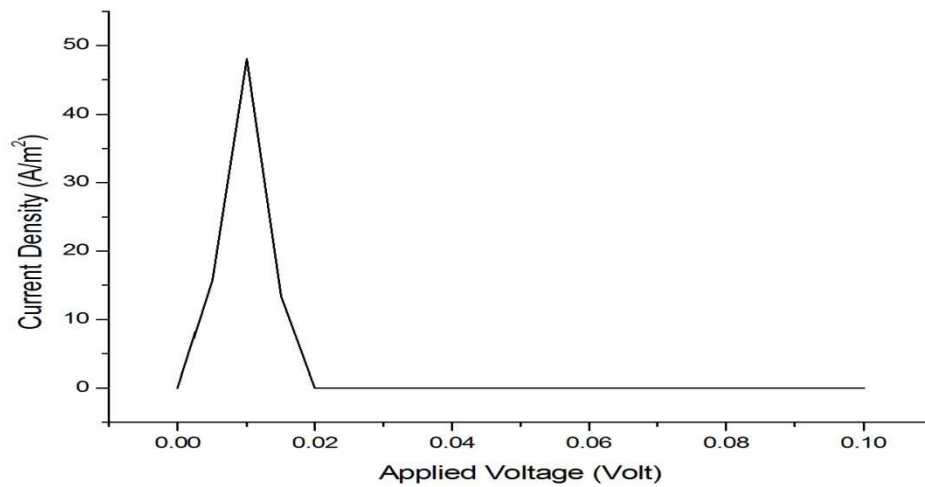
Figure 6.8 Zoom view of 1st NDR of *InGaAs-AlAs-InAs* based RTD

6.4.3. Analysis of the Simulated Result:

The simulated results are tabulated below.

Table 6.3 Simulated result of *InGaAs-AlAs-InAs* based RTD

Characteristics	Peak		Valley		PVCR
	J_p (A/m^2)	V_p (V)	J_v (A/m^2)	V_v (V)	
1st NDR	48.056	0.01	0.003	0.041	15992.76
2nd NDR	1.44×10^6	1.96	8.44×10^5	2.02	1.706

Discussion: From the simulated result tabulated in Table 6.3, it is found that introducing InAs as well material PVCR is improved and peak voltage is decreased. But introducing the thin layer of InAs should be maintained as précised manner, because length of InAs is very important. If InAs length is much more than desired value, then peak voltage will be at lower voltage but PVCR will decrease.

6.5. Conclusion

By analysing different 'In' based structure of RTD, the following conclusions are drawn:

- Higher figures of merit (PVCR) may be conveniently realized for the GaInAs/A1InAs system. Constructional features for these diodes are the same as for the GaAs/GaAlAs systems. Only GaInAs replaces GaAs and AlInAs replaces GaAlAs. The improvement for this system is essentially due to a larger value of the barrier potential and lower value of the effective mass in the well.

- Further improvement in device characteristics may achieved by using AlAs barrier layers in place of A1InAs barriers. From the simulated result, it is found that PVCR is very high than GaInAs/A1InAs based RTD. But NDR appears at higher voltages. To achieve PVCR at lower voltage, barrier thickness must be increased or well thickness must be decreased.

- By introducing InAs layer as well material the higher voltage problem associated with AlAs barrier can be minimized. This increases the PVCR and NDR occurs at lower voltages. But the dimension of InAs layer must be within a limit, otherwise PVCR can't be achieved at desired voltage.

CHAPTER:7

CONCLUSION & FUTURE SCOPE

CHAPTER: 7

CONCLUSION & FUTURE SCOPE

7.1. Summary

In this dissertation, after introducing the basic concepts of resonant tunneling, the transmission coefficient of a resonant tunneling structure has been derived theoretically and computed using MATLAB. Subsequently, the energy levels of a quantum well are determined numerically by MATLAB simulation and verified by simulating the well using SILVACO. The V-I characteristics has been critically studied, and the dependence of the peak and valley current, the corresponding voltages and the PVCR on various structural parameters of RTD along with the diode materials has been extensively investigated. On the basis of the investigations made in the dissertation, the key observations are summarized below:

i. The main goal of the researchers of RTD is to find higher PVCR at lower voltages. This can be achieved by using higher and wider right barrier. Bias reduces the heights of barriers, the right hand one particular, as well as the energy of the resonance. So, Device under bias condition is no longer a symmetric structure. So, device must be designed with thicker or higher right hand barriers at equilibrium, if they are to be reasonably symmetric, with higher peaks in T(E), when under bias. Though asymmetric structure has always less transmission probability than symmetric one. So, the total current is always less than the symmetric one. So, there is a trade off to choose proper barrier height.

ii. The wider barrier also results in peak current at lower operating voltage,but the amplitude of peak current density falls.

iii. The higher potential barrier is also useful to achieve multiple peaks, as the energy bound states become more confined in deeper well.

iv. A narrower quantum well is favourable to higher peak current density, but number of peak, i.e.number of NDR region gets limited.

v. Spacer layer helps to improve the PVCR, but an additional voltage drop is associated with the structure, shifting V_P to higher values.

vi. Use of material with lower electron effective mass makes the PVCR higher.

vii. Structure with InGaAs-AlAs performs better compared with other RTDs studied here. Only limitation of it is that the 1st current peakappears at higher voltage. This can be eliminatedmaking barriers wide, which in turn, will reduce the PVR. So a trade off is to be done in order to optimize the performance of the RTD.

viii. Introduction of a thin layer ofInAsin the middle of the well layer of InGaAs-AlAs based RTD improves performance of the device. However, dimension of the InAslayer should be very precisely chosen for the best result.

However, studies presented in the dissertation have few limitations:

➢ The theoretical calculation includes only basic resonant structure, i.e. a well sandwiched between two barrier layers. But in simulated structures, along with basic resonant tunneling structure two electrode regions are present. Therefore the peak voltages from SILVACO simulation are higher than theoretical value.

➢ The same thing happens in case of determination of bound energy states in the well. The simulated values are found to be larger than the theoretically estimated values.

➢ The simulation made here is 2-D in nature.

➢ Simulation of larger device structure is difficult due to meshing problem and is too time consuming. So, a small structure is simulated as replica of a largerone to investigate the qualitative features.

🔸 *7.2. Future Scope*

The most striking feature of RTD over all the other tunnelling-based devices is its multiple NDR regions. It provides multiple functionality to the device, and as a result makes it the

subject of intensecontemporary research.Our investigations can be further extended in the following directions:

   i.   More recent resonant tunneling diode models have incorporated additional important physical aspects such as the space charge effects, the 2-D accumulation layer in the RTD emitter region, the multiband effects,the phonon scattering and coulomb interaction between the carriers and traps. Sucheffects can also be incorporated in the model of RTD presented in the thesis to get more realistic results.

   ii.   In this thesis, the model of RTD possesses a single quantum well.If the single quantum well be replaced by MQW, multiple NDR regions should appear in its V-I characteristics. Analysis of such characteristics seems quite interesting.

   iii.   This work may be extended for structures based on other material system. It will help to find out the most appropriate materials yielding the best performance.

   iv.   RTD being a two terminal device suffers from inherent lack of control. So, modelling and simulation of RTT will be more useful for proper circuit applications.

   v.   Similar investigations may be made on HBT comprising of basic resonant tunnelling structure in it and will yield exciting results.

   vi.   Compared to conventional devices RTD and RTT take advantage of their higher speed of operation, low power dissipation and reduced circuit complexity due to higher functionality. So different logic circuit can be implemented and studied by the series and parallel combination of RTD and RTT.

References:

[1] L.L. Chang, L. Esaki, and R. Tsu, "Resonant tunneling in semiconductor double barriers," Applied Physics Letters, Vol. 24, pp. 593, 1974.

[2] T.C.L.G. Sollner, W.D. Goodhue, P.E. Tannenwald, C.D. Parker, and D.D. Peck, "Resonant tunneling through quantum wells at frequencies up to 2.5 THz," Applied Physics Letters, vol. 43, p. 588, 1983.

[3] Pinaki Mazumder, Shriram Kulkarni, Mayukh Bhattacharya, Jian Ping Sun, and George I. Haddad, "Digital Circuit Applications of Resonant Tunneling Devices," Proceedings of the IEEE, vol. 86, April 1998.

[4] A. Seabaugh, B. Brar, T. Broekaert, F. Morris, P. van der Wagt, and G. Frazier, "Resonant tunneling mixed-signal circuit technology," Solid-State Electronics, vol. 43, pp. 1355{1365, 1999.

[5] L. Esaki and R. Tsu, *IBM Internal Res. Rep. RC 2418, Mar.26* (1969)

[6] John H. Davies "The Physics Of Low-Dimensional Semiconductors -An Introduction", Cambridge University Press.

[7] D. K. Ferry, Quantum Mechanics, London: IOP Publishing Ltd., 2001.

[8] T R. Tsu and L. Esaki, "Tunneling in a finite superlattice", Journal of Applied Physics Letters, Vol. 22, No. 11, 1 June 1973, pp. 562-564.

[9] H. Mizuta and T. Tanoue, The Physics and Applications of Resonant Tunelling Diodes. Cambridge University Press, 1995. [14]

[10] S. Luryi, "Frequency limit of double-barrier resonant-tunneling oscillators," Applied Physics Letters, vol. 47, p. 490, 1985.

[11] S. Luryi, "Mechanism of operation of double-barrier resonant-tunneling ocsillators," International Electron Devices Meeting, 1985, pp. 666{669, 1985.

[12] S. Luryi, \Coherent versus incoherent resonant tunneling and implications for fast devices," Superlattices and Microstructures, vol. 5, p. 375, 1989.

[13] S. L. Rommel, T. E. Dillon, M. W. Dashiell, H. Feng, J. Kolodzey, P. R. Berger, P. E. Thompson, K. D. Hobart, R. Lake, A. C. Seabaugh, G. Klimeck and D. K. Blanks, "Room temperature operation of epitaxially grown $Si/Si_{0.5}Ge_{0.5}/Si$ resonant interband tunneling diodes," *Applied Physics letters,* vol. 73, no. 15, pp. 2191-2193, 1998.

[14] J.P. Sun et al., "Resonant Tunneling Diodes: Models and Properties", in PROCEEDINGS OF THE IEEE, VOL. 86, NO. 4, APRIL 1998, pp. 641-661.

[15] T. C. L. G. Sollner et al., "Quantum well oscillators", Journal of Applied Physics Letters, Vol. 45, No. 12, 15 December 1984, pp. 1319-1321.

[16] M. Tsuchiya, H. Sakaki and J. Yoshino, "Room temperature observation of differential negative resistance in an AlAs/GaAs/AlAs resonant tunneling diode," Japanese Journal of Applied Physics, vol. 24, no. 6, pp. L466-L468, 1985.

[17] C. I. Huang, M. J. Paulus, C. A. Bozada, S. C. Dudley, K. R. Evans, C. E. Stutz, R. L. Jones and M. E. Cheney, "AlGaAs/GaAs double barrier diodes with high peak-to-valley current ratio," Applied Physics Letters, vol. 51, no. 2, p. 121, 1987.

[18] T. Inata, S. Muto, Y. Nakata, T. Fujii, H. Ohnishi and S. Hiyamizu, *Jpn. J. Appl. Phys.* **25,** L983 (1986)

[19] P. D. Hadson, D. J. Robbins, R. H. Wallis, J. J. Davies and A. C. Marshall, *Electron. Lett.* **24,** 187 (1988)

[20] J. E. Oh, I. Mehdi, J. Pamulapati, P. K. Bhattacharya and G. I. Haddad, *J. Appl. Phys.* **65,** 842 (1989)

[21] S. Muto, T. Inata, Y. Sugiyama, Y. Nakata, T. Fujii, H. Ohnishi and S. Hiyamizu, *Jpn. J. Appl. Phys.* **26,** L220 (1987)

[22] T. Inata, S. Muto, Y. Nakata, S. Sasa, T. Fujii and S. Hiyamizu, *Jpn. J. Appl. Phys. Lett.* **26** L1332 (1987)

[23] S. Sen, F. Capasso, A. L. Hutchinson and A. Y. Cho, "Room temperature operation of Ga0.47In0.53As/Al0.48In0.52As resonant tunnelling diodes," Electronic Letters, vol. 23, p. 1229, 1987.

[24] J. E. Oh, I. Mehdi, J. Pamulapati, P. K. Bhattacharya and G. I. Haddad, "The effect of molecular-beam-epitaxial growth conditions on the electrical characteristics of In0.52Al0.48As/In0.53Ga0.47As resonant tunneling diodes," Journal of Applied Physics, vol. 65, no. 2, pp. 842-845, 1989.

[25] I. Mehdi and G. Haddad, "Lattice matched and pseudomorphic In0.53Ga0.47As/InxAl1-xAs resinant tunneling diodes with high current peak-to-valley ratio for millimeter-wave power generation," Journal of Applied Physics, vol. 67, p. 2643, 1990

[26] Tom P. E. Broekaert, Wai Lee, and Clifton G. Fonstad, "Pseudomorphic In0.53Ga0.47As/AlAs/InAs resonant tunneling diodes with peak tovalley current ratios of 30 at room temperature", Applied Physics Letters **53**, 1545 (1988);

[27] T. P. E. Broekaert and C. G. Fonstad, "In0.53Ga0.47As/AlAs resonant tunneling diodes with peak current densities in excess of 450 kA/cm2," Journal of Applied Physics, vol. 68, no. 8, p. 4310, 1990.

[28] Y. S. Moise,a) Y.-C. Kao, A. J. Katz, T. P. E. Broekaert, and F. G. Celii, Experimental sensitivity analysis of pseudomorphic InGaAs/AIAs resonanttunneling diodes, Journal of Applied Physics **78**, 6305 (1995);

[29] J. H. Smet, T. P. E. Broekaert and C. G. Fonstad, "Peak-to-valley current ratios as high as 50:1 at room temperature in pseudomorphic In0.53Ga0.47As/AlAs/InAs resonant tunneling diodes," Journal of Applied Physics, vol. 71, no. 5, p. 2475, 1992.

[30]   D. H. Chow, J. N. Schulman, E. Ozbay and D. M. Bloom, "High Speed InAs/AlSb and In0.53Ga0.47As/AlAs resonant tunneling diodes," MRS Proceedings, vol. 281, p. 269, 1992.

[31]   H. C. Liu, D. Landheer, M. Buchanan and D. C. Houghton, "Resonant tunneling in Si/Si1-xGex double-barrier structures," Applied Physics Letters, vol. 52, no. 21, p. 1809, 1988.

[32]   D. X. Xu, G. D. Shon, M. Willander and G. V. Hansson, "Variations of resonant tunneling properties with temperature in strained Si1-xGex/Si double-barrier structures," Applied Physics Letters, vol. 58, no. 22, p. 2500, 1991.

[33]   A. Zaslabsky, A. Grutzmacher, Y. H. Lee, W. Ziegler and T. O. Sedgwick, "Selective growth of Si/SiGe resonant tunneling diodes by atmospheric pressure chemical vapor deposition," Applied Physics Letters, vol. 61, p. 2872, 1992.

[34]   Y. Rajakarunanayake and T. C. McGill, "Si-Si1-xGex n-type resonant tunnel structures," Applied Physics Letters, vol. 55, no. 15, p. 1537, 1989.

[35]   K. Ismail, B. S. Meyerson and P. J. Wang, "Electron resonant tunneling in Si/SiGe double barrier diodes," Applied Physics Letters, vol. 59, no. 8, p. 973, 1991.

[36]   D. J. Paul, P. See, I. V. Zozoulenko, K.-F. Berggren, B. Kabius, B. Hollander and S. Manti, "Si/SiGe electron resonant tunneling diodes," Applied Physics Letters, vol. 77, no. 11, p. 1653, 2000.

[37] F. Capasso and R. A. Kiehl, "Resonant tunneling transistor with quantum well base and high-energy injection: A new negative differential resistance device," Journal of Applied Physics Letters, vol. 58, 1985, pp. 1366.

[38] B. Riccb and P. M. Solomon, "Tunable resonant tunneling semiconductor emitter structure," IBM Tech. Dig. Bull., vol. 27, p. 3053, 1984

[39] B. R. Nag, "Physics of Quantum Well Devices" , Solid-State Science and Technology Library, Vol. 7, Kluwer Academic Publishers, 2002.

[40] Kwok K. Ng-Complete Guide to Semiconductor Devices, Second Edition-Wiley-IEEE Press (2002)

[41] Masahiro Tsuchiya and Hiroyuki Sakaki, Dependence of resonant tunneling current on well widths in AlAs/GaAs/AlAs double barrier diode structures, Applied Physics Letters 49, 88 (1986)

[42] M. Tsuchiya and H. Sakaki, Jpn. J. Appl. Phys. 25, Ll85 (1986).

[43] F. Schulze-Kraasch, P. Velling, S. Neumann, W. Pros, Characterisation of ultra-thin III/V-heterostructures by convergent-beam-electron- and high-resolution-X-ray-diffraction, Materials Science and Engineering B 110 (2004) 161–167

APPENDIX - A

The program of the proposed structure shown in figure 3.2 is given below:

```
go atlas

mesh    diag.flip

x.mesh loc=0.00  spac=0.01
x.mesh loc=2.0   spac=0.01

y.mesh loc=0.0   spac=0.002
y.mesh loc=0.1   spac=0.001
y.mesh loc=0.102 spac=0.0001
y.mesh loc=0.112 spac=0.0001
y.mesh loc=0.114 spac=0.001
y.mesh loc=0.214 spac=0.002

region num=1 material=GaAs y.min=0.0
region num=2 material=AlGaAs x.comp=0.33 y.min=0.1 y.max=0.102
region num=3 material=GaAs y.min=0.102  y.max=0.112
region num=4 material=AlGaAs x.comp=0.33 y.min=0.112
y.max=0.114
region num=5 material=GaAs y.min=0.114  y.max=0.214


elec num=1 name=emitter top
elec num=2 name=collector bottom

MATERIAL NAME=GaAs AFFINITY=4.07
MATERIAL NAME=AlGaAs AFFINITY=3.74

#material  material=AlGaAs  align=0.65


doping reg=1 y.max=0.1 uniform n.type conc=1e18
doping reg=5 y.min=0.114 uniform n.type conc=1e18

save outf=dbar01_0.str
tonyplot dbar01_0.str -set dbar01_0.set


method carr=0
model     conmob  srh  auger  bgn
#contact     name=emmiter workf=4.97

probe name="Well charge " integrate charge  y.min=0.112
y.max=0.122
probe name="Emitter charge " integrate charge  y.min=0.0
y.max=0.1
```

```
probe name="Well state energy (eV)"  nbnd.ener  state=1
y=0.118 x=0
probe name="Emitter state energy (eV)"  nbnd.ener  state=2
y=0.1 x=0

extract
output band.param con.band val.band eigen=3
solve       init
save outf=rtd.str negf.log
tonyplot rtd.str

solve init
log outf= dbar01.log
solve name=emitter vemitter=0 vstep=0.01 vfinal=0.05
solve name=emitter vemitter=0.05 vstep=0.02 vfinal=0.6
solve name=emitter vemitter=0.6 vstep=0.05 vfinal=5
log off
tonyplot dbar01.log -set dbar01_log.set

quit
```